EVALUATION OF RELATIONSHIP BETWEEN SULFATE CONTENT AND ELECTRICAL RESISTIVITY

by

ZOBAIR AHMED

Presented to the Faculty of the Graduate School of

The University of Texas at Arlington in Partial Fulfilment

Of the Requirements

For the Degree of

MASTER OF SCIENCE IN CIVIL ENGINEERING

THE UNIVERSITY OF TEXAS AT ARLINGTON

December 2022

ACKNOWLEDGEMENT

I would like to express my gratitude towards my supervisor, Dr. MD Sahadat Hossain, for his continuous contribution and guidance during the course of my graduate studies. Having the chance to work on this research project under his supervision is an honor.

I am grateful to Dr. Xinbao Yu and Dr. Azijul Islam for their precious time. I really appreciate your valuable suggestions and advice. I would also like to acknowledge the Texas Department of Transportation for funding this study.

My sincere gratitude to all of the SWIS members who have offered me unwavering support. A special thanks to Yatindra Thorat for his support and help during the sample collection and laboratory testing.

Finally, but most importantly, I want to express my sincere thanks to my family, particularly to my parents, wife, and sibling, for their unending support and inspiration. I'm grateful to my Almighty for all the favors.

ABSTRACT

EVALUATION OF RELATIONSHIP BETWEEN SULFATE CONTENT AND RESISTIVITY IMAGING

Zobair Ahmed

The University of Texas at Arlington, 2022

Supervising Professor: Dr. MD Sahadat Hossain

Texas soils typically have sulfate content due to certain geologic formation types. Soil sulfate needs to be identified and quantified to minimize damage to infrastructure caused by sulfate-induced heave. Electrical Resistivity Imaging can identify the presence of sulfate content in the soil. Electrical Resistivity Imaging (ERI) is a non-destructive and fast way of obtaining continuous soil substructure profiles. Moisture fluctuations and soil heterogeneities can be found using an ERI approach. As a result, ERI is growing in popularity as a tool in geotechnical engineering, yet at the moment, it only offers qualitative data. It can be challenging to determine quantitative geotechnical information about the subsurface from qualitative images, such as the soil type, sulfate content, moisture content, level of saturation, and Atterberg limit.

This study aims to identify the relationship between the soil's electrical resistivity and sulfate content, and geotechnical parameters. Two soil samples from Fort Worth and El Paso were selected for laboratory experimentation. The Fort Worth Sample was high plastic clay, and El Paso was poorly graded sand. Existing sulfate content was measured using a colorimeter for the two soil samples. The laboratory resistivity of these two samples was measured with increasing unit weight and moisture content using Super String IP resistivity equipment. A gypsum solution of 1000 ppm was added and thoroughly mixed with soil to increase the sulfate content of the soil to simulate higher sulfate content. Therefore, sulfate addition of 1000 ppm followed by sulfate testing and resistivity testing was done repeatedly until both samples reached 11000 ppm. Resistivity values were plotted against moisture content (MC), sulfate content (SC), dry unit weight (DUW), void ratio(e), and degree of saturation (DOS) to find out the correlation among the geotechnical parameters of the soil with resistivity. The general trend was downward for MC, SC, DUW and

DOS but upward for void ratio. This correlation was used to find suitable parameters for the statistical modeling.

The geotechnical engineering properties of both samples were correlated with electrical resistance using different multiple linear regression (MLR) models developed in R-studio. In developing a multiple regression equation SC, MC, DUW, fine content (FC) was used as an independent parameter. The MLR model was validated based on the laboratory and field test data; therefore, the model can be used for estimating sulfate content.

Table of Content

1 CHAPTER 1: INTRODUCTION 1

1.1 Background 1

1.2 Problem Statement 2

1.3 Research Objective 3

1.4 Thesis Organization 3

2 CHAPTER 2: LITERATURE REVIEW 5

2.1 Introduction 5

2.2 Sulfate Bearing Soil 5

2.3 Form of Sulfate present in Soil 6

2.3.1 Primary Sources of Sulfate 7

2.3.2 Secondary Source of Sulfate 7

2.4 Mechanisms for Sulfate Heaving 8

2.4.1 Heaving caused by Crystal Growth 8

2.4.2 Heaving caused by Hydration 9

2.5 Sulfate Level 9

2.6 Heave Cases in Texas 10

2.6.1 Forensic Investigation of Premature Pavement Failure Resulting from Heave Caused by Soil Sulfate, Childress, County, U.S. 287 Texas 10

2.6.2 Sulfate Heave, 2.6.2 FM 201, Sabine County, Pineland, Texas 11
2.6.3 Sulfate Heave on U.S. 67 in Ellis County, Texas 12
2.6.4 Other Case Studies in Texas 13
2.6.5 Conductivity Test 14
2.6.6 Acetone Test 15
2.6.7 Barium Chloride Test 15
2.6.8 Colorimetry/Spectrophotometry 16
2.7 Evaluation of the Sulfate Test Procedures 17
2.8 Soil Resistivity 17
2.9 Formation of Clay Minerals 18
2.9.1 Kaolinite 19
2.9.2 Smectite 19
2.9.3 Illite 20
2.10 The Soil Resistivity Mixing Model 21
2.11 Factors affecting Soil Resistivity 22
2.11.1 Effect of Moisture of Soil 23
2.11.2 Effect of Unit Weight 24
2.11.3 Effect of Degree of Saturation 24
2.11.4 Relationship of Cation Exchange Capacity with Specific Surface Area 25
2.11.5 Temperature of soil 26

2.11.6 Soil Types and Resistivity Values 27
2.11.7 Current Frequency 28
2.11.8 Pore fluid composition 29
2.11.9 Presence of Salts 30
2.11.10 Sulphate Content of Pore Water 31
2.12 Determination of Geotechnical Parameters 32
2.12.1 Atterberg Limits 32
2.12.2 Compaction Parameters 33
2.12.3 Behavior of Consolidation 35
2.12.4 Hydraulic Conductivity 36
2.13 Electrical Resistivity Methods 38
2.13.1 Electrical resistivity tomography (ERT) 41
2.13.2 Capacitively coupled resistivity (CCR) 41
2.13.3 Data acquisition for Four-electrode resistivity systems 41
2.14 Limitation of previous studies 44
3 CHAPTER 3: METHODOLOGY 45
3.1 Introduction 45
3.2 Sample Collection 48
3.3 Test Methodology 49
3.3.1 Particle Size Distribution 49

3.3.2 Liquid limit and Plastic limit 51
3.3.3 Specific Gravity 53
3.3.4 Sulfate Content in Soil with Colorimetric Method 53
3.3.5 Laboratory Electrical Resistivity Testing 55
3.3.6 Sulfate Addition in the soil sample 56
3.4 Statistical Analysis 58
3.5 Model Validation 58
4 CHAPTER 4: RESULTS AND DISCUSSION 59
4.1 Geotechnical Properties 59
4.1.1 Grain Size Distribution 59
4.1.1.1 Fort Worth Sample 59
4.1.1.2 EL Paso Sample 59
4.1.2 Atterberg Limit Test 60
4.2 Laboratory Resistivity Test Results 61
4.3 Resistivity Results for Clayey Fort Worth Soil 61
4.3.1 Influential Parameters Related to Soil Properties 61
4.3.1.1 Resistivity and Sulfate Content 61
4.3.2 Influential Parameters Related to Phase Relationship 65
4.3.2.1 Moisture Content and Resistivity 65
5.2.1.2 Dry Unit Weight and Resistivity 69

4.3.2.2 Void ratio and resistivity 72
4.3.2.3 Degree of saturation and resistivity 75
4.4 Resistivity Results for Sandy El Paso Soil 76
4.4.1 Influential Parameter Related to Soil Properties 76
4.4.1.1 Sulfate Content and Resistivity 76
4.4.2 Influential Parameters related to Phase Relationship 79
4.4.2.1 Gravimetric Moisture Content and Resistivity 79
4.4.2.2 Dry Unit Weight and Resistivity 82
4.4.2.3 Void Ratio and Resistivity 84
4.4.2.4 Degree of Saturation and Resistivity 88
5 CHAPTER 5: STATISTICAL ANALYSIS 89
5.1 Introduction 89
5.2 Parameter Selection for Model 90
5.3 Multiple Linear Regression Analysis 92
5.3.1 Correlation Analysis 92
5.3.1.1 Response vs Predictor Plots 93
5.3.1.2 Predictor vs Predictor Plots 94
5.3.2 Development of Preliminary Model 96
5.3.3 Verification of Preliminary Model 97
5.4 MLR Model Form 98

5.4.1 Constant Error Variance 98
5.4.2 Normality 99
5.4.3 Outlier Test 100
5.4.4 Multicollinearity 103
5.4.5 Transformation of Variables and Check for MLR Assumptions 103
5.4.6 Final Model Selection 103
5.4.7 Best Subset Selection 103
5.4.8 Stepwise Regression 104
5.4.9 Validation of Final Prediction Model 105
6 CHAPTER 6: CONCLUSIONS AND FUTURE RECOMMENDATIONS 109
6.1 Introduction 109
6.2 Summary and Conclusions 109
6.3 Recommendation for Future Studies 110
7 REFERENCES 111

List of Figures

Figure 2-1: Texas Counties with measurable sulfate concentrations (>100 ppm). (Harris et al. 2004; Chen et al. 2005) 6

Figure 2-2: East side of the project area has a heaved area. (Chen et al. 2005) 11

Figure 2-3**:** Gypsum crystals can be discovered in the roadside drainage wash. (Harris et al.2006) 12

Figure 2-4: Near Midlothian, Texas, a Heave on US 67 (Wimsatt 1999) 13

Figure 2-5: Kaolinite formation diagram (© 2007-2010 The University of Waikato |www.sciencelearn.org.nz) 19

Figure 2-6 : Smectite formation diagram (© 2007-2010 The University of Waikato |www.sciencelearn.org.nz) 20

Figure 2-7: Formation of Illite 20

Figure 2-8: Changes in soil resistivity with soil saturation levels in several soil samples. (Abu-Hassanein et al. 1996). 25

Figure 2-9: Relationships between pore water conductivity and volumetric water content at different values (Kalinski and Kelly, 1993) 30

Figure 2-10: Variations in resistivity of samples when pore water contains sulfates (Akhtar et al, 2021) 32

Figure 2-11: Optimal Water Content and Electrical Resistivity Relationship: Liquid limit and plasticity index are two examples. (Abu Hassanein et al., 1996) 33

Figure 2-12: Compaction parameters and conductivity have a relationship (data from Abu-Hassanein et al., 1996; Abu-Hassanein, 1994). 34

Figure 2-13: Change in Conductivity and Void Ratio in Relation to Effective Stress (after McCarter and Desmazes, 1997). 35

Figure 2-14: Hydraulic and Electrical Conductivity Relationship (data from Abu-Hassanein, 1994) 38

Figure 2-15: electrode arrays that are frequently used in resistivity investigations. The current and potential electrode positions are indicated by the letters C1, C2, and P1, P2. It is typical to use the symbols A, B for the current electrodes and M, N for the potential electrodes for the symmetrical and gradient Schlumberger arrays. (Sharma, 1997)..... 39

Figure 2-16: Dipole-dipole resistivity pseudosection construction (Everette, 2013) 40

Figure 2-17: Top: Inverted resistivity image and measured apparent resistivity pseudo section for a hybrid Schlumberger -dipole-dipole electrode arrangement (Bottom). The apparent resistivity determined using the inverted cross section is shown in the middle figure. (Everette, 2013)..... 41

Figure 2-18: Traditional four-electrode resistivity system (Samouëlian et al., 2005; Aizebeokhai, 2010) 42

Figure 2-19: Conventional four-electrode resistivity technique (ASTM G57, 2006) 43

Figure 3-1: Workflow of the study 45

Figure 3-2 Soil collection locations 48

Figure 3-3: Sieves used for Sieve Analysis 50

Figure 3-4: Particle size distribution testing using the hydrometer procedure 51

Figure 3-5: Liquid limit testing involves (a) flattening the soil in the device cup, (b) creating a groove in the center, and (c) contacting the groove after blowing. 52

Figure 3-6: Rolling device and cracked and shattered threats of 3 mm plastic limit testing..... 52

Figure 3-7: Specific gravity testing of soil 53

Figure 3-8: Photograph of a Colorimeter used for sulfate determination..... 54

Figure 3-9: Illustrated Tex-145-E Method for Soluble Sulfates Determination in Soil 55

Figure 3-10: Preparation of soil samples in steps a and b, a schematic setup for a laboratory electrical resistivity test, and a practical setup for a laboratory resistivity test are all included... 56

Figure 3-11 : (a) Pulverizing sample; (b) Measuring sulfate sample (c) Mixing sulfate with water; (d) Mixed sulfate with soil 57

Figure 4-1: Grain size distribution curve for El Paso & Fort Worth sample. 59

Figure 4-2: Plasticity Chart of Fort Worth and El Paso Soil 60

Figure 4-3: Relationship between sulfate content and resistivity in different moisture content level. 63

Figure 4-4: Resistivity vs Sulfate content for different dry unit weight. 64

Figure 4-5: Relationship between FW soil's electrical resistance and moisture content. 68

Figure 4-6: Relationship between soil compaction's unit weight and resistivity..... 71

Figure 4-7: Relationship between electrical resistivity and void ratio. 74

Figure 4-8: Resistivity and saturation level are correlated. 75

Figure 4-9: Relationship between sulfate content and resistivity in different moisture content level. 77

Figure 4-10: Resistivity vs Sulfate Content for different dry unit weight. 78

Figure 4-11: Electrical resistivity and moisture content of EP soil: a relationship. 81

Figure 4-12: Relationship between resistivity and unit weight of compacted El Paso soil..... 84

Figure 4-13: Relationship between electrical resistivity and void ratio. 87

Figure 4-14: Relationship between electrical resistivity and degree of saturation. 88

Figure 5-1: Model development steps..... 89

Figure 5-2: Relationship between soil phase (geoengineer.org)..... 91

Figure 5-3: Response vs Predictor Plots. 93

Figure 5-4: The correlation among the predictor variables (R, MC, SC, DUW) 94

Figure 5-5: The correlation among the predictor variables (R, FC, SC, DUW)..... 95

Figure 5-6: Residuals vs Fitted Values Plot for the Preliminary Model..... 99

Figure 5-7: Normal Probability Plot for the Final Model..... 99

Figure 5-8: Outlier test by using DFFITS..... 101

Figure 5-9: Outlier test by using Cook's Distance..... 101

Figure 5-10: Outlier test by using DFBETAS 102

Figure 5-11: Validation of Final Prediction Model 105

Figure 5-12: Resistivity line data for field validation. 107

List of Tables

Table 2-1: Mineral Clay, Type of Layer, and Typical Chemical Formula (Yang, 2002)..... 21

Table 2-2: Moisture Content's Effect on Soil Resistivity (Pozdnyakov et al. (2006)) 23

Table 2-3: Effect of Temperature on Soil Resistivity (Keller and Frischknecht (1966)) 27

Table 2-4: Different Soil Types' Resistivity Values by Kaufman and Hoekstra (2001) and Palacky (1987)..... 28

Table 2-5: Effect of Soil Resistivity and Salt Content (Wenner, 1915) 31

Table 3-1: Test numbers for Fort Worth sample 46

Table 3-2: Test numbers for El Paso: 47

Table 3-3 : Depth of samples taken for testing..... 48

Table 4-1: Atterberg Limits of EL Paso and Fort Worth samples..... 60

Table 4-2 Change in resistivity with unit weight for different sulfate content at 10% moisture content..... 72

Table 5-1: Correlation among the Predictor Variables..... 96

Table 5-2: Correlation between the Resistivity and Predictor Variable 96

Table 5-3: The parameter estimates..... 97

Table 5-4: The analysis of variance (ANOVA) summary..... 97

CHAPTER 1: INTRODUCTION

1.1 Background

Most of the states in the United States and many other nations across the world have naturally expansive soils (Chen, 1988). In North Texas, subgrade soils are particularly prevalent in Southeast Arlington, Dallas, and Fort Worth expansive soils are known to be problematic because of their excessive swell and shrinkage, low strength, and other features (Chen, 2005) Expansive soils typically experience significant volumetric changes as a result of seasonal moisture fluctuations. These volumetric movements cause subgrades to break, and when the soil absorbs water as a result, this causes the soil to swell (Nelson and Miller, 1992). Low subgrade strength and volumetric movements both impair the pavement's structural integrity and induce fractures and differential heave movements. The expense of maintaining and repairing these damaged pavements is substantial (Nelson and Miller, 1992). One way to identify anything is to: 1) pinpoint the soil formation and soil mineralogy inside the alignment; 2) pinpoint the soil and climatic characteristics; 3) evaluate the drainage features in the aligning areas; and 4) conduct a visual inspection of the site or borrow source. All of the approaches used in this work are meticulous, time-consuming, and difficult. Therefore, it is crucial to determine the amount of problematic sulfate levels in the soil quickly before applying any kind of strengthening treatment.

An investigation of a site that is not destructive is done using electrical resistivity imaging. The technique is less expensive, and it allows for quick subsurface exploration of a vast area. However, soil test borings are typically employed to explore the subsurface. Standard Penetration Tests (SPT), Cone Penetration Tests (CPT), Vane Shear Tests, Dilatometer Tests, and Pressure Meter Tests are other often used methods in geotechnical inquiry. These techniques all offer information about a spot at various subsurface depths. Additionally, resistivity The subsoil can be continuously learned about through imaging, both vertically and horizontally. The benefits of RI over traditional techniques can be summed up as follows: (1) Provide continuous images of the subsurface; (2) Has the capacity to cover a large area in a short amount of time; (3) Is less expensive; (4) Is able to identify heterogeneity and high moisture zone; and (5) Data can be processed quickly. The use of RI has considerably increased as a result of these advantages. It is one of the most practical techniques for geohazard investigations and preliminary subsurface investigation currently accessible. As a result, RI can be seen as an alternative to soil boring for

site exploration and geohazard study as well as a useful technique for determining the existence of sulfate in Texas.

1.2 Problem Statement

To reduce infrastructure damage from sulfate-induced heave, soil sulfate must be recognized and measured. Currently, laboratory experiments, in-situ tests, and geophysical surveys are used to explore the engineering characteristics and chemical characteristics of geomaterials. Using electrical resistivity imaging, sulfate content in the soil can be detected. The presence of sulfate in soil is identified using colorimetric laboratory testing. To find out these features in a controlled environment, laboratory tests are a trusted method.

For subsurface study, a variety of in-situ tests are employed; nevertheless, these techniques offer information at some site-specific sites. In order to analyze geotechnical parameters, as well as sulfate content, and offer a continuous image of the subsoil, a subsurface investigation approach is needed. A continuous profile can aid to solve the geotechnical investigation's current issue. A potential method to obtain a continuous profile of the subsurface is resistivity imaging (RI). This technique provides an easy way to pinpoint moisture heterogeneity and variance in the area under investigation (Hossain et al. 2010).

Numerous research have been done to explain how surface conductance and pore fluid conductivity relate to resistivity (Archie, 1942; Sauer et al. 1955; Waxman and Smits, 1968; Shah and Singh, 2005). However, because of the inherent complexity of the soil-water matrix and the interconnectedness of the key components, a general explanation for how electrical conduction varies with soil qualities is not yet available. Additionally, the experimental techniques used to ascertain the characteristics of pore water and surface conductance are sometimes expensive and time-consuming.

Therefore, this research focuses on establishing correlations to understand the effects of sulfate content on resistivity.

1.3 Research Objective

The goal of this study is to ascertain how the soil's soluble sulfate concentration and electrical resistivity are related. To achieve this goal, the following program was implemented:

- Determination of the type of soil according to Unified Soil Classification System (USCS).
- Determination of the variation of soil resistivity with moisture content, sulfate content, dry unit weight, degree of saturation, void ratio for both soil samples.
- Establishing a model of multiple linear regression.
- The multiple linear regression model's validation.

1.4 Thesis Organization

This thesis consists of five chapters: Chapter 1: Introduction, Chapter 2: Literature Review of Sulfates in Soil and Electrical resistivity Imaging, Chapter 3: Methodology, Chapter 4: Results and Discussion, Chapter 5: Statistical Analysis, Chapter 6: Conclusions and Recommendations

Chapter 1 provides the introduction to the sulfate study, the electrical resistivity method the research objectives, and thesis organization.

Chapter 2 provides a thorough summary of research that includes: The causes of sulfates in soils, the mechanics of heaving, case studies on sulfate-induced heave, and a comparison of sulfate testing techniques are all covered in this article. A brief history of the electrical resistivity system and procedures is covered after the study of sulfate heave. Both the text of the chapter and the References section at the end of the paper contain a list of all the sources consulted in its creation.

Chapter 3 presents the soil selection and sampling, different methodologies that were followed to test the soil properties and the test methods that were considered for the sulfate testing, the procedures and equipment associated with those methods.

Chapter 4 provides results and discussions of conducted tests.

Chapter 5 provides discussion how data for both sandy and clayey soils were used to create multiple linear regression models. The laboratory and field results were also used to validate the models.

Chapter 6 provides an overview of test outcomes. On the above subjects, this chapter also provides conclusions and links. Finally, this chapter offers recommendations for additional testing and analysis as well as implications for more recent investigations.

Following chapter 6, all references used for this study are provided.

CHAPTER 2: LITERATURE REVIEW

2.1 Introduction

This chapter aims to be a thorough compilation of the mechanisms underlying electrical resistivity imaging, the mechanisms underlying problems connected to sulfate heave, and some case studies of concerns caused by sulfate heave in the state of Texas. The University of Texas at Arlington Library's traditional library resources, databases, electronic search engines, and a variety of reports and technical papers were used to compile the literature review presented in this chapter. The introduction to sulfate heave, documentation of sulfate manifestations in soils, and then a discussion of soil resistance makes up the structure of the literature review.

2.2 Sulfate Bearing Soil

There are sulfate-bearing soils in many parts of the US, but they are most common in the west and southwest. Texas, Nevada, Louisiana, Kansas, Colorado, and Oklahoma are among these states (Solanki et al. 2010). According to studies, gypsum is the most prevalent sulfate mineral in soils in the Dallas area, and particular geologic formations have large concentrations of sulfates. Gypsum (CaSO4.2H2O), which has a comparatively low solubility (2.6 gm/L) level when compared to both sodium sulfate Na2SO4 (408 gm/L) and magnesium sulfate or MgSO4 (260 gm/L), is the most prevalent sulfate mineral found in soils. In order to avoid infrastructure damage from sulfate-induced heave, it is crucial to identify and measure sulfate-bearing soils in these areas. As more and more design experts become aware of the consequences of sulfate associated heave on civil engineering projects, sulfate related heave and failures have become more well-known over time. The Eagle Ford formation in the DFW region was linked to one of the worst instances of sulfate-induced heave, with sulfate concentrations ranging from 4,000 ppm to 27,800 ppm (Chen et al., 2005).

Sulfate-induced heave, also known as chemical swelling, is a chronic condition that frequently gets worse with time (Hunter 1988). In contrast to physical heaving, chemical heaving frequently has a steady or rising rate over time (Ferris et al. 1991). The Eagle Ford formation, which has previously been proven to be extremely problematic for sulfate-induced heave, is highlighted in Figure 2-1 on the following page, which also shows specific counties in the state of

Texas with sulfate-bearing soils (Harris et al. 2004; Chen et al. 2005).

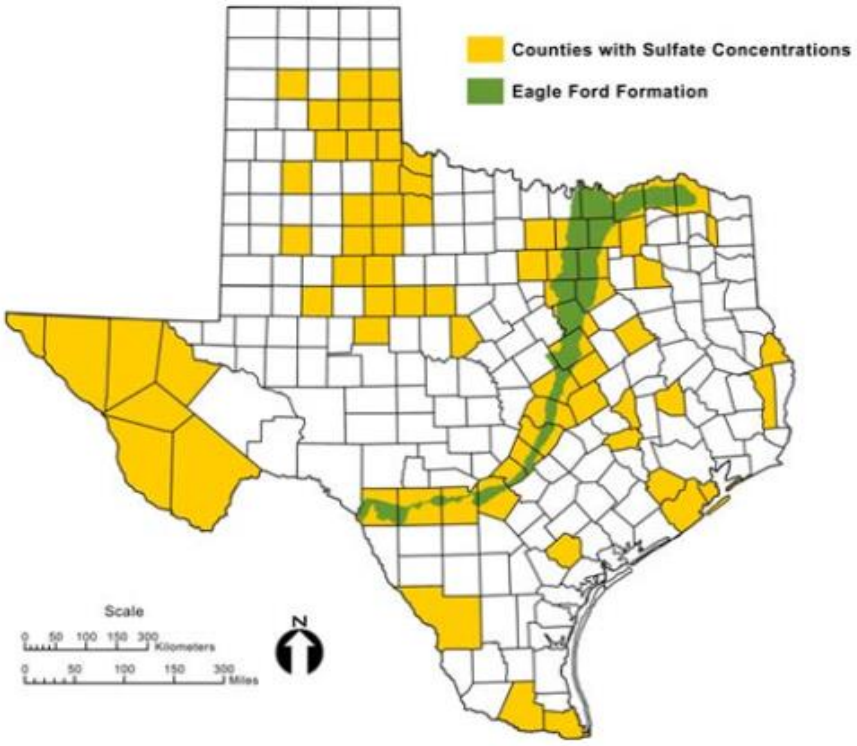

Figure 2-1: Texas Counties with measurable sulfate concentrations (>100 ppm). (Harris et al. 2004; Chen et al. 2005)

2.3 Form of Sulfate present in Soil

There are many different sulfate compounds in nature and soil, and they can appear as a solid, liquid, or vapor (Chikyala 2007). Sulfates can be found in solid forms in soils and rocks, while they can also be found in liquid forms in air and water (Hawkins et al 1998). In soils, sulfates can appear in two different ways. Primary sulfate sources and secondary sulfate sources are the two types. While secondary sources are the byproducts of other chemical reactions, including oxidation, or from engineering methods, primary sources of sulfate derive from chemicals that exist or are created naturally. The sections below describe both main and secondary sulfate sources because they can both cause sulfate heave.

2.3.1 Primary Sources of Sulfate

The majority of sulfate minerals are formed and deposited by salt water evaporation and salt precipitation (Zanbeck et al. 1986). This process often results in the formation of anhydrite (CaSO4), gypsum or calcium sulfate dihydrate (CaSO4.2H2O), halite (NaCl), and dolomite (CaMg(CO3)2) (Zanbeck et al. 1986). Both dolomite, a carbonate mineral, and halite, which is more frequently referred to as sea salt, are not sulfate minerals. In order to make the conversation thorough, these minerals were included. More frequently encountered in the upper crust, evaporation minerals appear as evaporate, clay, or fine-grained sediment deposits (Zanbeck et al. 1986). Because clay or fine-grained sedimentary layers make up the majority of Texas soils, gypsum is the most prevalent primary sulfate source in Texas soil. Gypsum can also be created artificially by the breakdown of anhydrite into an aqueous solution, which subsequently recrystallizes to form gypsum, in addition to being created naturally through the evaporation and precipitation mechanism previously mentioned (Indiana Geological Survey).

Thenordite or sodium sulfate Na2SO4, and Epsomite, or magnesium sulfate, are two additional significant sources of sulfates in soil aside from gypsum (MgSO4.7H2O). More arid places are more likely to experience sodium and magnesium sulfate manifestations (Hilgard 1906; FAO 2001;12 Bing et al. 2007).

2.3.2 Secondary Source of Sulfate

Secondary sources of sulfate can take many different shapes. One secondary source of sulfates in soils comes from the decomposition of pyrites.

This is an example of sulfate transportation through ground water flows (Dermatas, 1995; Natarajan 2004). Additionally, water sources used in construction may include soluble sulfates. For instance, Bush Road in Georgia was the subject of a forensic study by Rollings et al. in 1999. Distress cracks and bumps from soil heave were found five months after construction. The research came to the conclusion that Ettringite development in the subgrade material was what caused the breakdown. Initial geotechnical testing, however, found no sulfates in the subgrade soil, despite the fact that the subgrade soil had been cemented. At the conclusion of the study, it was found that sulfates were present in water from a nearby well that was used for mixing concrete and field

compaction, and that the introduction of this sulfate water to the subgrade soil in combination with the cement stabilization caused sulfate heave.

Similar to the Yongam Dam in China, which was also contaminated by sulfate-bearing building water that eventually caused Thaumasite to develop and the concrete used to build the dam to degrade (Mingyu et al. 2006).

2.4 Mechanisms for Sulfate Heaving

Portland cement concrete was first subject to sulfate assault in the early 19th century (ACI1982; DePuy 1994). The creation of Ettringite and Thaumasite minerals from calcium-rich cement, sulfate, and free alumina was established at that time (ACI 1982). Cohen also provided an explanation for how ettringite forms and then grows in concrete (1983). Cohen identified crystal growth and hydration as the two distinct growth mechanisms for ettringite and thaumasite. The same two expansion processes were also established in soil (Dermatas 1995). Due to Ettringite's creation and/or directed crystal development, the first mechanism promotes expansion (Ogawa and Roy, 1982). The second is a full solution mechanism in which Ettringite's swelling as a result of hydration is related to expansion (Mehta 1973; Mehta and Wang 1982).

2.4.1 Heaving caused by Crystal Growth

According to crystal growth theory, Ettringite nucleation sites can become concentrated with aluminum, calcium, and sulfates, which can then combine to produce more Ettringite, basically adding to the Ettringite molecule's internal lattice structure (Ogawa and Roy 1982). Theoretically, this crystal formation takes place during the early phases of cement hydration, and as water is added to the solution, the crystals take on their characteristic needle shape. As the crystals grow, they start to interact with one another, applying pressure on one another and expanding the system as a whole. The strains and pressures caused by the pressure from the crystal development are then applied to the nearby soil. Heave happens when the load generated by crystal growth surpasses the capacity of the restraining medium. Ettringite crystallization prefers high pH ranges. Alkaline earth metals like calcium and alumina dissolve more easily as a solution grows more basic. These components dissolve, which triggers the reaction and produces Ettringite. Compared to concrete, soil is more malleable and can accommodate some Ettringite development. However, as the

reaction progresses, the soil eventually loses its ability to withstand the stresses and pressures caused by the development of the Ettringite crystals and heaves, shifting the stress to the next line of least resistance.

2.4.2 Heaving caused by Hydration

Mehta argued that swelling could occur from dehydration (1973). According to the notion, a comprehensive solution process governs the creation of ettringite. The rate of hydration of aluminum lowers noticeably in the presence of saturated calcium hydroxide $Ca(OH)_2$, resulting in the formation of colloidal and gel-like crystals in Ettringite. The resulting colloidal crystal gels are hydroscopic in nature and can adsorb substantial amounts of water molecules because of their vast surface area and net negative charge. The gel expands as more water molecules are taken up by the system, putting pressure and strain on the medium around it. According to Mehta and Wang (1982), the size of the crystals and the amount of water adsorption both directly affect how much the Ettringite gel expands. It was discovered that coarser colloidal crystal gels expanded more than finer colloidal crystal gels. The amount of hydroxyl is a component that affects the type of crystals. While low hydroxyl levels produce rod-like crystals that expand significantly less, high hydroxyl levels produce colloidal crystal gels.

2.5 Sulfate Level

Establishing problematic threshold levels for sulfates in soils is a challenging subject. In some circumstances, these levels are stated to be between 1,500 and 5,000 parts per million (ppm), but in other cases, threshold levels of 10,000 ppm are reported (Harris et al 2004; Puppala et al. 2005; Adams et al. 2008). Unfortunately, these threshold levels are heavily influenced by environmental factors, stabilizing methods, and soil characteristics as plasticity, density, and void ratio (Puppala 2005). Setting threshold levels "across the board" is therefore quite difficult (Adams et al. 2008). Although this will only partially address the issues with sulfate heave thresholds, research is being done to create sulfate threshold values depending on mineralogy and geological depositional circumstances (Adams et al. 2008).

2.6 Heave Cases in Texas

Sulfate-induced heave has been described in numerous case studies from the United States, the United Kingdom, and China (Hawkins 1987; Little 1989; Wimsatt 1999; Chen et al., 2005; Mingyu 2006; Rollings et al. 2006; Zhiming, 2008; Adams 2008; Bagley et al. 2009; Puppala et al. 2010). These case studies were mostly carried out in order to identify the causes of infrastructure failures, which led to the need for them. The infrastructure failures in the examples discussed in the following sections are primarily the result of incorrect stabilization or identification of sulfate soils and are brought on by the growth of Ettringite or Thaumasite. These investigations' specifics, the findings reached, and advancements in the field of sulfate heave forensics are detailed.

2.6.1 Forensic Investigation of Premature Pavement Failure Resulting from Heave Caused by Soil Sulfate, Childress, County, U.S. 287 Texas

Large fractures and swells in the pavement close to the Bear Creek Bridge on U.S. 287 in Childress County, Texas, were investigated by TXDOT's Materials and Pavement Division (Zhiming 2008). Prior to 2001, the northbound and southbound lanes had both undergone reconstructions. After the rehabilitation, the pavement near Baylor Creek had considerable fatigue cracking and swelling for around two years. At that time, repair work involving milling and inlays was started. Gypsum interbeds and the 9 in subgrade, which was treated with lime at 3% by dry weight of soil, interacted to generate the heave associated with the early collapse of this pavement. The location of the gypsum interbeds next to the pavement construction is shown in Figure 2-2 on the following page.

Subgrade soil samples were taken from the lanes that run north and south and sent for laboratory analysis. The North bound lane had significantly worse distress and heave, which was supported by sulfate testing that found soils there had sulfate concentrations above 35,000 ppm. Testing revealed that the sulfate concentration in the southbound lane was low. Following additional testing, it was shown that soils bound to the north had finer grains than soils tied to the south. This contributes to the understanding of why the heave in the northbound lane was greater.

Figure 2-2: East side of the project area has a heaved area. (Chen et al. 2005)

2.6.2 Sulfate Heave, 2.6.2 FM 201, Sabine County, Pineland, Texas

In East Texas, close to the city of Lufkin, FM 201 is situated immediately east of U.S. 96. Large "roller coaster"-style bumps in the road, which were a TXDOT project, were found to be the result of inadequate stabilization of expanding soils. The Eocene Yazoo Formation, which is clay and sandy with interbeds of silt and glauconitic sand and marine fossils, served as the foundation for the project. The drainage wash surrounding the pavement was filled with gypsum beds. Areas of substantial expansion were used to extract pavement and subgrade cores, which were then analyzed. These samples contained ettringite, and Figure 2-3 below displays some of the gypsum crystal forms identified in the drainage washes from the investigation. The top two feet of the subgrade were completely removed for this building job, and select fill stabilized with cement was used to replace it (Harris et al. 2006).

Figure 2-3**:** Gypsum crystals can be discovered in the roadside drainage wash. (Harris et al.2006)

2.6.3 Sulfate Heave on U.S. 67 in Ellis County, Texas

Sulfate-induced heave was found to be the cause of the deterioration of a pavement structure in a research done by Wimsatt 1999 in collaboration with TXDOT on U.S. 67. As a widening project for US 67, the project was started. Lime was used to stabilize the subgrade at 10% and 11% of the soil's dry weight. Following stabilization, the subgrade was sealed to cure. Construction workers discover numerous equally spaced heave ridges as depicted in Figure 2-4 when they arrive at the site the day after a significant rainstorm that occurred while the concrete was being cured. Research was initiated to determine the precise source of the distress heaves. The Eagle Ford Formation was used in a research study on distress heave, which is similar to the US 82 experiment. The only term for the gypsum is selenite. In this particular case study, it was found that ettringite was produced by the reaction of the soil's gypsum with the lime stabilization. Due to heave brought on by the growth of ettringite, the pavement structure ultimately broke before construction was complete. X-ray diffraction and SEM analysis were used to determine that the expanding mineral was Ettringite. After extensive testing in the lab, it was discovered that 67 soil samples from the United States had sulfate amounts ranging from 11,000 to 32,000 ppm. The removal of the subgrade and replacement with carefully chosen fill that didn't require stabilization turned out to be the best course of action for this project. This was chosen since there was still some gypsum in the soil that had not yet fully reacted and could lead to further expansion. One of the study's

findings was that sulfates in the field may be more precisely identified before construction using the Geologic Atlas of Texas, conductivity tests, and sulfate concentration testing.

Figure 2-4: Near Midlothian, Texas, a Heave on US 67 (Wimsatt 1999)

2.6.4 Other Case Studies in Texas

The interchange between SH 161 and SH 183 in Dallas County is one example of heave in Texas. In one case, sulfate concentrations as high as 27,000 ppm were discovered. In response to this finding, the soil was prepared for construction by mixing lime and ground granulated blast furnace slag (GGBFS). On FM 3338 in Webb County, another incident occurred in 2005. Sulfates on the order of 40,000 ppm were found in this study, and they had to be reduced by using a mixture of lime, GGBFS, and clay star product. Additionally, sulfate-related heave was observed on SH 118 in Brewster County, far West Texas, close to the city of El Paso. While cement is usually utilized to stop subgrade material erosion in Texas' more arid regions instead of lime for stabilization. In this instance, significant amounts of gypsum that had evaporated were found at the subgrade's peak. Studies are still being conducted to decide the optimum strategy for paving rehabilitation. Another instance of sulfate-related problems was seen in Culberson County in TXDOT's El Paso District on SH 54, despite suggestions like fly ash not being adopted. In this

instance, sulfate heave caused culverts to deform and head walls to crack. It was discovered that sulfate heave was caused by gypsum in the soil reacting with the cement stabilizer. The culverts had to be changed, and an untreated backfill had to be used. The USFHWA Report FHWATX-06/0-4240-4 by Harris (2006) contains all of the cases that were used in the presentation. These cases demonstrate that stabilizer interactions with gypsum are the main cause of sulfate-related heave in Texas. Additionally, while all projects in Texas experience sulfate heave, they differ in terms of project location, climate, soil type, and stabilizer type.

The Texas Department of Transportation uses a number of sulfate measuring procedures, including the conductivity test recommended by Bredenkamp and Lytton (1995), the modified Acetone Test of Bower and Huss (1948) approved by the USDA, the Barium Chloride Test, and the Colorimetry Test.

2.6.5 Conductivity Test

The procedures for doing the conductivity test are outlined below:

1. The conductivity and pH meters are calibrated in accordance with the manufacturer's recommendations. With standards that are near to those values, conductivity and pH are estimated and calibrated. For instance, because a sample high in carbonate will be basic, standardizing pH should also include a pH 10 standard..
2. A 125 ml (HDPE) Nalgene brand container containing 2.5 g of air-dried soil is being measured to the nearest 0.1 g.
3. Double-distilled water is measured at 100 g to the nearest 0.1 g.
4. Samples are put on a BurrellTM Model 75 wrist-action shaker and shaken for a minute on the highest setting.
5. After removing the samples from the shaker, the Accumet Model AR50 pH/Conductivity Meter is used to test the conductivity and pH.
6. The samples were placed on the wrist-action shaker for 10 minutes at the highest setting after 50 minutes.
7. After removing the samples from the shaker, conductivity and pH readings are made right away.
8. This technique was carried out hourly for the first eight hours.

9. Samples were shaken twice the next day—once in the morning and once in the afternoon—using the wrist action shaker's highest setting for a total of 10 minutes.
10. pH and conductivity were assessed right after shaking.
11. This process was repeated for a number of days until the conductivity was constant.

2.6.6 Acetone Test

This test, which was modified by the USDA to be a quick and affordable field method for identifying sulfates in soil, was initially a quantitative technique created by Bower and Huss (1948). (Figure 2-5). The following steps are taken when applying this technique:

1. Adding 10 g of air-dried soil to a 250 ml (HDPE) Nalgene centrifuge bottle is the first step.
2. Next, at a 1:10 soil to solvent ratio, 100 ml of double-distilled water was added to the 250 ml centrifuge bottle.
3. The Burrell Model 75 wrist-action shaker is used to thoroughly shake the material for 15 minutes.
4. The extract is filtered into 250 ml beakers using WhatmanTM #42, 5-inch diameter filter paper. With fine-grained soils, centrifugation could be required to get rid of every particle in suspension.
5. A 40 ml glass centrifuge tube is filled with approximately 5 ml of the extract.
6. Add 5 ml of acetone and stir it into the solution in the centrifuge tube. If gypsum is present, a murky suspension or a white precipitate will be seen after 5 to 10 minutes. Gypsum will be detected by this test, however it does not provide a quantitative result. Sulfate is present in the sample on the right but not in the sample on the left.

2.6.7 Barium Chloride Test

The soil testing kit includes the technique for this test, which is written in terms of the kit's equipment. The test procedure is as follows:

1. Marked amounts of Universal Extracting Solution are added to the test tube distilled water with 3 percent acetic acid and 10 percent sodium acetate.
2. One level measure of orange soil is added to the test tube.
3. After capping the test tube, it is shaken for a minute.

4. The extract solution is poured into the funnel with the filter paper in it, and the filtrate is collected.
5. Five drops of clear filtrate are added with a transfer pipette to a turbidity vial.
6. Add one drop of the 0.2 percent HCl and 5% BaCl22H2O sulfate test solution and gently stir to combine.
7. A color chart for sulfate is being drawn out in neutral lighting. The turbidity vial is placed 0.5 inches above the center black strip on the chart. The sample's turbidity is compared to a turbidity standard.
8. PPM unit is used to measure sulfate.

2.6.8 Colorimetry/Spectrophotometry

The AQUAfastTM II Colorimeter/Spectrophotometer is used in this method to measure how much light passes through the sample. The procedures outlined in the manual, with a modification for soils, are as follows:

1. A 125 ml Nalgene container is filled with 100 ml of double-distilled water and 5. g of air-dried soil.
2. The Burrell wrist-action shaker is used to vigorously shake the sample for 15 minutes.
3. After removing the sample from the shaker and filtering it through Whatman #42, 9.0 cm filter paper into a 250 ml beaker, centrifugation may be required to completely remove the fine-grained soil particles that are suspended.
4. Fill the sample vial with filtrate to the 10 ml mark, and then clean the bottle with Kimwipes or another soft job wipe.
5. The device is turned to "ON."
6. The desired technique is displayed when holding down the MODE key.
7. You press the ZERO/TEST key. The method symbol indicates zero calibration for around three seconds.
8. The vial is taken out of the sample chamber after zero calibration.
9. Without touching the sulfate tablet with hands, add it to the vial and crush it right away with the included white plastic rod.

10. The ZERO/TEST key is once more pressed. The result is displayed after around three seconds of the method sign flashing. The final reading is averaged from a minimum of three readings.

2.7 Evaluation of the Sulfate Test Procedures

The Conductivity Test is a useful method for locating potential sulfate-rich soils, although it will produce high results in a soil with other salts. This examination is quick and simple to complete in the field. It is advised to use this method as a screening tool. Perform laboratory tests to ascertain whether sulfates are the source of any elevated conductivity results if there are any.

Sulfates can be detected by the barium chloride test at low concentrations, but it is challenging to conduct in carbonate-rich soils and takes longer to complete because of filtration. Barium chloride is also extremely poisonous. As a result, it is not advised to apply this test on Texas soils given that many of the sulfate-bearing soils also include a significant amount of carbonate minerals.

Sulfates can be found using the Acetone Test. Because the sample must be filtered before analysis, this test's analysis time is a problem. To identify various sulfate concentrations, the dilution ratio can be changed. Although this test is non-quantitative, it will find real sulfates.

A laboratory or field office could use the colorimetric/spectrophotometric test. It can provide lab test accuracy that is comparable to IC. Test Method Tex-620-J could be supplemented or replaced by this approach, according to results from colorimetric/spectrophotometric testing. This test can be completed in about 25 to 30 minutes, and the equipment required costs around $400.

The researcher decides to utilize the Colorimetric Test to measure the soil's sulfate content based on the recommendations made above by the Texas Transportation Institute.

2.8 Soil Resistivity

The ability of soil to oppose, resist, and reduce the flow of electrical current through it is measured as soil resistivity. Due to variations in composition, moisture content, and temperature, it varies over both its depth and breadth. The resistivity decreases to a specific minimum value with increased wetness. Conduction in coarse-grained soil is primarily electrolytic and is

influenced by the linked pore space, granular skeleton, electrolyte conductivity, and saturation level (Santamarina et al. 2001).

Numerous conductors and resistors have a uniform cross section and an even flow of electricity. Thus, the more precise but more popular electrical resistivity formula or equation can be developed:

$$\rho = \frac{RA}{L}$$

Where:

ρ is the resistivity of the material in ohm metres, Ω·m

R is the material's uniform specimen's electrical resistance, expressed in ohms.

L is the material's length in meters, m

A is the specimen's cross-sectional area, measured in square meters, m2., m^2

Electrical resistivity is a characteristic parameter of soils that is strongly influenced by the microstructure of the soil, including its porosity, electrical conductivity of the pore fluid, saturation level, solid particle size and distribution, ions concentration, and distribution in the pore fluid of various soil layers, among other factors. Geotechnical researchers have recently expressed worry about the use of electrical resistivity in geotechnical engineering. Its value has been linked to a number of strata conditions, such as the depth of an aquifer or bedrock, the injection of salt or pollutants close to the surface of the ground, an underwater line, and the thickness of particular layers, with success in ground survey and mapping.

2.9 Formation of Clay Minerals

There are three or four major categories of clays: kaolinite, montmorillonite-smectite, illite, and chlorite, depending on the academic source. Chlorites are occasionally categorized as a different group within the phyllosilicates, and are not necessarily thought of as clay. These categories contain about 30 different types of "pure" clays, however the majority of "natural" clay deposits are a combination of these various types and other weathering minerals.

2.9.1 Kaolinite

The main mineral in kaolin clays is kaolinite. It is a 1:1 clay mineral, with the silicate and aluminate layers of the basic unit closely bound to one another in two dimensions.

Tetrahedral octahedral (TO) layered structure with close packing is seen throughout the entire material. Kaolinite does not shrink when dry or swell when wet as a result of its tight packing, which makes it look like the pages of a closed book.

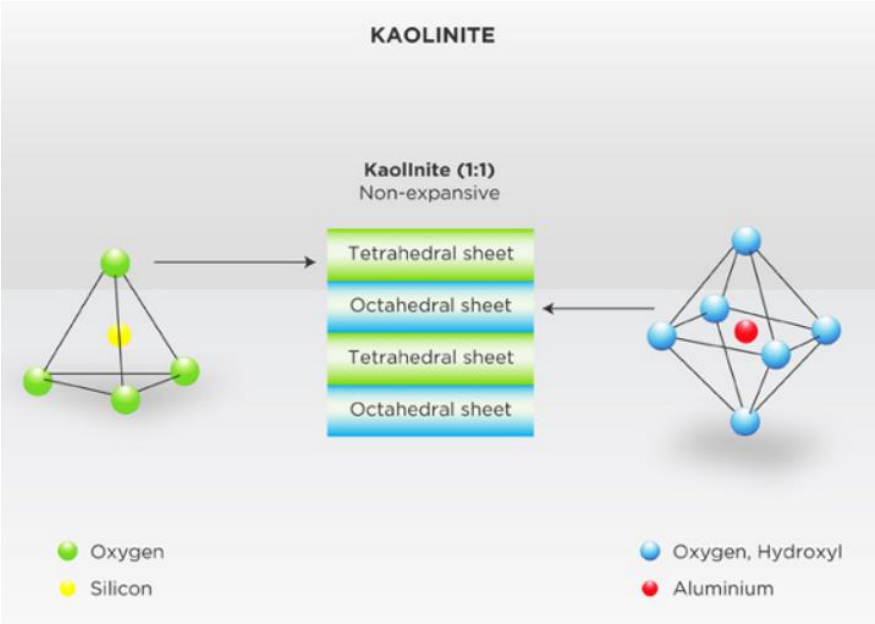

Figure 2-5: Kaolinite formation diagram (© 2007-2010 The University of Waikato |www.sciencelearn.org.nz)

2.9.2 Smectite

Bentonite clays include smectite minerals. These minerals have a tetrahedral/octahedral/tetrahedral (TOT) sheet structure as opposed to kaolinite's TO sheet arrangement. As a result, there is space between each TOT unit in a TOT TOT TOT TOT layout. Because water may get between the layers, bentonite clays expand when wet and contract when dry.

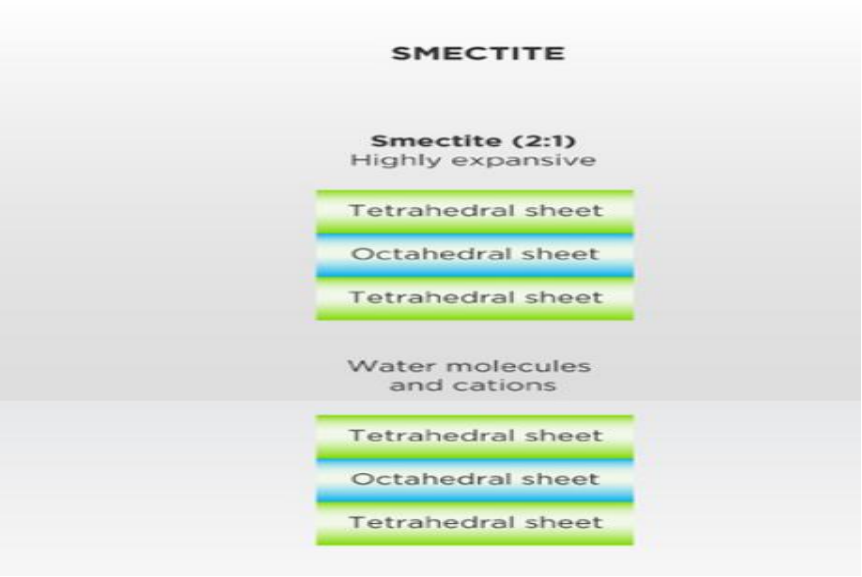

Figure 2-6 : Smectite formation diagram (© 2007-2010 The University of Waikato |www.sciencelearn.org.nz)

2.9.3 Illite

Similar to montromorillonite, illite is made up of two sheets of silica and one sheet of alumina. The structure is hence known as a 2:1 mineral. Potassium holds the fundamental layers together in illite. The link between the layers is quite strong thanks to the potassium present. Figure 2-7 shows a schematic of the Illite's structure.

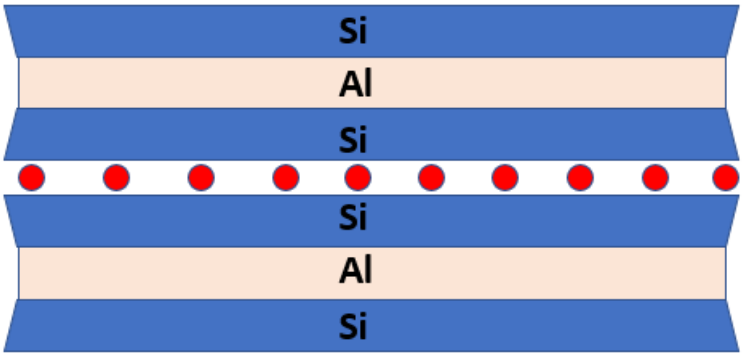

Figure 2-7: Formation of Illite

Table 2.1 presents the clay material, layer type, and typical chemical formula.

Table 2-1: Mineral Clay, Type of Layer, and Typical Chemical Formula (Yang, 2002)

Clay Mineral	Layer type	Typical Chemical Formula
Kaolinite	1:1	$[Si_4]\ Al_4O_{10}(OH)_8.nH_2O$ (n= 0 or 4)
Smectite	2:1	$M_x\ [Si_8]Al_{3.2}Fe_{0.2}Mg_{0.6}O_{20}(OH)_4$
Illite	2:1	$M_x\ [Si_{6.8}Al_{1.2}]Al_3Fe_{0.25}Mg_{0.75}O_{20}(OH)_4$

2.10 The Soil Resistivity Mixing Model

Equations known as electrical mixing models link the bulk resistivity of the conducting medium to the resistivity of the various porous media components. According to Archie (1942), the bulk electrical resistivity of a saturated soil is empirically connected to the electrical resistivity of its pore fluid, w, and the geometry of the soil's pore spaces, among many other things. Later, the Archie model was expanded to include partially saturated porous medium (Keller and Frischknecht, 1966), and is represented as follows:

$$\rho = a\rho_w n^{-m} S^{-p}$$

where S is the degree of saturation, n is the soil's porosity, an is the compaction constant, m is the cementation exponent, and p is the saturation exponent. Pore tortuosity and the interconnectedness of the pore network are both measured by the exponent m. (Dullien, 1992). The literary constant an is based on empirical observations rather than any theoretical underpinnings. The interstitial water in the soil matrix is reflected by the saturation exponent, p. Regression analyses are frequently used to determine the a, m, and p values.

The Archie model is relevant as long as the pore fluid resistivity is low and there are only trace amounts of conducting clay minerals in the soil, despite the fact that it oversimplifies the parameters affecting electrical measurements in soils. For circumstances where surface conductance is not trivial, Waxman and Smits (1968) developed a model based on two electrical resistors connected in parallel, and it is given as:

$$\rho = \frac{a\rho_w n^{-m} S^{1-p}}{S + \rho_w BQ}$$

where Q is the clay's cation exchange capacity per unit pore volume, and B is the analogous conductance of counter ions on the diffuse double layer, or ions with the opposite charge to that of the surface. Typically, Waxman and Thomas' empirical data is used to calculate the B term (1974). The BQ word, which is expressed in Siemens per meter, refers to the surface conductivity along the double layer.

Mixing models are typically presented in geophysics literature as a ratio of the pore fluid resistivity to the bulk soil resistivity. The formation factor, abbreviated F, is a ratio that is presented as

$$F = \frac{\rho}{\rho_w}$$

A generalized version of Archie's law for fine-grained soil was described by Shah and Singh (2005). Shah and Singh (2005) claim that the cementation component of Archie's law takes surface conductivity into account. Therefore, it was not required to include the soil matrix's conductivity while describing Archie's law for fine-grained soil. In terms of conductivity, Shah and Singh (2005) hypothesized a link as follows:

$$\sigma_b = c * \sigma_w * \theta^m$$

where = volumetric moisture content, _w = pore-water conductivity, and b = bulk conductivity of the soil. For the soil with a clay component less than 5%, the observed values of c and m were 1.45 and 1.25, respectively.

When creating mixing models, media with a predominance of nonconductive soil particles, such as clean sands and gravels, are best suited for the application of the formation factor (Archie, 1942). This is due to the implicit prediction made by the formation factor that the resistivity of a soil-water matrix is inversely linked to the amount of pore water in the matrix (Mitchell, 1993).

2.11 Factors affecting Soil Resistivity

Depending on the level of compaction, moisture content, temperature, and the presence of conducting salts, soil resistivity for a certain type of soil can vary significantly.

2.11.1 Effect of Moisture of Soil

For good soil conductivity, moisture is a necessity. Because the moisture content of the soil might change with the season, it is desirable to place the electrodes at a depth where moisture will be present all year long to prevent too much variation in soil resistivity over the yearly weather cycle.

Table 2-2: Moisture Content's Effect on Soil Resistivity (Pozdnyakov et al. (2006))

Moisture Content (%)	Resistivity (in Ohm-meter)		
	Topsoil	Sandy Loam	Red Clay
2	***	1850	***
4	***	600	***
6	1350	380	***
8	900	280	***
10	600	220	***
12	360	170	1800
14	250	140	550
16	200	120	200
18	150	100	140
20	120	90	100
22	100	80	90
24	100	70	80

Pozdnyakov et al. (2006) described how soil and water interacted when electrical potential was applied. Pozdnyakov et al. (2006) found that water has a significant impact on the mobility of electrical charge in soil. The surface of soil particles is covered with diffuse double layers of electrical charges now present. Adsorbed charges in the solution were released as water was added,

bringing it from a dry state in the atmosphere to a saturated state. As a result, the presence of water increases the mobility of electrical charges.

2.11.2 Effect of Unit Weight

The study of Abu-Hassanein et al. can explain how soil resistivity varies with unit weight (1996). The degree of saturation was correlated with an increase in moist unit weight. At high saturation levels, the bridging between the particles becomes more evident. Additionally, clay clod remolding, eliminating interclod voids, and particle reorientation were linked to an increase in wet unit weight (Abu-Hassanein et al. 1996). As a result, soil resistivity reduces as moist unit weight increases. Mitchell and Soga (2005) claim that as clay soil is remolded, the size of the big pores decreases, and the flocculated open fabric breaks down. The outcome was a substantial unit weight reduction in the conduction channel in the soil.

2.11.3 Effect of Degree of Saturation

The degree of saturation is a single geotechnical metric that may be used to combine the water content and dry unit weight. As the water content or dry unit weight rises, the saturation level rises (Abu-Hassanein et al. 1996). Clay clods, intercloud macrovoids, and clay particle orientation all alter as the saturation level is increased (Lambe 1958). As a result, soil resistivity reduced as saturation level increased.

Similar findings were made in a study by Kibria and Hossain (2012) that examined the impact of electrical resistivity's degree of saturation. The results are depicted in figure 2-8:

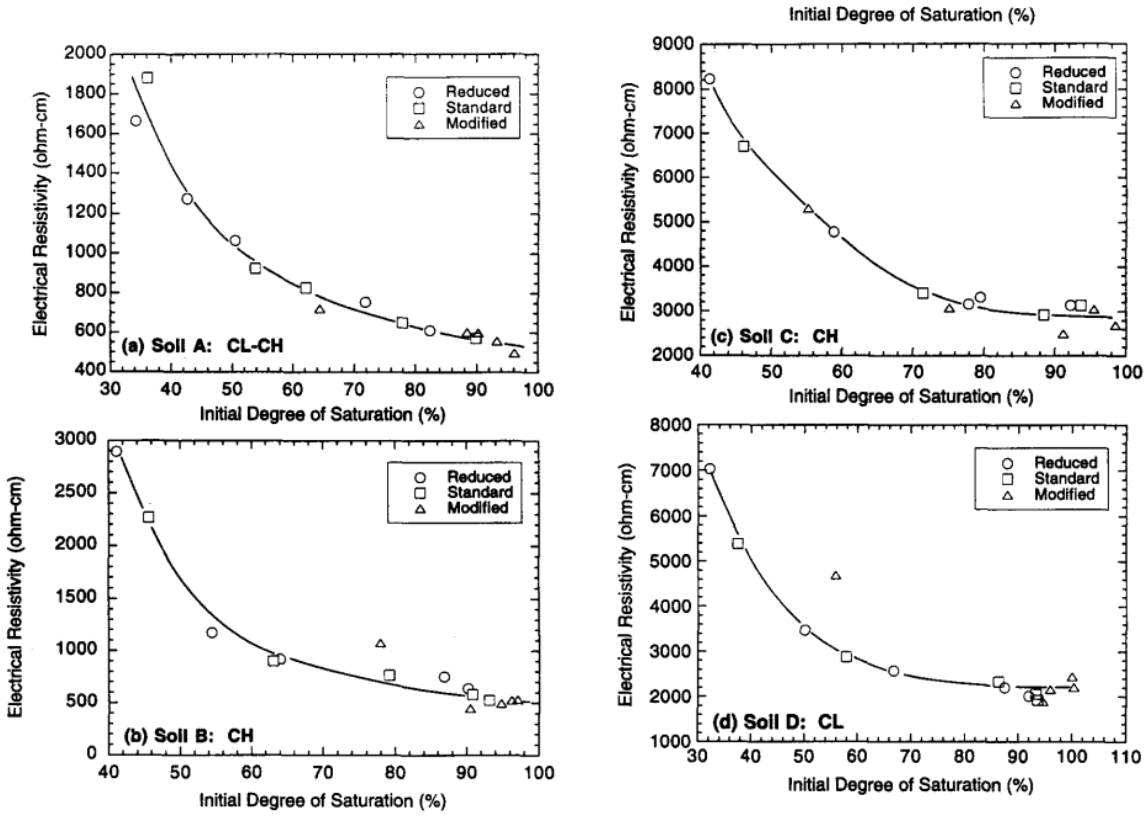

Figure 2-8: Changes in soil resistivity with soil saturation levels in several soil samples. (Abu-Hassanein et al. 1996).

2.11.4 Relationship of Cation Exchange Capacity with Specific Surface Area

In medium and fine-grained soil, adsorbed cations contribute significantly to electrical resistance. The study establishes a link between soil properties such as adsorbed ions, pore water conductivity, and surface charge and their cation exchange capacity (CEC) (Friedman, 2005; Tabbagh and Cozenza, 2007; Schwartz et al. 2008)

A study on the electrical resistivity responses of high plastic clays at various moisture levels and unit weights was published by Kibria and Hossain in 2012. The authors claimed that in fine-grained soil, particular surface area had a significant impact on electrical conductivity. The study found that soils with a high specific surface area needed a lot of moisture to generate a water film. As a result, testing carried out at low moisture levels revealed that the soils with a high SSA had a high electrical resistance (below saturation).

2.11.5 Temperature of soil

The electrical resistance of soil is influenced by temperature as well. The electrical resistance of soil lowers as temperature rises because it makes the ions more mobile. According to Keller and Frischknecht (1966), a standard electrical resistivity measured at 18°C (18) by the same method can be used to determine the electrical resistivity of soil PT at a temperature of eC:

$$\rho_T = \frac{\rho_{18}}{1 + \alpha(T - 18)}$$

Where, α= an empirical parameter that is approximately $0.025°C^{-1}$

Below is the table of change in resistivity with temperature.

Table 2-3: Effect of Temperature on Soil Resistivity (Keller and Frischknecht (1966))

Temperature (°C)	Resistivity (in ohmmeter)
-5	700
0	300
10	80
20	70
30	60
40	50
50	40

2.11.6 Soil Types and Resistivity Values

There have been numerous attempts to determine the kind of soil based on the magnitude of the resistivity. Piegari and Di Maio (2013) used a combination of Archie (1942) and Van Gnuchten (1980) models on a number of lab and field tests to arrive at an empirical link between soil resistivity and suction. Electrical resistivity can be utilized to explain the structure of the tilled soil, claim field research by Besson et al. (2004). In addition, Seladji et al. (2010) performed a series of lab tests to investigate how soil compaction affects electrical resistivity.

Additionally, there have been numerous attempts to link field resistivity measurements to different soil types or classes of soil. The more important research were carried out by Palacky and Kaufman (2001) and Kaufman and Hoekstra (2001). (1987). Table 2.4 provides a summary of their findings.

Table 2-4: Different Soil Types' Resistivity Values by Kaufman and Hoekstra (2001) and Palacky (1987)

Soil Type	Soil Classification	Resistivity (Ω.cm) (Kaufman and Hoekstra, 2001)	Resistivity (Ω.cm) (Palacky, 1987)
CLAYS	CH	1,000-5,000	300-10,000
	CL	2,400-6,000	-
	OL	2,650-7,500	-
SILTS	ML	2,650-7,250	-
	SC	4,650-17,800	-
	MH	7,150-24,000	-
SAND	SM	9,600-45,250	47,500-1000,000
GRAVEL	GW	56,300-91,800	47,500-1,000,000
	GC	12,900-40,500	-
	GP	91,500-233,250	-

A lot of the various soil types overlap, according to Kaufman and Hoekstra (2001). Additionally, for comparable soil types, Palacky (1987) provided a different range of values. While Kaufman and Hoekstra reported substantially higher upper bound resistivity values for sand, he measured far lower lower bound resistivity values for clays (2001). Palacky asserts that gravels can have resistivities that are far higher than those reported by Kaufman and Hoekstra (2001). The challenge of determining soil type and geotechnical qualities from electrical resistivity data collected in the field is somewhat illustrated by these two articles.

2.11.7 Current Frequency

In studies using experimental methods, it has been discovered that the electrical resistivity and dielectric constant of soil are both affected by the frequency range at which they are measured (Rinaldi and Cuestas, 2002; Arulanandan, 1991; Mitchell and Arulanandan, 1968). For clayey soils, fluctuations in the electric field lead to the release of ions from the double layer at high frequencies, increasing the soil's overall conductivity. Double layer relaxation is the name given to this phenomena, which has been seen to happen at frequencies higher than 100 kHz (Rinaldi

and Cuestas, 2002). Most soils' total conductivity and ohmic conductivity are equal at frequencies lower than 100 kHz (Rinaldi and Cuestas, 2002).

2.11.8 Pore fluid composition

The mobility of the ions in the fluid filling the pores has an impact on the electrical conductivity. The content and viscosity of the water affect conductivity (Scollar et al., 1990). Knowing the concentration of dissolved ions is necessary for resistivity experiments that estimate the water content. Early research attempting to calculate soil water content encountered the challenge of estimating soil salinity fluctuation (Rhoades et al., 1977). The possible routes of conduction are determined by the amount of water in the soil since salts must be in an ionized condition to conduct the current. Electrical resistivity and salinity were found to be closely correlated for soil water contents ranging from saturation to -3 kPa water potential by Shea and Luthin (1961). Thus, measurements must be taken at the same water content in order to estimate the soil salinity using electrical resistance. Since saturation is regarded as a standardized condition, the soil salinity is typically measured at this point. The volumetric water content was calculated by Kalinski and Kelly (1993) using Eq. (12) and pore solution resistivities (pw) of 1, 2, and 3 mmho/cm. They discovered that the electrical resistance reduces as the water conductivity increases for a fixed water content (Fig. 3). Additionally, due to variations in ion mobility, the various ions (H+, OH-, SO4 2-, Na+, and Cl-) present in the solution do not effect the conductivity in the same way. This explains why soil solutions with the same concentration and various ionic compositions may exhibit various electrical conductivities. This leads to a wide variety of potential electrical conductivities due to changes in concentration and ionic composition in different soil regions. Bernstone et al. (1998) also used this feature to outline the landfill structure. Several researchers have studied salt water intrusion into coastal areas using the stark resistivity contrast between salt water- and fresh water-saturated zones (Nowroozi et al., 1999; Acworth, 1999; Yaramanci, 2000). According to Van Dam and Meulenkamp (1967), fresh, brackish, and

salinwater are each represented by soil resistivity values of 40, 12 and 3 m, respectively.

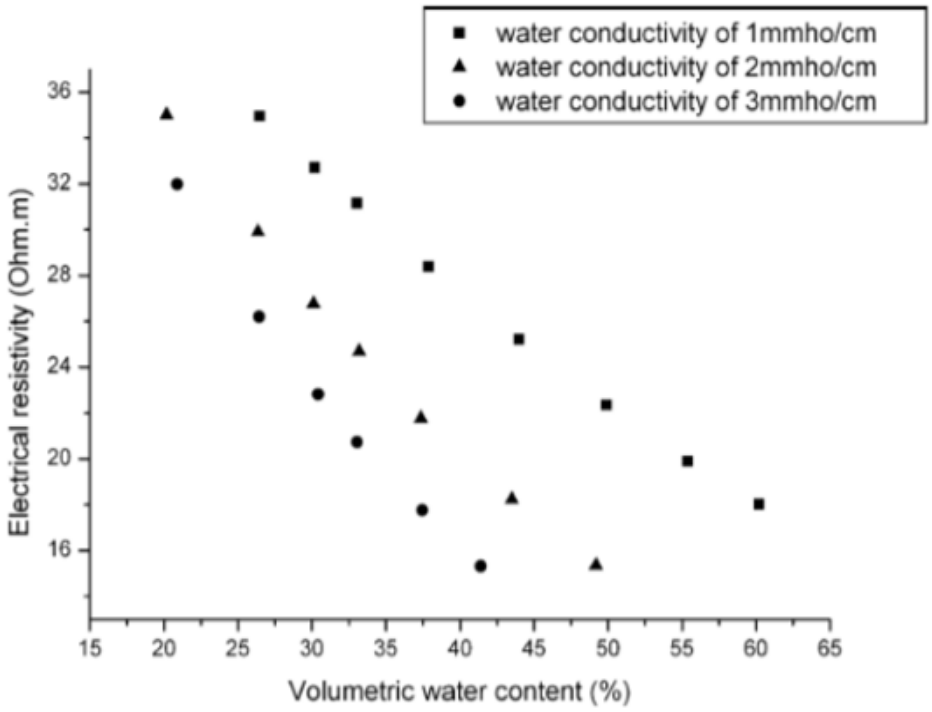

Figure 2-9: Relationships between pore water conductivity and volumetric water content at different values (Kalinski and Kelly, 1993)

2.11.9 Presence of Salts

For reducing resistivity, conducting salts may be introduced externally or found naturally in the soil. In general, soil additives consist of chlorides, nitrates, and sulfates of sodium, potassium, magnesium, or calcium. However, adding these salts might have corrosive effects that are sometimes unfavorable for the environment. Particularly, calcium sulfate in the soil is harmful to concrete foundations, hence its usage for improving electrode quality should be restricted to electrodes that are located far from such foundations. Additionally, they have a tendency to stray away from the area around the electrode with time. Additionally, in order to lower the resistivity, these additional salts must first dissolve in the soil's moisture, therefore it should be possible to supply water to the area around the electrode to speed up this process, especially in dry areas..

Due to the molecular makeup of these soils' low retentive abilities, saturation causes the essential ions to be washed away. The essential charge to convey current is provided by dissolved salts from a vast range of widely used, well-known substances like sodium chloride, copper sulfate, and sodium carbonate (in Table 2-5) Report No. 258, published in the Bulletin of the Bureau of Standards, Vol. 12, No. 3, October 11, 1915, by F. Wenner, is titled "A Method of Measuring Earth Resistivity."

Table 2-5: Effect of Soil Resistivity and Salt Content (Wenner, 1915)

For sandy loam, 15.0% moisture	
Salt content	Resistivity, Ohm-m
No salt added	107
1.0% salt added	4.6
20.0% salt added	1

2.11.10 Sulphate Content of Pore Water

Significant differences in sulphate contents were detected between the samples, per the IC of extracted pore water. As a result, at various saturation levels, the pore water's sulphate ions were associated with resistivity. According to Figure 2-10, a rise in sulfate ions causes a marked decline in resistivity. For a rise in sulphate concentrations from 88.5 to 878.7 mg/L at 25% saturation, resistance decreased from 435 to 32 Ohm-m. High sulphate concentrations may result in improved ionic conduction, which would explain the observed variances.

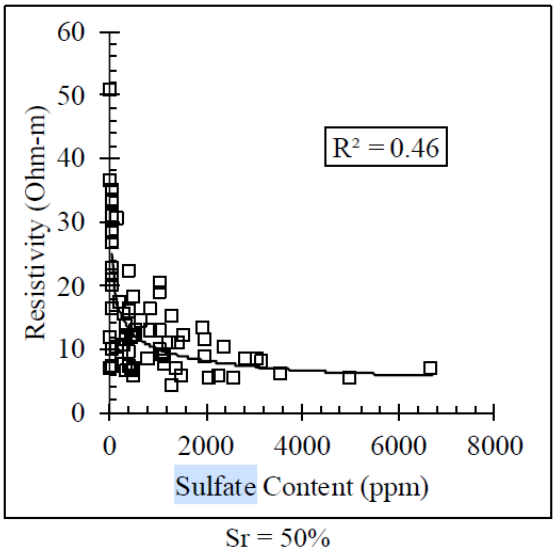

Figure 2-10: Variations in resistivity of samples when pore water contains sulfates (Akhtar et al, 2021)

2.12 Determination of Geotechnical Parameters

2.12.1 Atterberg Limits

To determine the connection between resistivity and Atterberg Limits, research has been done. With Atterberg limits, Abu Hassanein et al. (1996) studied variations in electrical resistivity. Using the Standard Proctor technique, soil samples were compacted at the ideal moisture content and dry unit weight. As shown in Figure 2-11, it was discovered that soil with higher LL and PI had lower resistivity. Figure 2-11 further demonstrates how electrical resistivity tends to decrease with an increase in LL and PI as a power function. Only samples with a high coarse proportion showed an exception. High resistivity was found in soils with a 47% coarse component. The samples' mineralogy and the pattern of declining resistivity with increasing LL and PI were both in agreement. The LL and PI of clay samples with higher smectite content are higher. These soils have increased surface conductivity and are more active. The diffuse double layer exerts significant influence on the LL and PI of non-swelling clay. Clay's surface conductivity is heavily reliant on the diffuse double layer. Electrical resistance thus depends on the soil's Atterberg limits. Eagle Ford dirt was described by Akhtar et al. in 2022.

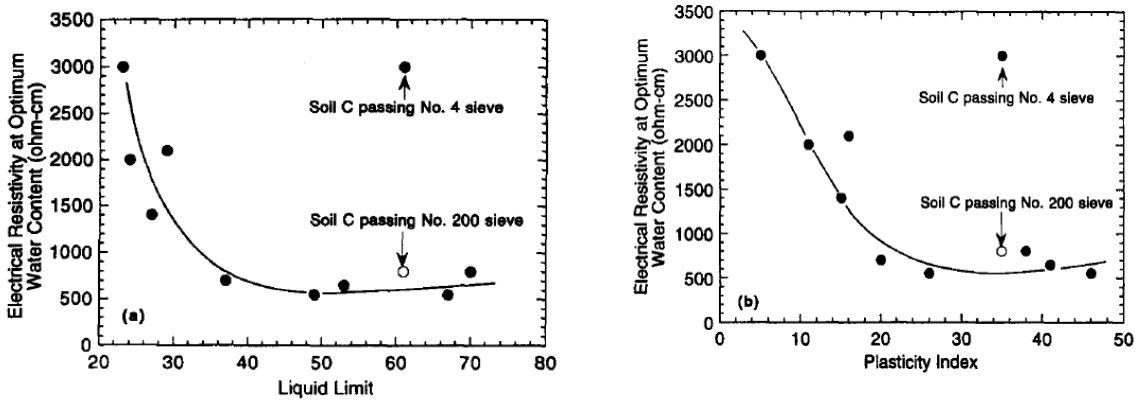

Figure 2-11: Optimal Water Content and Electrical Resistivity Relationship: Liquid limit and plasticity index are two examples. (Abu Hassanein et al., 1996)

2.12.2 Compaction Parameters

According to Rinaldi and Cuestas (2002), Abu-Hassanein et al. (1996), Kalinski and Kelly (1994), and McCarter (1984), electrical resistivity measurements have been used to assess soil compaction. For most types of soil, there is a strong link between the vacancy ratio and the bulk electrical resistivity. It was also noted that a soil's bulk electrical resistance was high when compacted dry with the ideal moisture level. However, when the soil is properly moist and compacted, the resistivity for that same soil is lower (Abu-Hassanein et al., 1996). As long as the compactive effort is consistent, electrical resistivity testing can be performed to identify whether a soil is compacted wet of optimum or wet of the line of optimums. Figure 2-12 assesses the findings from Abu-Hassanein et al. (1996) and Abu-Hassanein in more detail (1994). The relationship between numerous clays' maximum dry densities, void ratios at varying moisture levels, bulk electrical conductivities, and surface conductivities is depicted in the picture. The pattern shows that when conductivity rises, void ratio rises as well, and maximum dry density falls. In general, it has been found that the void ratio rises with increasing clay content for clays compacted to their ideal moisture content and maximum dry density. Figure 2-12 shows that surface conductivity initially grows significantly more slowly with rising void ratio and decreasing density than bulk electrical conductivity. This pattern demonstrates that the pore fluid conductivity has a greater impact on the bulk conductivity of clay soils with relatively low clay concentrations.

The surface conductivity of clay soils, in contrast, changes relatively little in relation to the compaction parameters. Figure 2-12 seems to suggest that surface conductivity is a more appropriate indication of compaction parameters than bulk conductivity due to the uncertainties involved with pore fluid conductivity measurements, such as the chemical composition and concentration of the pore fluid.

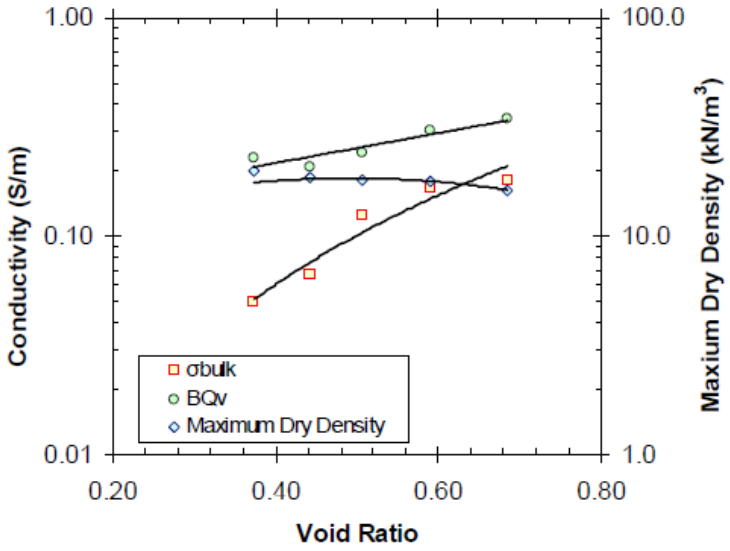

Figure 2-12: Compaction parameters and conductivity have a relationship (data from Abu-Hassanein et al., 1996; Abu-Hassanein, 1994).

Based on the Figure 2-16, the following relationships can be developed:

$$\gamma_{D(max)} = \alpha_3 (BQ_v)^{-\beta_3}$$

$$e_{opt} = \alpha_4 (BQ_v)^{\beta_4}$$

Where eopt = void ratio at optimal moisture content, 4 = 1.97, 4 = 1.01; D(max) = maximum dry density given in units of kN/m3, 3 = 12.3, 3 = 0.29; The unit of BQv in Equations 6 and 7 is siemens/m. And values are most likely effects of the clay mineralogy, just like the relations seen for Atterberg limits.

2.12.3 Behavior of Consolidation

McCarter and Desmazes (1997) assessed changes in electrical conductivity measurements in response to one-dimensional consolidation using a modified consolidation cell. These results imply that it is possible to evaluate the behavior of soil consolidation using electrical measures. For instance, it is discovered that electrical conductivity measurements accurately forecast the highest historical pressure.

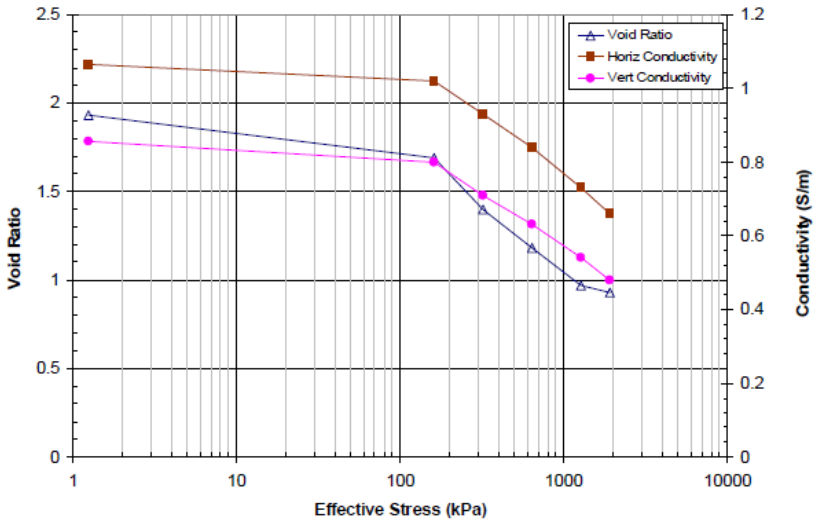

Figure 2-13: Change in Conductivity and Void Ratio in Relation to Effective Stress (after McCarter and Desmazes, 1997).

Keep in mind that the vacancy ratio and vertical conductivity have the strongest correlations. The only source of volumetric strain in a one-dimensional consolidation is vertical strain (i.e., vol = x + y + z, but x = y = 0 makes vol = z). The void ratio has altered as a result of the reduction in sample height, which denotes a change in the vertical component of the empty space. It would seem that since the vertical component of the empty space has changed, the observed vertical conductivity has also changed. Figure 2-13 depicts the relationship between the initial vertical conductivity and the initial void ratio, as well as the relationship between the change in conductivity and the modification of void ratio. According to the one-dimensional consolidation theory, the settlement can be expressed as follows in terms of conductivity:

$$S = \frac{\Delta e}{1 + e_0} H = \frac{\Delta \sigma_v}{1 + \sigma_{v0}} (\xi) H$$

where e_o stands for the initial void ratio, v for vertical conductivity change, v_o for initial conductivity, represents the factor relating conductivity and void ratio, and H for sample height. Then, for one-dimensional consolidation of normally consolidated clays, the compression index, cc, can be written asand H for sample height, and denotes the factor relating conductivity and void ratio. The compression index, cc, for clays that are typically consolidated in one dimension is then stated as

$$c_c = \frac{\xi(\Delta \sigma_v)}{\log \frac{p}{p_0}}$$

where p = consolidating pressure and p_o = initial pressure.

Measurements of horizontal conductivity are proportionally higher than those of vertical conductivity, as seen in Figure 2-13. The, thats that, thats that, thats that, s thate, the s, the s, the the (horizontal conductivity is greater than the vertical conductivity). McCarter and Desmazes (1997) found that the average kh/kv value was 1.35. An average h/v value of 1.31 is obtained from the data in Figure 2-13. Given this, electrical conductivity might be considered a good instrument for figuring out the hydraulic anisotropy of soils.

2.12.4 Hydraulic Conductivity

Many of the same variables that affect electrical conductivity also affect hydraulic conductivity. The electrical conductivity of soils is influenced by the pore space properties (such as porosity, structure, saturation, and tortuosity) and pore fluid chemistry. Hydraulic conductivity has been proven to be impacted by these parameters as well (Benson et al, 1994; Benson and Daniel, 1990; Mitchell et al., 1965). However, according to Abu-Hassanein et al. (1996), only few soils have a specific link between hydraulic conductivity and electrical conductivity. They cite research by Mazac et al. (1990), who came to the conclusion that for clean sandy soils, hydraulic conductivity and electrical conductivity have an inverse relationship. However, there is a direct correlation between hydraulic conductivity and electrical conductivity for silty and clayey soils. According to their findings, Abu-Hassanein et al. (1996) came to the conclusion that variations in

surface conductivity were the main cause of the direct correlation between hydraulic conductivity and electrical conductivity for soils. It should be emphasized, too, that the Abu-Hassanein et al. (1996) data contrasted electrical resistivity measurements made from one set of soil samples with hydraulic conductivity measurements made from another set of soil samples. This contradiction might be responsible for some of the scatter mentioned in their original text. Hydraulic conductivity and porosity were plotted by Rinaldi and Cuestas (2002), who then used a regression analysis to establish a link between the two variables. The Archie (1942) equation's formation factor was then calculated using the porosity function, and a link between electrical conductivity and that value was established. They noted that, rather than being directly correlated with electrical resistivity, hydraulic conductivity was connected to the formation factor. Figure 2-18 displays a sample of data from Abu-Hassanein (1994). The link between hydraulic conductivity and electrical conductivity is depicted in the figure. The picture also depicts the association between porosity and hydraulic conductivity. Using the Waxman and Smits (1968) equation, the porosity is estimated from the soil data corresponding to the ideal moisture content and maximum dry density and then back computed using resistivity readings. The image illustrates how hydraulic conductivity and clay porosity are closely related, and how porosity may be predicted using the proper electrical mixing model. The image also demonstrates that for compacted clays, bulk conductivity measurements rather than surface conductivity more accurately reflect a direct relationship between electrical conductivity and hydraulic conductivity.

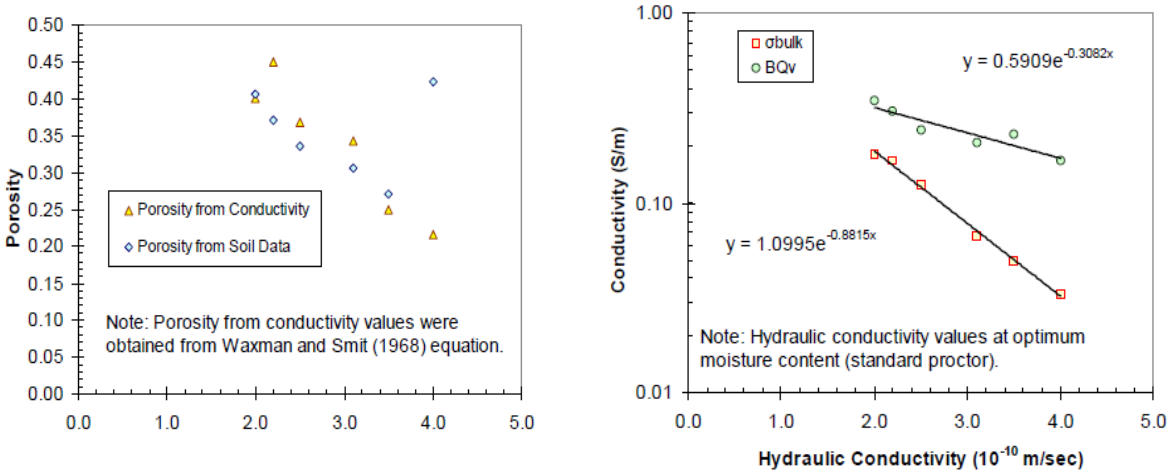

Figure 2-14: Hydraulic and Electrical Conductivity Relationship (data from Abu-Hassanein, 1994)

2.13 Electrical Resistivity Methods

Electrical resistivity, a property that determines how well a substance resists electrical current flow, quantifies this resistance. In geophysical testing, the electrical resistivity method has a long history, and Conrad Schlumberger's seminal work in France in 1912 is primarily to blame for its widespread fame. (1991 Dahlin).

At least four electrodes, including two current electrodes and two voltage potential electrodes, are needed for electrical resistivity studies. The array is the configuration of the electrodes and the order of measurements, and various arrays have been created over time. For instance, a Wenner array (Figure 2-14(a)) is used to measure the electrical resistivity. To do this, a voltage potential is created by passing an electrical current between two electrodes that are put into the ground (current electrodes and potential electrodes), and the resultant voltage potential is then measured (Herman, 2001). Several of the most common resistivity arrays are shown in Figure 2-15.

In the DC electrical resistivity method, a pair of electrodes are used to inject an electric current into the ground directly, and the resulting voltage V is then measured between a different set of electrodes. the and the the the the and, and the, and the, and the, and the,, and and, and the

time the and this was considered by 2013 (Everette). The measurement that would have been taken if the subsurface's entire surface were uniform is referred to as the apparent resistivity for each measurement (Everett, 2013). A pseudo section is a plotted map of the apparent resistivity at these places. (Loke, 1999).

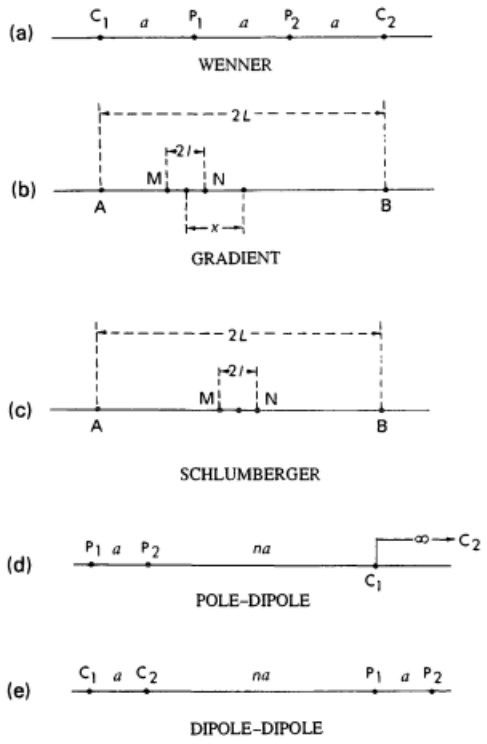

Figure 2-15: electrode arrays that are frequently used in resistivity investigations. The current and potential electrode positions are indicated by the letters C1, C2, and P1, P2. It is typical to use the symbols A, B for the current electrodes and M, N for the potential electrodes for the symmetrical and gradient Schlumberger arrays. (Sharma, 1997)

In Figure 215 (d), a pseudo section made from a dipole-dipole array is constructed, and the measured apparent resistivity for the current electrode pairs AB and potential electrode pairs PQ is displayed at the intersection of two 45° angles that cut through the electrode pairs. The apparent resistivity is determined at various depths and locations by moving the electrode pairs. 2013 (Everette). The pseudo section, however, only offers a hazy estimation of the real resistivity of the subsurface. True resistivity of the ground can be ascertained by a procedure called inversion, which necessitates intricate mathematical computations (Figure 2-16). Different electrical signals are used by electrical resistivity to identify changes in soil layer and moisture content. Electrical signal current type variation, soil layer change and electrical frequency all come to role for finding the

results just like sending different vibrations can find the dynamic impact factors of a bridge using Vehicle-Bridge Interaction modeling (Shuvrodev et al. 2021) to identify bridge damage (Shohel et al. 2022 Similar to how sending different vibrations can find the dynamic impact factors of a bridge using Vehicle-Bridge Interaction modeling (Shuvrodev et al. 2021) to identify bridge damage, electrical signal current type variation, soil layer change, and electrical frequency all play a role in finding the results (Shohel et al. 2022).

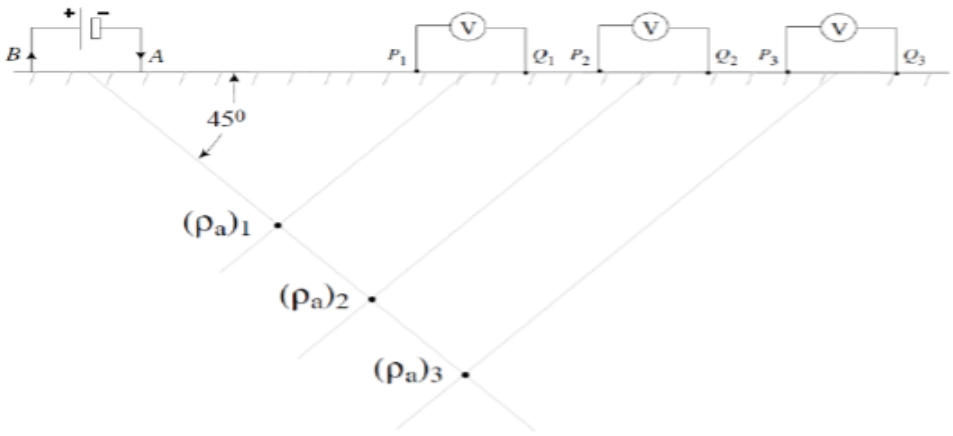

Figure 2-16: Dipole-dipole resistivity pseudosection construction (Everette, 2013)

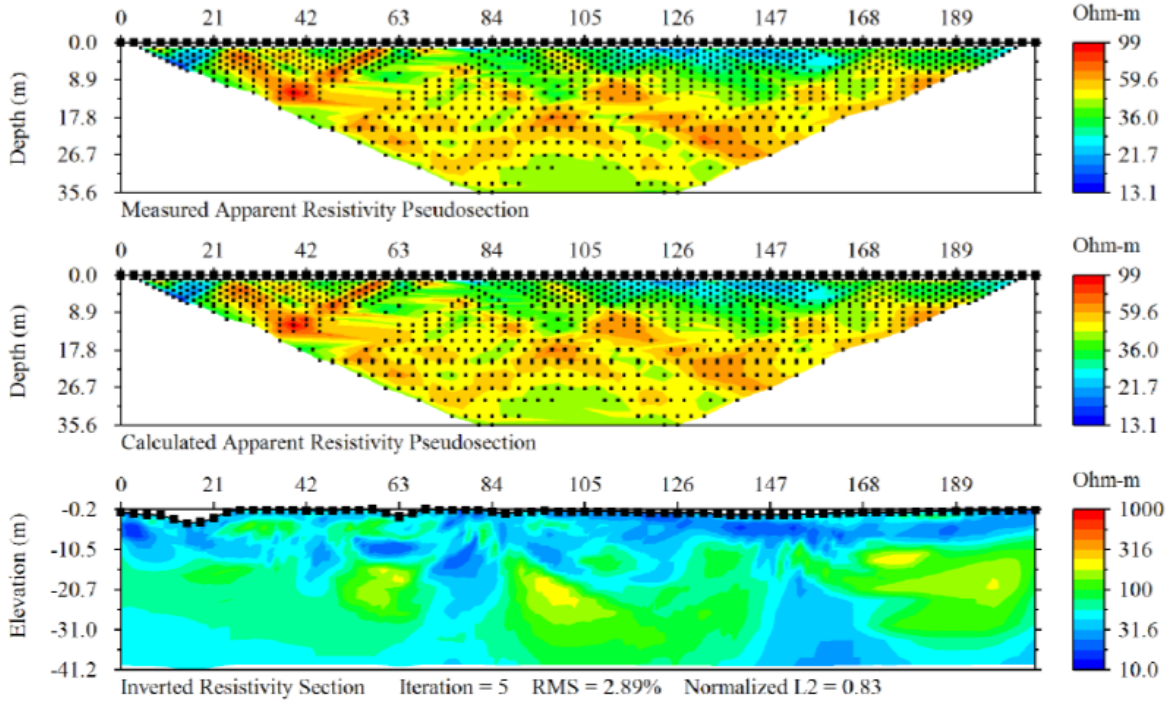

Figure 2-17: Top: Inverted resistivity image and measured apparent resistivity pseudo section for a hybrid Schlumberger -dipole-dipole electrode arrangement (Bottom). The apparent resistivity determined using the inverted cross section is shown in the middle figure. (Everette, 2013)

2.13.1 Electrical resistivity tomography (ERT)

A resistivity depth model at the midpoint is produced by an electrical resistivity sounding in which the electrode spacings are changed without changing the midpoint (z). It is possible to perform lateral profiling of (x) over a constrained depth range by moving the array along a horizontal profile and keeping the same electrode spacings. However, using this approach in complex geologies presents significant obstacles (Everette, 2013).

2.13.2 Capacitively coupled resistivity (CCR)

Utilizing capacitively coupled resistivity is a relatively quick way to gather data on electrical resistivity in the field (CCR). Five receivers and one transmitter are used in a geometrics OhmMapper. Resistivity measurements at various depths are possible by adjusting the distances between the transmitter and the first receiver as well as between each receiver. The fact that CCR does not require direct contact with the ground, in contrast to traditional DC electrical resistivity approaches, is a benefit of this technology (Chlaib, 2014). Two benefits result from this: first, it shortens the setup time for repeated measurements and, second, it permits measurement on hard surfaces like sidewalks where electrode penetration is not possible or desirable. While the device continuously gathers data and creates the pseudosection using the GPS data in real time, the Ohm Mapper can be pulled behind a vehicle or by people moving at walking pace (about 2 km/hr). However, many passes may be necessary to collect data at various depths depending on the investigation's aim. Similar to any other geophysical method, larger spacings correspond to deeper readings but lesser resolution.

2.13.3 Data acquisition for Four-electrode resistivity systems

A resistivity meter, four metal stakes (electrodes), and cables connecting the electrodes to the resistivity meter make up the conventional four-electrode resistivity system. Two essential components of the system are connected to the current and voltage electrodes by cables: the power unit and the voltage measuring unit (e.g., Samoulian et al., 2005; Aizebeokhai, 2010). Figure 2-18 depicts the main elements of the traditional four-electrode resistivity setup.

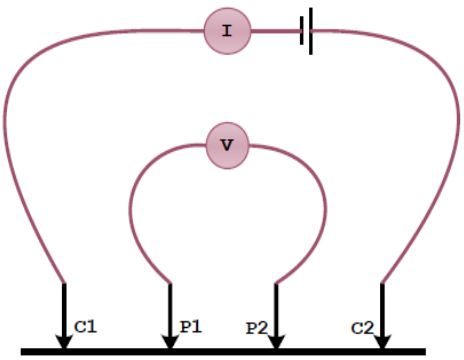

Figure 2-18: Traditional four-electrode resistivity system (Samouëlian et al., 2005; Aizebeokhai, 2010)

In field investigations, vertical electrical sounding (VES), horizontal profiling or Constant Separation Traversing (CST), and horizontal mapping are used for traditional 1D data collecting (Reynolds, 1997). The resistivity change with depth can be obtained by performing a set of measurements at a fixed array midpoint with gradually increasing distances between the electrodes. Interpretation of VES curves presupposes resistivity models in 1D horizontal layers (Zohdy, 1989). The depth of the bedrock, the water table, and the thickness of horizontal layers can all be determined using this method in hydrogeological and engineering applications. To perform CST, an array with fixed electrode spacing is moved along a profile to detect changes in lateral resistance. The data taken are qualitatively evaluated in order to map the locations of vertical features, such as faults, and the thickness of overburden layers. To map lateral resistivity changes, horizontal mapping (i.e., combining several CST profiles) is helpful (Reynolds, 1997).

The four-electrode approach is defined on a laboratory scale in BS 1377-3 (1990) and ASTM G57 (2006). An instantaneous measurement of soil (or water) resistivity can be made using a typical resistivity cell, such as a Miller soil box. The measurement setup for the four-electrode approach is shown in Figure 2-19. The current is injected between the outer two pins (or plates), and the voltage difference between the inner voltage pins is monitored. Equation, where A is the cross-sectional area of the box (m2) and L is the distance between the voltage pins (m), can be used to calculate the resistivity. In BS 1377-3 (1990) and ASTM G57, the four-electrode technique is described on a laboratory scale (2006). An instantaneous measurement of soil (or water) resistivity can be made using a typical resistivity cell, such as a Miller soil box. The measurement

setup for the four-electrode approach is shown in Figure 2-19. The current is injected between the outer two pins (or plates), and the voltage difference between the inner voltage pins is monitored. Equation can be used to compute the resistivity where L is the distance between the voltage pins and A is the cross-sectional area of the box (m2) (m).

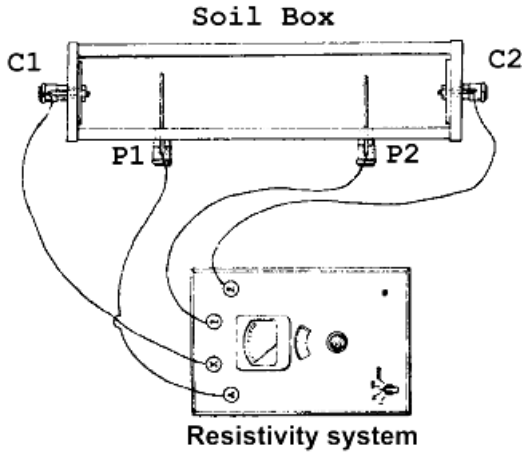

Figure 2-19: Conventional four-electrode resistivity technique (ASTM G57, 2006)

The two-electrode technique (AASHTO T288-91, 2004; ASTM G187, 2005) involves removing the voltage pins and connecting the voltage wires to the current ends. L would therefore be the separation between the outer electrodes. The measured soil resistivity should, in theory, be the same and irrespective of the method used, whether it be a two-electrode or a four-electrode approach.

2.14 Limitation of previous studies

The complex nature of soil-water systems imparts difficulty in development of electrical resistivity imaging equations for various geotechnical parameters. Several soil characteristics must be considered. To create a fully practical equation that may be used to estimate sulfate content using resistivity value, laboratory results need to be combined with statistical analysis. Previously, resistivity model attempted to take pore water conductivity and various clay qualities into consideration. However, a thorough study needs to be done to integrate the sulfate content in relationship with the resistivity.

CHAPTER 3: METHODOLOGY

3.1 Introduction

The purpose of this research is to ascertain how the sulfate concentration and geotechnical characteristics of the soil in Texas affect electrical resistivity. Fort Worth and El Paso were the two distinct districts from which soil samples were taken. To identify the soil type, index characteristics, and sulfate concentration, laboratory testing was done on the samples that were obtained. In the lab, electrical resistivity was also evaluated to ascertain their association. Testing using spectrophotometry was done to find out how much soluble sulfate was in the soil samples. In figure 3-1, a summary of the research approach is given.:

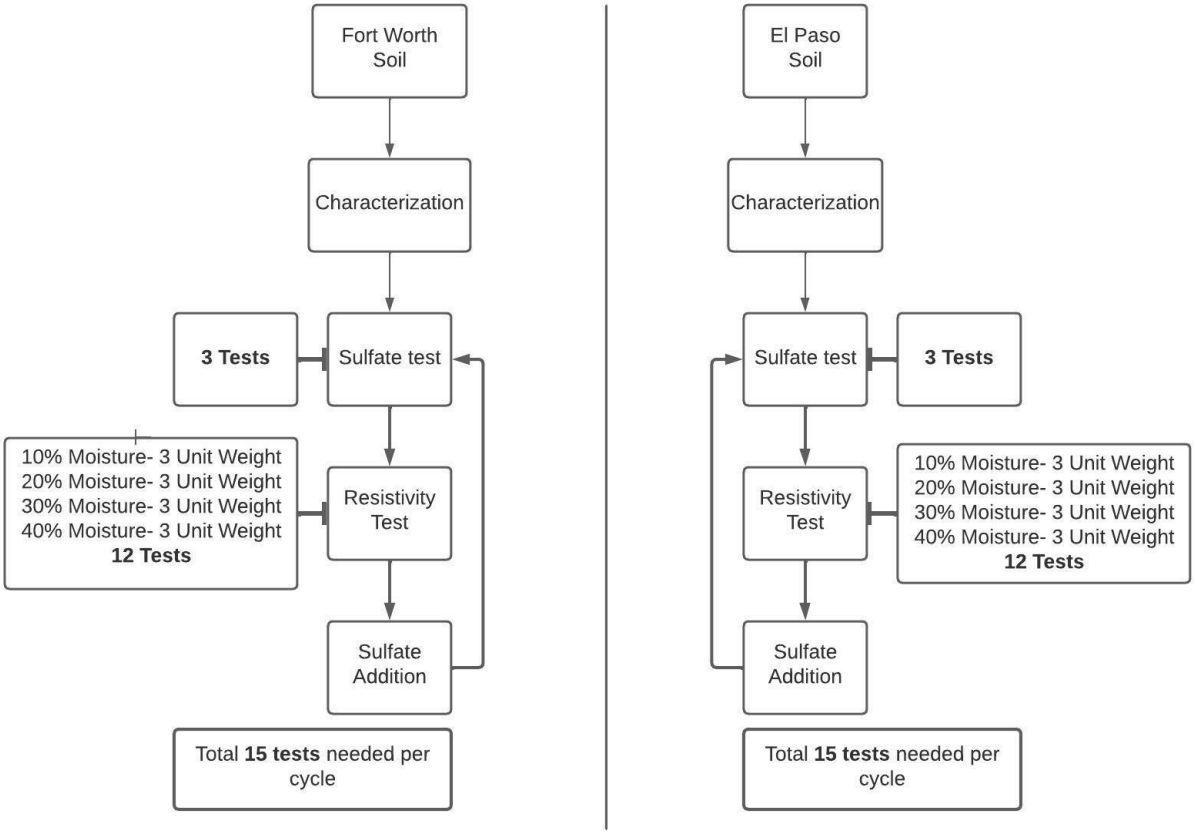

Figure 3-1: Workflow of the study

Table 3-1: Test numbers for Fort Worth sample

Sulfate content	Sulfate Test	Moisture Content	Resistivity Test		
			Unit Weight		
			11.8KN/m3	13.4 KN/m3	14.9 Kn/m3
2500 Ppm	3	10%	1	1	1
		20%	1	1	1
		30%	1	1	1
		40%	1	1	1
3000 Ppm	3	10%	1	1	1
		20%	1	1	1
		30%	1	1	1
		40%	1	1	1
4000 Ppm	3	10%	1	1	1
		20%	1	1	1
		30%	1	1	1
		40%	1	1	1
5000 Ppm	3	10%	1	1	1
		20%	1	1	1
		30%	1	1	1
		40%	1	1	1
6000 Ppm	3	10%	1	1	1
		20%	1	1	1
		30%	1	1	1
		40%	1	1	1
7000 Ppm	3	10%	1	1	1
		20%	1	1	1
		30%	1	1	1
		40%	1	1	1
8000 Ppm	3	10%	1	1	1
		20%	1	1	1
		30%	1	1	1
		40%	1	1	1
9000 Ppm	3	10%	1	1	1
		20%	1	1	1
		30%	1	1	1
		40%	1	1	1
10000 Ppm	3	10%	1	1	1
		20%	1	1	1
		30%	1	1	1
		40%	1	1	1
11000 Ppm	3	10%	1	1	1
		20%	1	1	1
		30%	1	1	1
		40%	1	1	1
Total Tests			150		

Test number done for the sample taken from El Paso is tabulated below in table 3-2:

Sulfate content	Sulfate Test	Moisture Content	Resistivity Test		
			Unit Weight		
			11.8 KN/m3	13.4 Kn/m3	14.9 KN/m3
1000 Ppm	3	10%	1	1	1
		20%	1	1	1
		30%	1	1	1
		40%	1	1	1
2000 Ppm	3	10%	1	1	1
		20%	1	1	1
		30%	1	1	1
		40%	1	1	1
3000 Ppm	3	10%	1	1	1
		20%	1	1	1
		30%	1	1	1
		40%	1	1	1
4000 Ppm	3	10%	1	1	1
		20%	1	1	1
		30%	1	1	1
		40%	1	1	1
5000 Ppm	3	10%	1	1	1
		20%	1	1	1
		30%	1	1	1
		40%	1	1	1
6000 Ppm	3	10%	1	1	1
		20%	1	1	1
		30%	1	1	1
		40%	1	1	1
7000 Ppm	3	10%	1	1	1
		20%	1	1	1
		30%	1	1	1
		40%	1	1	1
8000 Ppm	3	10%	1	1	1
		20%	1	1	1
		30%	1	1	1
		40%	1	1	1
9000 Ppm	3	10%	1	1	1
		20%	1	1	1
		30%	1	1	1
		40%	1	1	1
10000 Ppm	3	10%	1	1	1
		20%	1	1	1
		30%	1	1	1
		40%	1	1	1
11000 Ppm	3	10%	1	1	1
		20%	1	1	1
		30%	1	1	1
		40%	1	1	1
Total Tests			165		

Table 3-2: Test numbers for El Paso:

3.2 Sample Collection

Soil samples were collected from two districts of Texas prior to this study. Sample collection locations are presented in Figure 3-2. One sample from each site was taken from the collected samples.

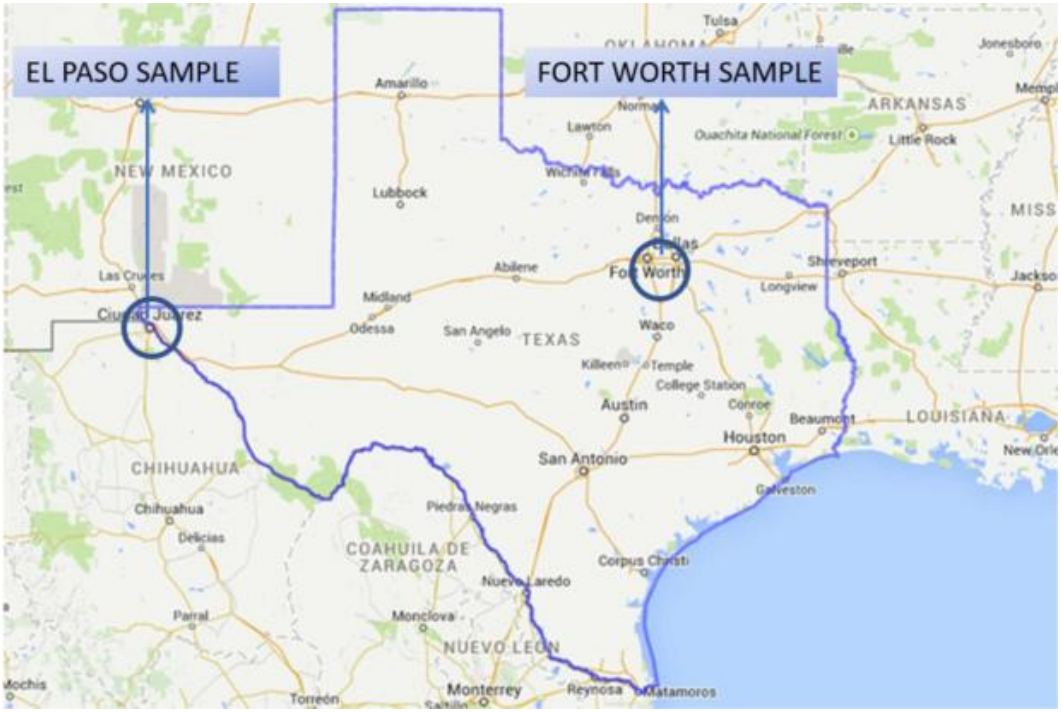

Figure 3-2 Soil collection locations

Fort Worth sample was sampled from North side of the I-30 and Fielder Road intesection. The other sample was collected from El-Paso. Sample name along with sample depth is showed in the Table 3-3.

Table 3-3 : Depth of samples taken for testing

Sample Name	Depth
Fort Worth	15′

El-Paso	25′

3.3 Test Methodology

To accomplish the goals of the investigation, a comprehensive laboratory experimental program was started. Using the results of tests for liquid limits and plastic limits, sieve analysis, and the Unified Soil Classification System (USCS), the gathered soil samples were categorized. Soluble sulfate contents were calculated using colorimetry. Different circumstances were used in the laboratory to measure the soil samples' resistivity.

3.3.1 Particle Size Distribution

One of the most crucial aspects of soil that has an impact on engineering is the particle size distribution. This characteristic describes how the soil would react to water. Additionally, the particle size distribution affects the plasticity, permeability, electric conductivity, consolidation, shear strength, and chemical diffusion. In this investigation, laboratory sieve analyses were carried out in accordance with ASTM D422 on the samples that were obtained..

500 g of dried samples were used in a sieve analysis to evaluate the distribution of particle sizes. The rubber-covered pestle and mortar were used to separate the clumped-together particles. A set of US standard sieves were used to measure the grain size distribution (No. 4, 10, 20, 40, 60, 100, 200 and pan). Additionally, a lid was positioned at the top to conceal the sample. Prior to staking, the weight of each sieve was determined. A motorized sieve shaker was used to shake a stack of sieves. The sieve stack was removed after 10 minutes. Each sieve's combined weight with the sample was calculated. To stop big clumps of small particles in soil samples held on sieve No. 200 from accumulating, wet washing was done. The sieve was positioned beneath a bowl. Continue washing the sample until only clean water is flowing out. The final sample was baked to dry it, and its weight was calculated. The geotechnical engineering laboratory of the UTA used sieve analysis, which was depicted in Figure 3-3.

Figure 3-3: Sieves used for Sieve Analysis

The particle sizes and the fine content relative to a certain diameter were determined using the hydrometer method in accordance with ASTM D7928-17 standard test procedure. Material passing through a No. 10 (2.0 mm) or finer sieve was used for the test.

The sedimentation specimen was first treated with approximately 5.0 grams of sodium hexametaphosphate that had been dissolved in water. A spatula was used to thoroughly mix the contents until all of the soil aggregations were broken up. The slurry needs to soak all night (at least 12 hours). The slurry was then placed into the hydrometer cylinder after being stirred up with a device. There was enough distilled water poured to raise the water level to 1000 ml. The cylinder was then positioned in a water bath at a consistent temperature.

The contents of the container were thoroughly stirred for about a minute, until the dirt suspension reached the bath's temperature. After setting the hydrometer cylinder on the table, the hydrometer was instantly dropped into the suspension, and the time was noted. After two minutes from the moment the graduate was placed on the table, the hydrometer's meniscus peak was measured to the nearest 0.5 g per liter. The cylinder was taken out and put back into the bath of constant temperature. After the start of sedimentation, readings from the hydrometer were taken at intervals of 1, 2, 4, 15, 30, 60, 240, and 1440 minutes. Using the equations presented in ASTM D7928-17, particle diameters and the fine content than a specific diameter were determined.

Figure 3-4: Particle size distribution testing using the hydrometer procedure

3.3.2 Liquid limit and Plastic limit

The percentage of water in a cohesive soil at the arbitrary border between the semi-liquid and plastic states is known as the liquid limit (ASTM D4318-17). First, a spray bottle was used to evenly spritz the sample with water before adding small amounts of distilled water to the soil. The liquid limit device cup was then filled with an appropriate amount of dirt, flattened, and then divided using a grooving tool at the point of maximum thickness. To close the groove, the cup was raised and dropped at a rate of two drips per second until it reached roughly 13 mm (appropriate moisture contents should yield to 15 to 35 number of blows). Three different moisture contents were used for each test repetition. Samples were then dried in an oven for 24 hours at a temperature between 100 and 110 degrees Celsius to determine the moisture content. The liquid limit of the soil specimen was determined to be the moisture content equal to 25 blows. The testing process utilizing the liquid limit device is shown in Figure 3-5.

(a) (b) (c)

Figure 3-5: Liquid limit testing involves (a) flattening the soil in the device cup, (b) creating a groove in the center, and (c) contacting the groove after blowing.

The lowest moisture level, expressed as a percentage, of a cohesive soil at the transition between the plastic and semi-solid stages is known as the plastic limit (ASTM D4318-17). First, distilled water was added to the soil and repeatedly kneaded in order to ascertain the plastic limit. After that, enough soil was spread out on a glass plate and rolled back and forth until threads that were about one-eighth inch (3 mm) in diameter were created and shattered into bits. Samples were then dried for 24 hours at 100–110 degrees Celsius in the oven to measure the moisture content. The soil specimen's plastic limit was determined to be the moisture content associated with this stage.

(a) (b)

Figure 3-6: Rolling device and cracked and shattered threats of 3 mm plastic limit testing

3.3.3 Specific Gravity

The specific gravity of soil samples was determined using a water pycnometer in line with ASTM D854-14 standard test protocol. Approximately 50 grams of dry soil material passed through the test's No. 10 (2.00 mm) sieve. The pycnometer was filled with about half distilled water before the dirt was added. The weights of the pycnometer with specimens and the pycnometer that was empty were determined separately. A partial vacuum was used to release the trapped air between the soil particles. It begins by introducing a little vacuum, which is gradually raised until the water in the flash boils. Water was then weighed after being added up to the pycnometer's graduation point. The aggregate weight was calculated after the distilled water was poured into a pristine pycnometer. The ASTM D54-14 calculations were used to calculate the soil's specific gravity. The testing process on the clayey soil samples is shown in Figure 3-7.

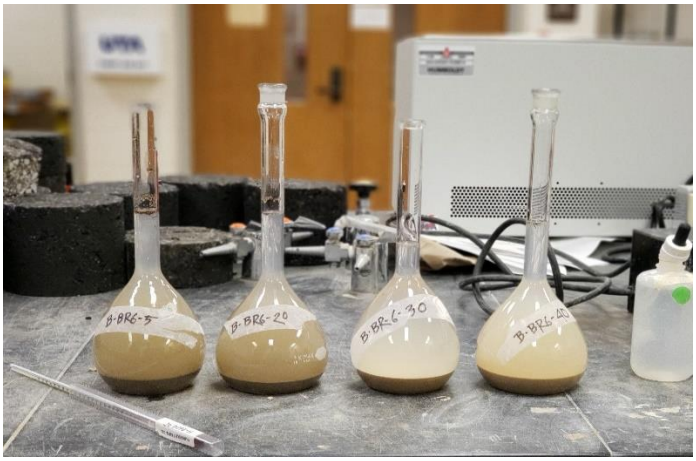

Figure 3-7: Specific gravity testing of soil

3.3.4 Sulfate Content in Soil with Colorimetric Method

The Texas Department of Transportation developed the TXDOT approach in 2005. This technique relies on turbidity. The first step in preparing the sample for this procedure is to dry 300 g of the field sample at 60°C (140°F) for an hour. After drying, the soil is ground until it can pass through a 0.422 mm (U.S. No. 40) screen. This particular process must be repeated twice, and the concentrations that result are averaged to determine the final sulfate value. The following step involves adding 200 mL of DI water to a flask with 10g of the sample. The flask is then sealed and forcefully shaken by hand for about a minute. After that, the sample is allowed to sit for at least

12 hours. The sample is shaken for 1 minute after it has sat for 12 hours before being filtered through Whatman 42® (fine porosity) filter paper or a comparable filter paper. Following the collection of the filtrate, 10 ml of the filtrate are pipette-transferred into the glass vile that is used in the particular colorimetric apparatus. The glass vile is then cleaned with Kimwipes® or a comparable product to get rid of any dirt or fingerprints that could affect the readings. The colorimetric device (Figure 3-8) is then filled with the glass vile, and it is zeroed to confirm that it is calibrated.

One sulfate pill is then inserted, and it is thoroughly crushed with a plastic rod once the vial has been withdrawn. Sulfates will cause the solution to get milky or hazy in hue if they are present. The vile is then tested after being reinserted into the colorimeter. The readings are averaged when utilizing this method, which calls for a minimum of three readings. The sample's ppm is calculated by multiplying the average reading value by the initial dilution ratio (for example, a 1:20 dilution with an average reading of 100 equals 2000 ppm).

Figure 3-8: Photograph of a Colorimeter used for sulfate determination

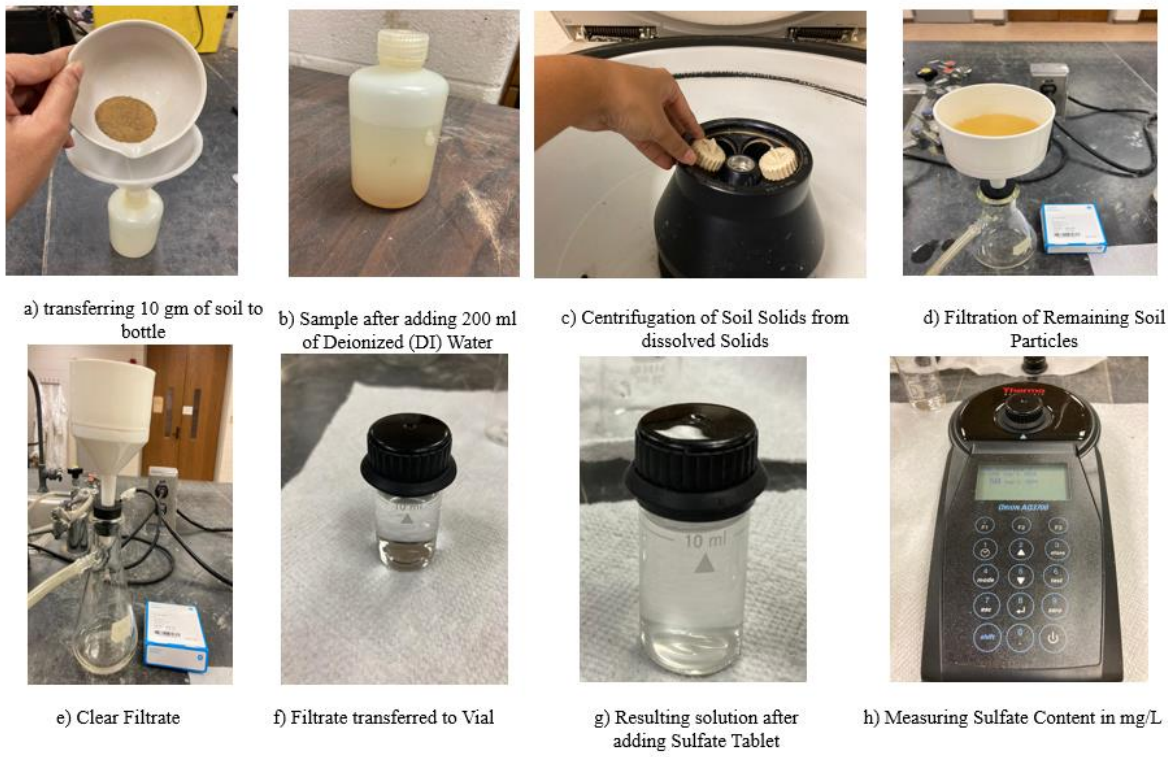

Figure 3-9: Illustrated Tex-145-E Method for Soluble Sulfates Determination in Soil

3.3.5 Laboratory Electrical Resistivity Testing

On the disturbed samples taken from boreholes and subjected to various electrical resistivity tests, various moisture contents, and dry unit weights were taken into consideration. The laboratory experiment was carried out using a four-electrode soil box, a current source, resistance measuring tools, and electrical connections. The soil was first blended with a certain quantity of water (between 10% and 40%). After that, the earth was packed into the box to the required level of compaction (in the range of 75 to 95 pounds per cubic feet). The potential drop between two sites at the specimen was measured after the equipment was installed. Direct current was provided using two electrodes situated at the end of the soil resistivity box. Figure 3-10 shows how to prepare soil samples and set up an experiment for resistivity tests in a lab.

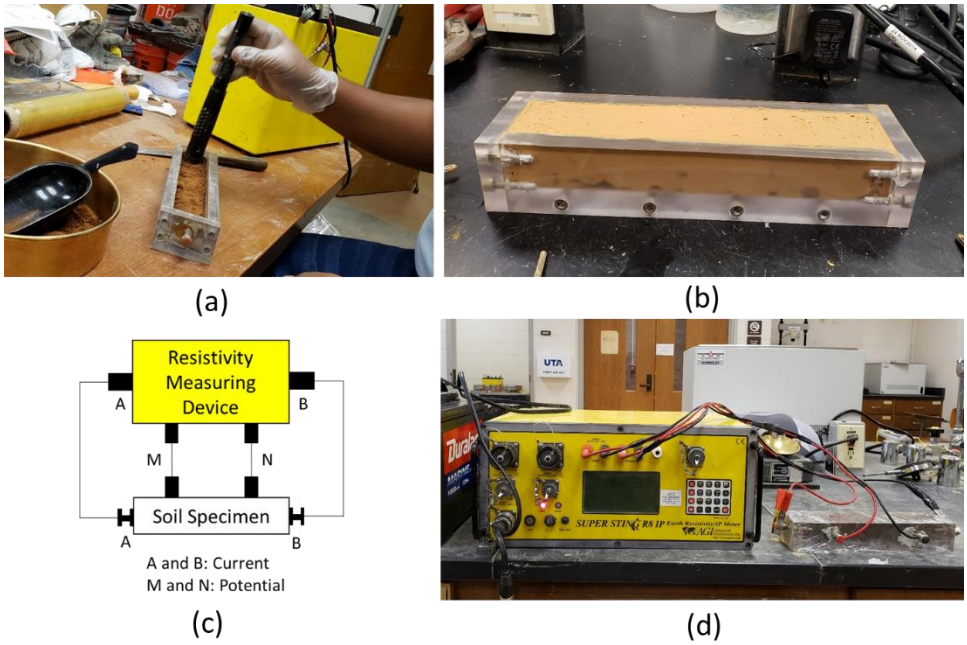

Figure 3-10: Preparation of soil samples in steps a and b, a schematic setup for a laboratory electrical resistivity test, and a practical setup for a laboratory resistivity test are all included.

After measurements of electrical resistivity, to consider the effect of temperature variations on the obtained values, the observed resistivity values were corrected for a uniform temperature of 15.5 degrees of Centigrade (60ᵒ F) according to the ASTM G187-05.

3.3.6 Sulfate Addition in the soil sample

After every resistivity test soil sample was pulverized and sulfate was added using Gypsum.

As the test required, every increment of the sulfate content needed to be 1000 ppm. To add this amount of soluble sulfate content into the soil, 1000 ml water was taken and 1.79 grams of Gypsum ($CaSO_4.2H_2O$) was added to the water and stirred until the gypsum was turned into solution. As the goal was to get 1000 ppm increment that needed 1gm/1000mL of water. So, the needed Gypsum was 0.0104 mole. Therefore, as the Molar Weight of Gypsum is 172.19 gm/mole weight of gypsum needed to get to 0.104 mole is 1.79 grams of gypsum into the 1000ml water.

After adding the gypsum mixed water, the soil sample was stirred continuously to ensure homogeneous mixing of sulfate. After mixing the soil was kept in the oven for drying. After drying

the soil was taken out to test for the sulfate content using the Tex-145-E Method. Figure 3-11 to 3-14 shows the mixing method.

$$\frac{mole*molecular\ weight}{L} = \frac{g}{L} \ ; \quad 1\ ppm = \frac{1mg}{L}$$

(a)

(b)

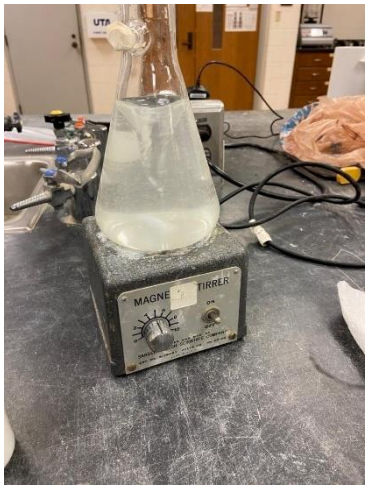

(c)

(d)

Figure 3-11 : (a) Pulverizing sample; (b) Measuring sulfate sample (c) Mixing sulfate with water; (d) Mixed sulfate with soil

3.4 Statistical Analysis

Multiple linear regression (MLR) studies were utilized to link the experimental resistivity value to the soil geotechnical engineering parameters. The multiple linear regression modeling was performed using the statistical analysis program R Studio. The statistical model was created using data from the experimental program. For samples of sandy soil and compacted soil, different MLR models were created. Prior to hand, important variables relating to soil characteristics were identified. The initial analysis was followed by verification of the following MLR modeling assumptions.

- Constant Variance check
- Normality check
- Independent error terms
- Presence of outlier
- Multicollinearity, and
- Applicability of regression on current data set
- Transformation of parameter if needed.

3.5 Model Validation

The created models were used to forecast the soil's sulfate concentration. A lab resistivity was done for increasing sulfate content and combination of compaction and moisture content. The model used the resistivity measurements to validate the estimated and obtained sulfate content of the soil.

CHAPTER 4: RESULTS AND DISCUSSION

4.1 Geotechnical Properties

4.1.1 Grain Size Distribution

Grain Size distribution was done for the samples collected from the boreholes.

4.1.1.1 Fort Worth Sample

Fort Worth Sample was taken from North Fielder Road, Fort Worth. The sample depth was 15 feet. From the grain size distribution curve in Figure 4-1, it is observed that 19.9% soil is sandy there. Therefore, Fort Worth sample is characterized as Clayey Sample.

4.1.1.2 EL Paso Sample

El Paso sample was taken from depth of 20-25 feet. From the grain size distribution curve in Figure 4-1, it is observed that 58.3% soil is sandy there. Therefore, El Paso sample is characterized as Sandy Sample.

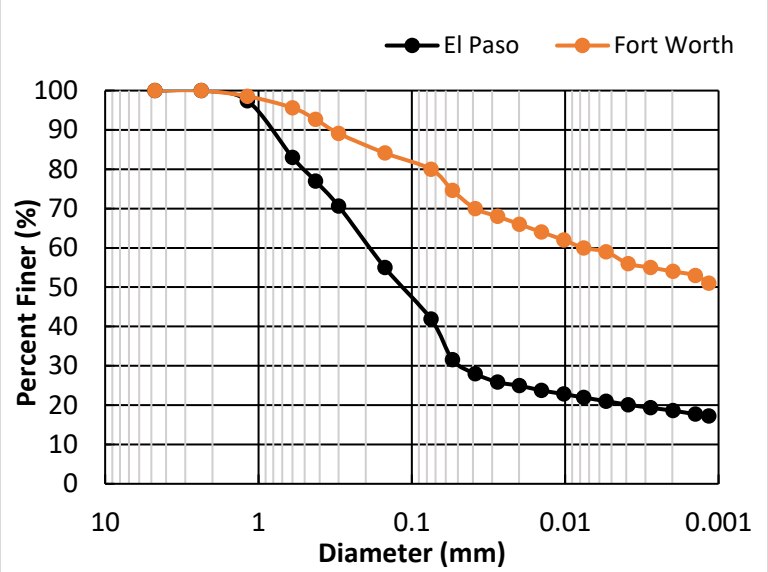

Figure 4-1: Grain size distribution curve for El Paso & Fort Worth sample.

4.1.2 Atterberg Limit Test

For the purpose of determining the plastic and liquid limits of the soil sample, Atterberg limit tests were performed. By deducting the liquid limit from the plastic limit, the plasticity index was calculated. The Liquid Limit and Plastic Limit of the soil sample are displayed in Table 4-1. Figures 4-2 display the plasticity chart for the soil samples utilized in this investigation.

Table 4-1: Atterberg Limits of EL Paso and Fort Worth samples

Sample	Liquid Limit	Plasticity Index
El Paso	43%	27 %
Fort Worth	53%	37%

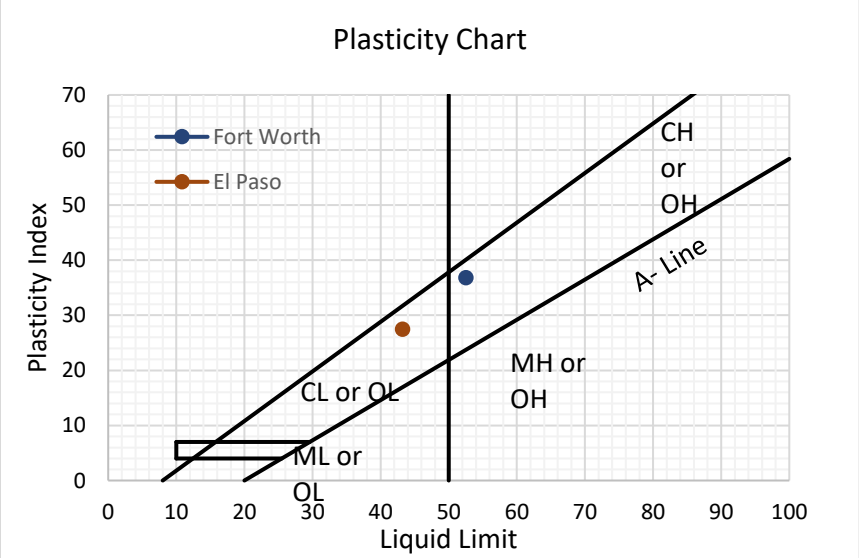

Figure 4-2: Plasticity Chart of Fort Worth and El Paso Soil

From the plasticity chart of Fort Worth soil from Figure 4-2 and grain size distribution curve Figure 4-1, Fort Worth sample was characterized as High Plasticity Clay (CH).

From the grain size distribution curve from Figure 4-2 and plasticity chart from Figure 4-2, it was found that EL paso sample was Poorly Graded Sandy Sample.

4.2 Laboratory Resistivity Test Results

This section investigates the relationship between sulfate concentration, significant parameters associated with soil characteristics, and phase interactions with electrical resistivity. To ascertain the relationship between soil moisture content, void ratio, degree of saturation, and electrical resistivity, laboratory studies were carried out. Both clayey and sandy samples of disturbed soil were included in the tests. We'll talk about how the diverse soil qualities affect the electrical resistivity values in clayey soils and sandy soils.

4.3 Resistivity Results for Clayey Fort Worth Soil

4.3.1 Influential Parameters Related to Soil Properties

Using compacted clays, it was possible to measure how the characteristics of the soil affected the electrical resistivity results. The amount of saturation was maintained throughout to decrease the impact of saturation on the results of the resistivity analysis (Kibria & Hossain, 2015). There were a number of predefined saturation levels used to identify the important variables.

4.3.1.1 Resistivity and Sulfate Content

To regulate the samples' sulfate concentration, sulfate was applied. As a result, the sulfate ions in the pore water were linked to resistivity at different saturation levels. The soil samples' conductivity is increased by sulfate ions. The relationship between resistivity and sulfate concentration is depicted in Figure 4-3.

The resistivity decreases at lower moisture contents of 10% and 20% as the sulfate content increases for all variable unit weights. However, compared to the lower rate of change at 20% moisture content, the rate of change in resistivity is much higher for the 10% moisture level. The

rate of change in resistivity is not enhanced for the 30% moisture content. Lastly, a 40% moisture content causes little to no change in resistance.

In Figure 4-3, it is observed that different unit weight will have impact on the resistivity value. For 10% moisture content, for all the sulfate content levels resistivity value for 11.8 KN/m^3 has significantly higher resistivity value opposed to the 13.4 KN/m^3 or 14.9 KN/m^3. However, as the moisture content goes higher to 30% or 40% the effect of dry unit weight on resistivity value declines.

It is observed in Figure 4-3 that there is an average 58 Ohm-m drop in resistivity value for the difference in moisture content of 10% to 30%. However, this difference is not same for all the sulfate content levels. As the sulfate content goes higher, this difference in resistivity for gain in moisture content goes lower. Though this trend is followed throughout all three-unit weight ranges, the amplitude of difference in resistivity for 10% and 30% is not same for all three-unit weight. For 13.4 KN/m^3 we can see average drop in resistivity of 24 Ohm-m for shifting in 10% to 30% moisture content and for 14.9 KN/m^3 we can see average drop in resistivity of 10 Ohm-m for shifting in 10% to 30% moisture content,

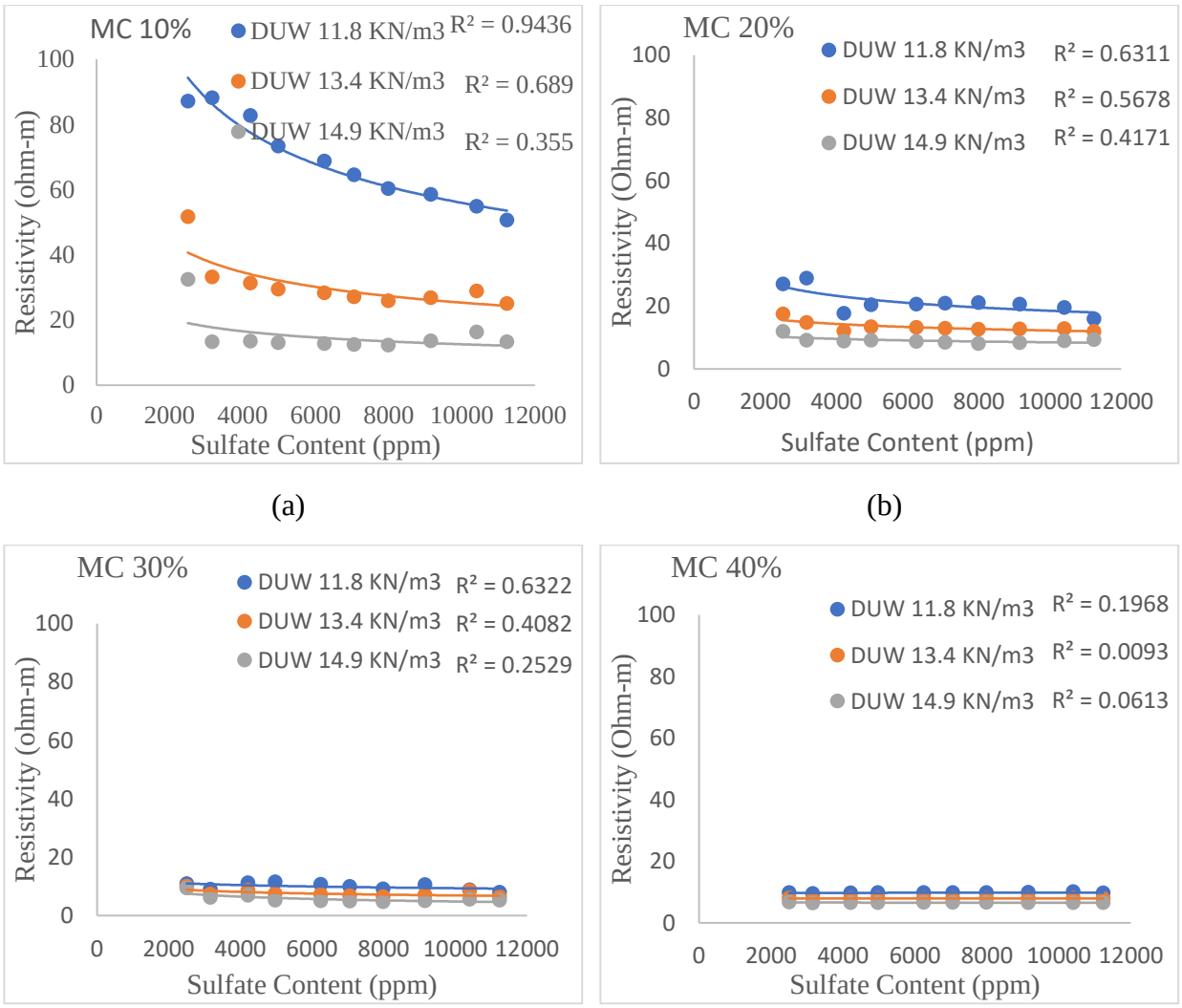

Figure 4-3: Relationship between sulfate content and resistivity in different moisture content level.

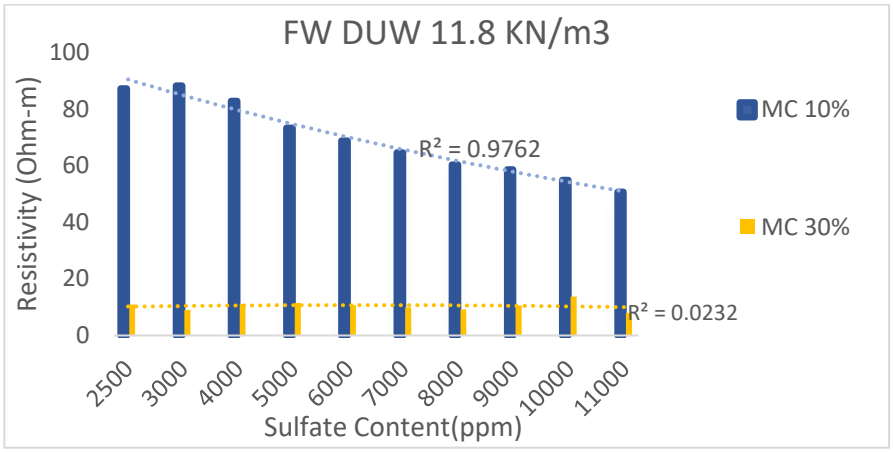

(a)

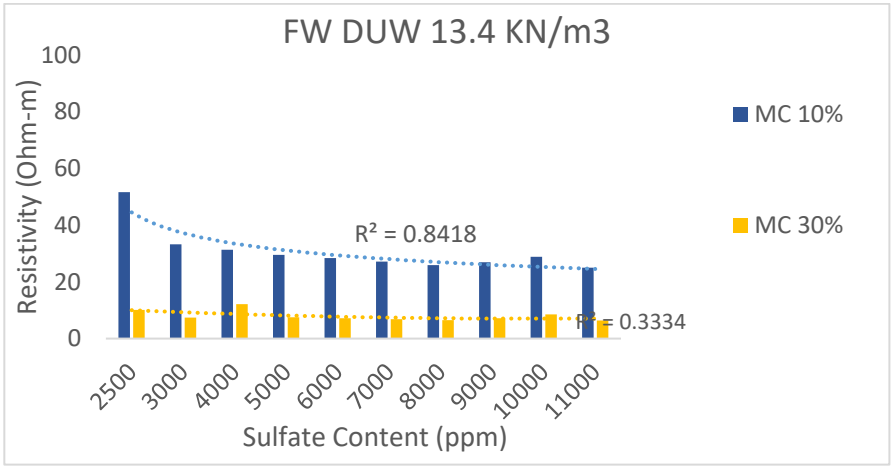

(b)

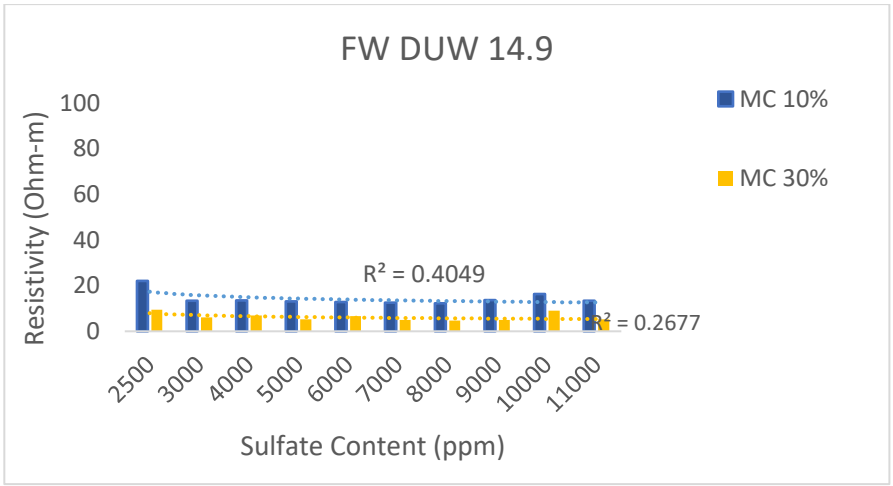

(c)

Figure 4-4: Resistivity vs Sulfate content for different dry unit weight.

4.3.2 Influential Parameters Related to Phase Relationship

Gravimetric moisture content, void ratio, unit weight, volumetric moisture content, and saturation level were all individually studied for their effects on compacted clays. Gravimetric moisture, specific gravity, dry unit weight, and void ratio, on the other hand, determine the volumetric moisture content and degree of saturation. In order to determine how electrical resistance reacts in compacted clay, various conditions are examined, including gravimetric moisture content, void ratio, volumetric moisture content, saturation level, and dry unit weight.

4.3.2.1 Moisture Content and Resistivity

Figure 4-5 shows the variation in electrical resistivity of clayey soil with different gravimetric moisture contents at variable unit weights and sulfate contents. The moisture content impacts heavily on the fluctuation of electrical resistivity.

In this investigation, the average resistivity values for 11.8 KN/m3 dry unit weight and 10%, 20%, 30%, and 40% moisture content were determined to be 68.95 Ohm-m, 21.34 Ohm-m, 10.46 Ohm-m, and 9.78 Ohm-m, respectively, with standard deviations of 13.52 Ohm-m, 3.88 Ohm-m, 1.60 Ohm-m, and 0.141 Ohm-m.

The resistivity value was determined to be 30.82 Ohm-m with a standard deviation of 7.74 Ohm-m for the case of 13.4 KN/m3 and 10%, 20%, 30%, and 40% moisture content, 13.45 Ohm-m with a standard deviation of 1.64 Ohm-m, 7.62 Ohm-m with a standard deviation of 1.15 Ohm-m, and 7.92 Ohm-m with a standard deviation of 0.08 Ohm-m, respectively.

The resistivity was determined to be 15.34 Ohm-m with standard deviations of 6.11 Ohm-m, 9.14 Ohm-m with standard deviation of 1.08 Ohm-m, 5.82 Ohm-m with standard deviation of 1.42 Ohm-m, and 6.57 Ohm-m with standard deviation of 0.08 Ohm-m for soil with 14.9 KN/m3 and 10%, 20%, 30%, and 40% moisture content, respectively.

A massive reduction of electrical conductivity was observed between 10% and 30% of moisture content; however, the reduction rate of electrical resistivity with moisture content is rather low after 30% moisture content. This phenomenon can be explained through the study done by Pozdnyakov (2006). Pozdnyakov (2006) separated a graph of electrical resistance vs the natural

logarithm of moisture content into many sections. Adsorbed water, film water, film capillary water, capillary water, and gravity water are the portions of the curve that are labeled. The author claims that as moisture content rises, electrical resistance in the adsorption water zone rapidly lowers. Even though the water molecules are immobile in the adsorbed water zone, the dipolar water produces a conductive route for electrical current.

Elevated moisture levels in the adsorption zone result in a significant reduction in electrical resistance. The rate of fall diminishes as the Van der Waals force rises in the film water zone.. Water from the pores in the water film flows from the film to the fissure after it has reached its maximum thickness. Because molecular attraction dominates capillary attraction in the film capillary water zone, both the capillary zone and the capillary water zone undergo a step-down in the rate of decrease. Because water molecules in gravitational water zones move independently of electrical charges, electrical resistance is largely independent of the amount of water present.

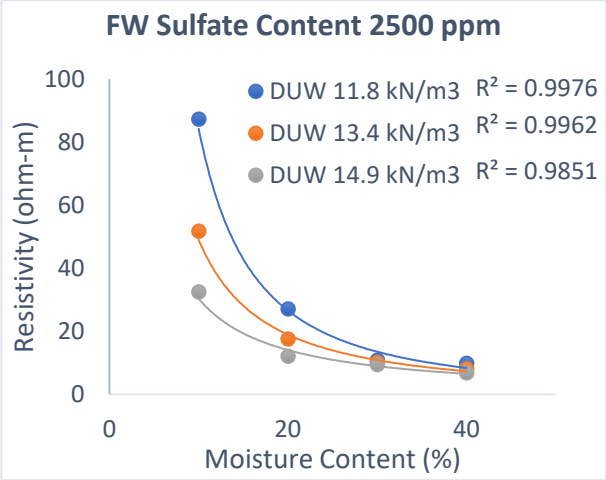
FW Sulfate Content 2500 ppm
DUW 11.8 kN/m3 R² = 0.9976
DUW 13.4 kN/m3 R² = 0.9962
DUW 14.9 kN/m3 R² = 0.9851
Resistivity (ohm-m)
Moisture Content (%)

(a)

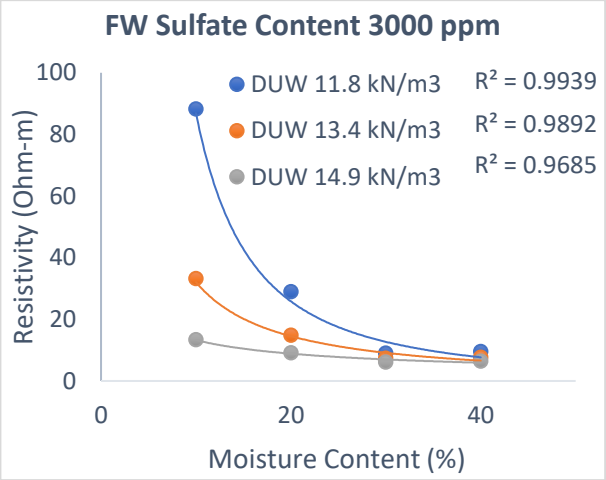
FW Sulfate Content 3000 ppm
DUW 11.8 kN/m3 R² = 0.9939
DUW 13.4 kN/m3 R² = 0.9892
DUW 14.9 kN/m3 R² = 0.9685
Resistivity (Ohm-m)
Moisture Content (%)

(b)

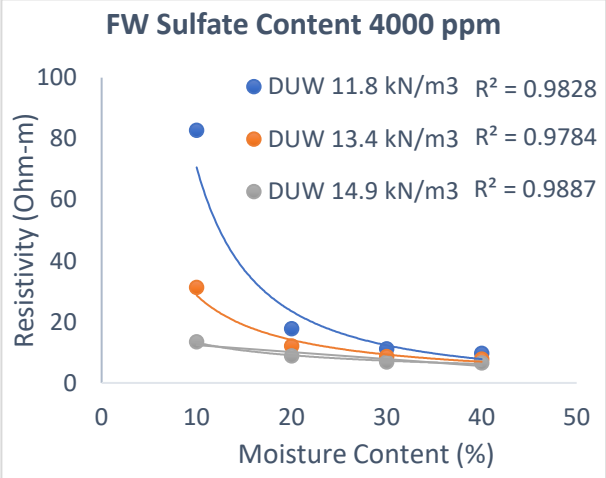
FW Sulfate Content 4000 ppm
DUW 11.8 kN/m3 R² = 0.9828
DUW 13.4 kN/m3 R² = 0.9784
DUW 14.9 kN/m3 R² = 0.9887
Resistivity (Ohm-m)
Moisture Content (%)

(c)

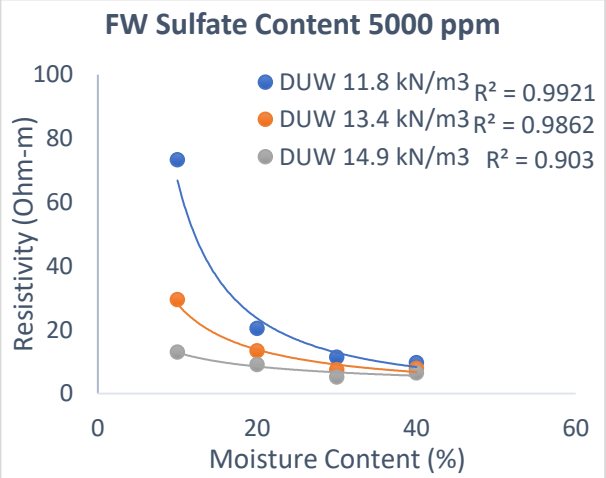
FW Sulfate Content 5000 ppm
DUW 11.8 kN/m3 R² = 0.9921
DUW 13.4 kN/m3 R² = 0.9862
DUW 14.9 kN/m3 R² = 0.903
Resistivity (Ohm-m)
Moisture Content (%)

(d)

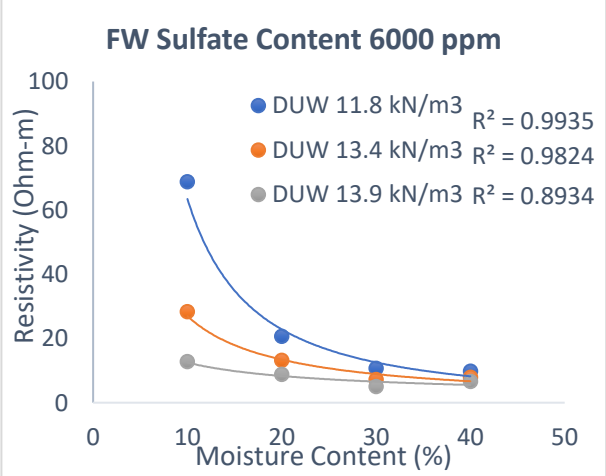
FW Sulfate Content 6000 ppm
DUW 11.8 kN/m3 R² = 0.9935
DUW 13.4 kN/m3 R² = 0.9824
DUW 13.9 kN/m3 R² = 0.8934
Resistivity (Ohm-m)
Moisture Content (%)

(e)

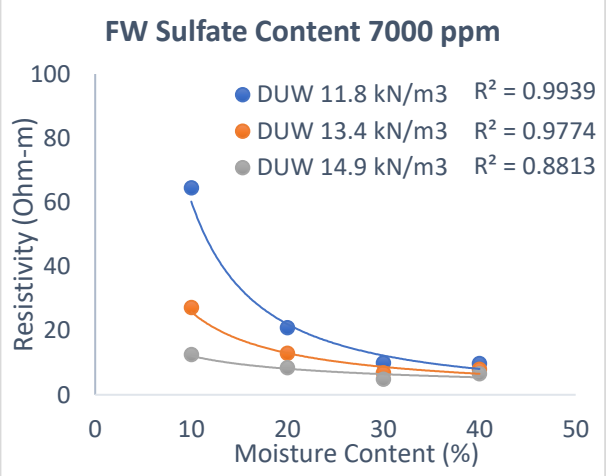
FW Sulfate Content 7000 ppm
DUW 11.8 kN/m3 R² = 0.9939
DUW 13.4 kN/m3 R² = 0.9774
DUW 14.9 kN/m3 R² = 0.8813
Resistivity (Ohm-m)
Moisture Content (%)

(f)

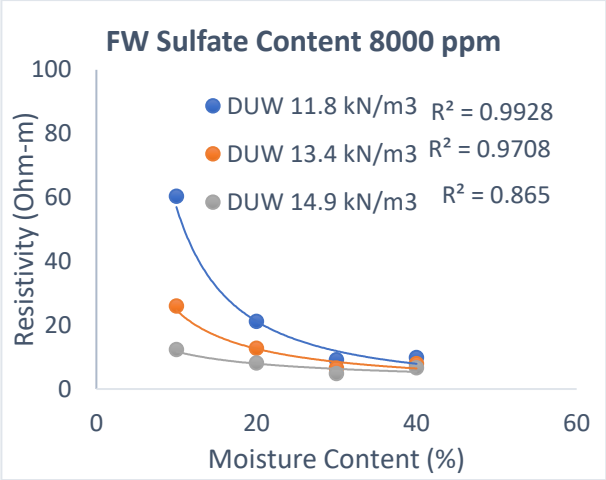

(g)

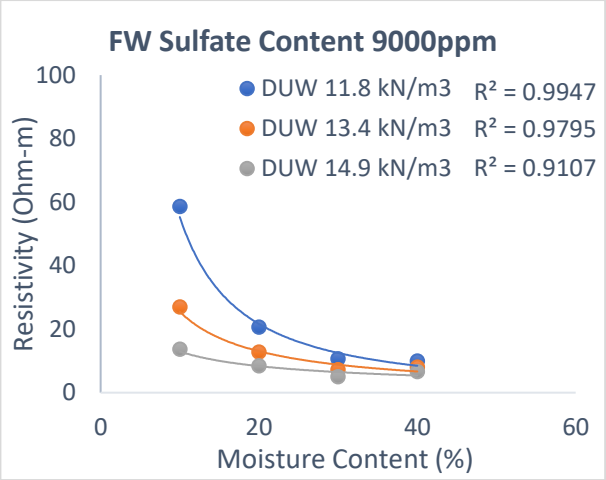

(h)

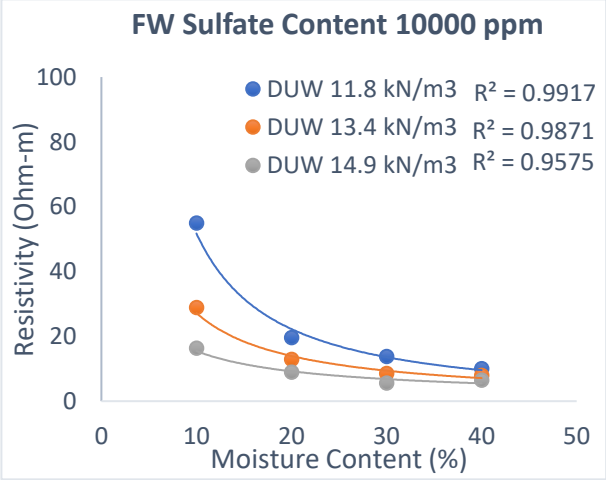

(i)

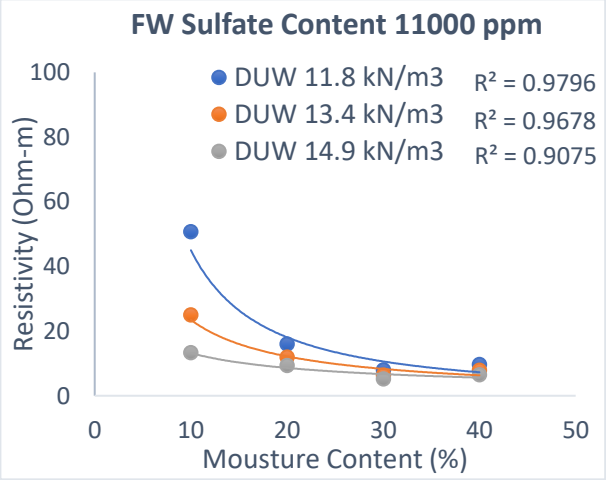

(j)

Figure 4-5: Relationship between FW soil's electrical resistance and moisture content.

Changes in resistivity with change in Dry Unit Weight for different moisture contents are tabulated below in Table

Table 5-4: Resistivity value for different unit weight

Dry Unit Weight (KN/m^3)	MC 10%		MC 20%		MC 30%		MC 40%	
11.8	68.95	13.52	21.34	3.88	10.46	1.608	9.78	0.141
13.4	30.82	7.74	13.45	1.64	7.62	1.15	7.92	0.08
14.9	15.34	6.11	9.14	1.08	5.82	1.42	6.57	0.08

5.2.1.2 Dry Unit Weight and Resistivity

In Figure 4-6 for different moisture content resistivity is expressed as a function of dry unit weight. It is seen that the resistivity decreases as the unit weight increase, however, the rate of decrease is not the same for all the sulfate content levels. The average decrease in resistivity for increase of unit weight from 11.8 KN/m^3 to 14.9 KN/m^3 is 77.7% for 10% moisture content, 57.17% for 20% moisture content, 44.48% for 30% moisture content and 31.5% for 40% moisture content.

The rate of change in resistivity with increasing unit weight for 10% moisture content is the highest. However, the rate decreases as the moisture content goes up.

Furthermore, another parameter is important while describing the relationship between unit weight and resistivity value. From the Figure 4-6, it is seen that the rate of change in resistivity with unit weight decreases with the increase of sulfate content.

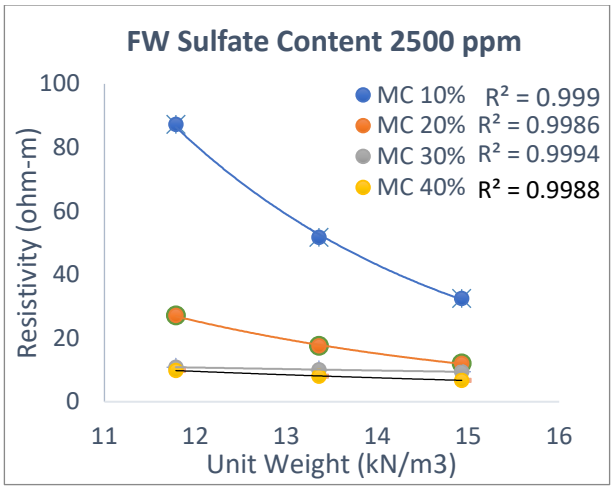
FW Sulfate Content 2500 ppm
Resistivity (ohm-m)
Unit Weight (kN/m3)
MC 10% R² = 0.999
MC 20% R² = 0.9986
MC 30% R² = 0.9994
MC 40% R² = 0.9988

(a)

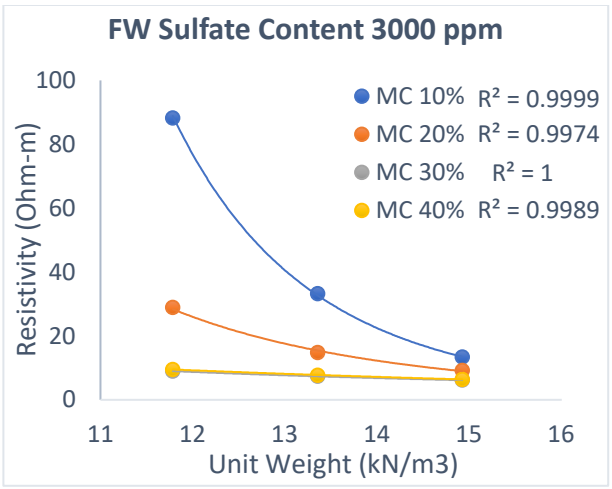
FW Sulfate Content 3000 ppm
Resistivity (Ohm-m)
Unit Weight (kN/m3)
MC 10% R² = 0.9999
MC 20% R² = 0.9974
MC 30% R² = 1
MC 40% R² = 0.9989

(b)

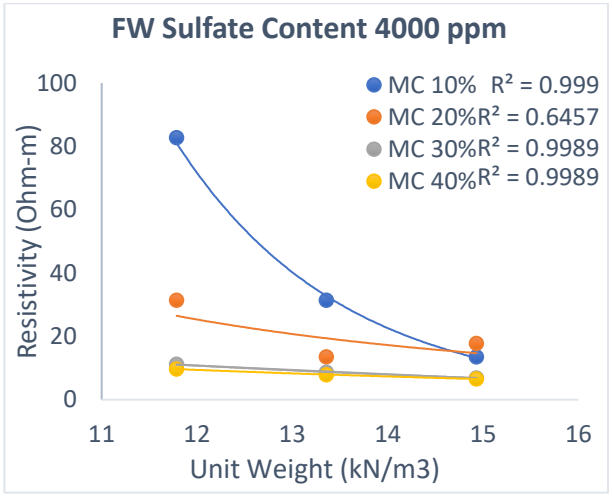
FW Sulfate Content 4000 ppm
Resistivity (Ohm-m)
Unit Weight (kN/m3)
MC 10% R² = 0.999
MC 20%R² = 0.6457
MC 30%R² = 0.9989
MC 40%R² = 0.9989

(c)

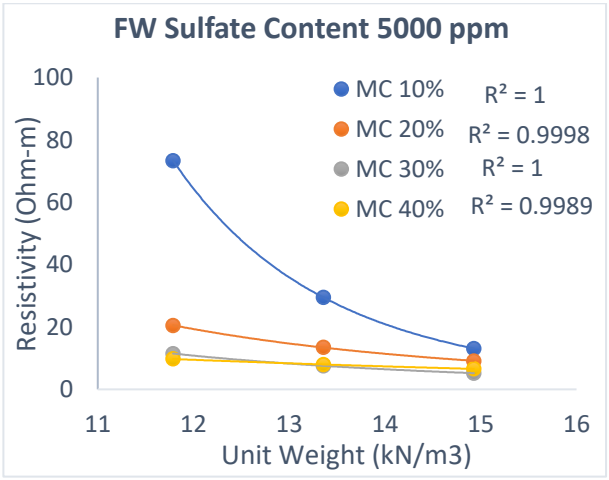
FW Sulfate Content 5000 ppm
Resistivity (Ohm-m)
Unit Weight (kN/m3)
MC 10% R² = 1
MC 20% R² = 0.9998
MC 30% R² = 1
MC 40% R² = 0.9989

(d)

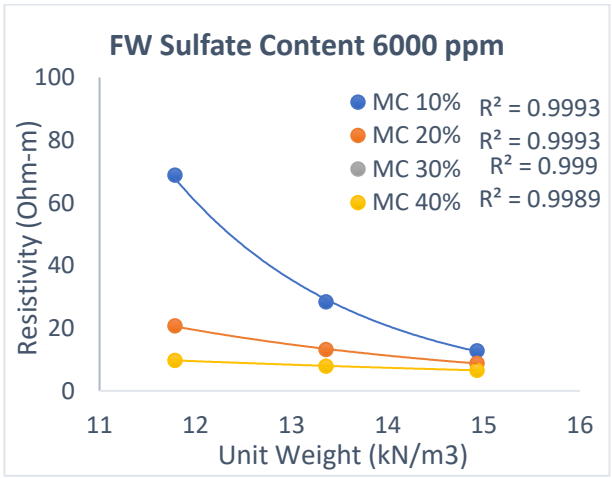
FW Sulfate Content 6000 ppm
Resistivity (Ohm-m)
Unit Weight (kN/m3)
MC 10% R² = 0.9993
MC 20% R² = 0.9993
MC 30% R² = 0.999
MC 40% R² = 0.9989

(e)

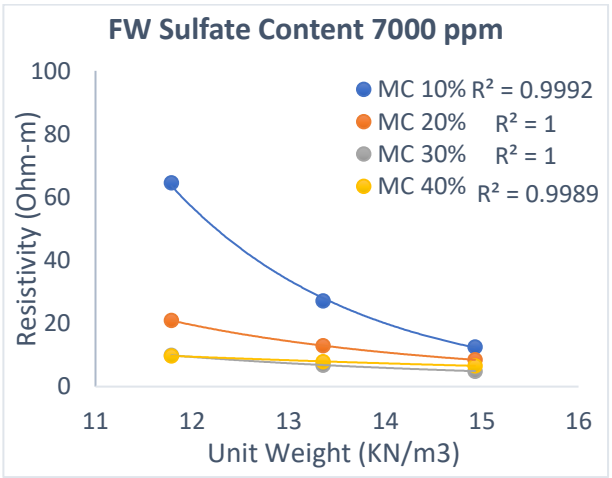
FW Sulfate Content 7000 ppm
Resistivity (Ohm-m)
Unit Weight (KN/m3)
MC 10% R² = 0.9992
MC 20% R² = 1
MC 30% R² = 1
MC 40% R² = 0.9989

(f)

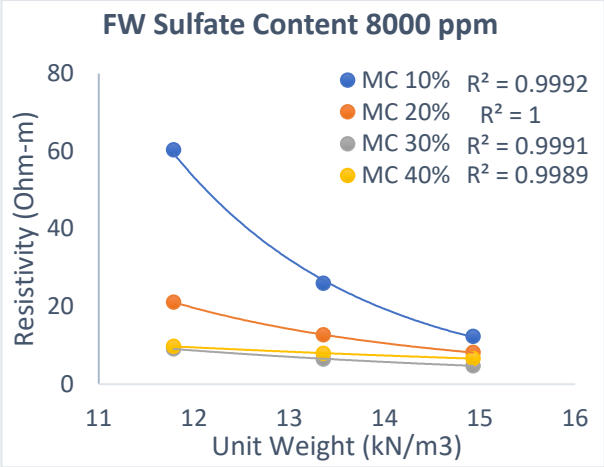

(a)

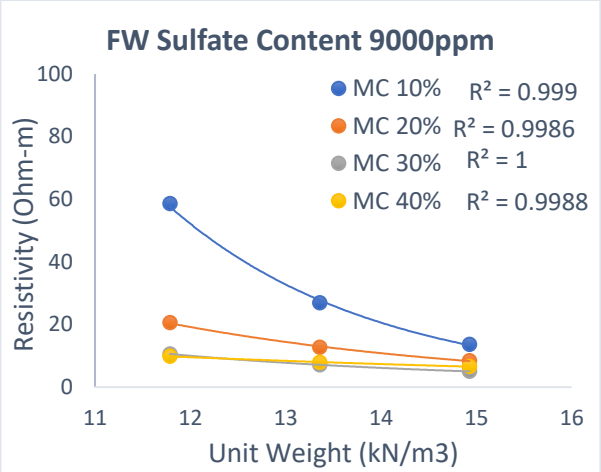

(b)

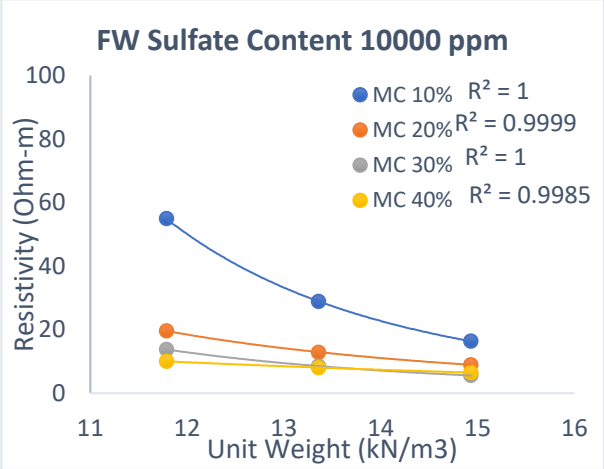

(c)

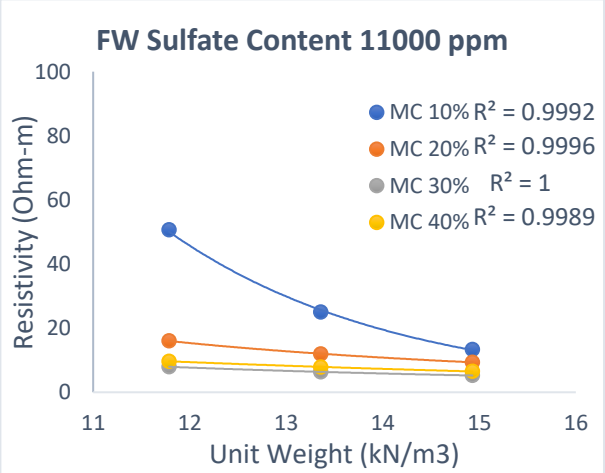

(d)

Figure 4-6: Relationship between soil compaction's unit weight and resistivity

Table 4-2 Change in resistivity with unit weight for different sulfate content at 10% moisture content.

Sulfate Content (ppm)	Resistivity value for DUW 11.8 KN/m^3	Resistivity value for γ_d = 14.9 KN/m^3	Percent change in resistivity (%)
3000	88.21	13.38	84.83
5000	73.36	13.05	82.18
10000	54.92	16.36	70.20

Table 5-2 shows for 10% moisture content resistivity drops 84.83% for compacting the sample from 11.8 KN/m^3 to 14.9 KN/m^3 at 3000 ppm of sulfate content in the clayey soil. Figure 4-6 shows the percent change in resistivity values for compaction from 11.8 KN/m^3 to 14.9 KN/m^3 for 10%, 20%, 30%, 40% moisture content.

For moisture content 10% and 20% the change in resistivity is higher for lower sulfate levels and lower for higher sulfate contents. However, for 30% to 40% moisture content this change is almost constant.

4.3.2.2 Void ratio and resistivity

The change of resistivity with change in void ratio at diverse moisture content was plotted in Figure 4-7. A trend was observed as the void ratio was increasing the resistivity was decreasing. The resistivity value increased along with the general trend of the void ratio, which was observed to be growing. However, depending on the soil type and moisture level, the rate of growth varies. When the soil has less moisture but high liquid limit which denotes a high fine content, typically exhibits a higher growing rate of resistivity.

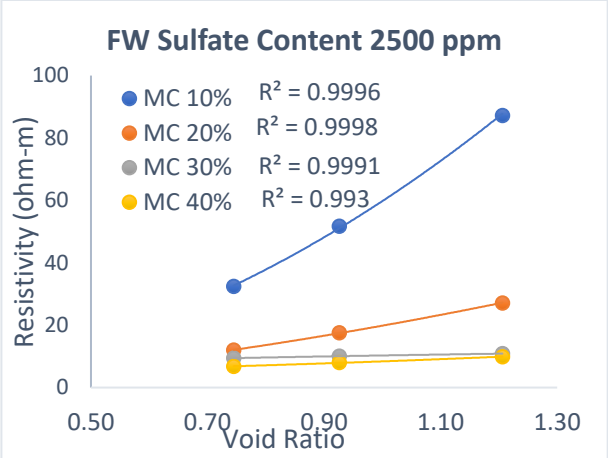
FW Sulfate Content 2500 ppm
MC 10% R² = 0.9996
MC 20% R² = 0.9998
MC 30% R² = 0.9991
MC 40% R² = 0.993
Resistivity (ohm-m)
Void Ratio
0
20
40
60
80
100
0.50
0.70
0.90
1.10
1.30

(a)

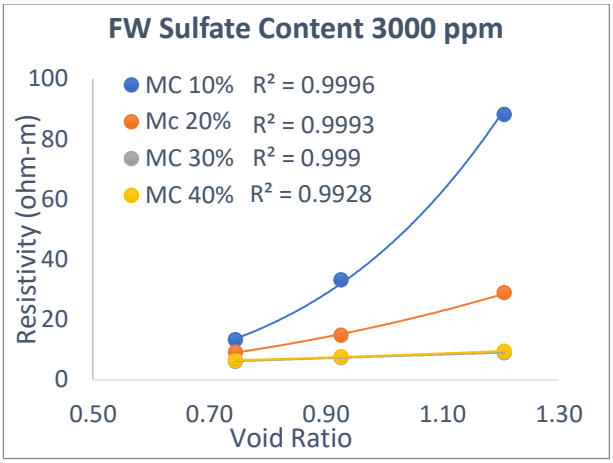
FW Sulfate Content 3000 ppm
MC 10% R² = 0.9996
Mc 20% R² = 0.9993
MC 30% R² = 0.999
MC 40% R² = 0.9928
Resistivity (ohm-m)
Void Ratio
0
20
40
60
80
100
0.50
0.70
0.90
1.10
1.30

(b)

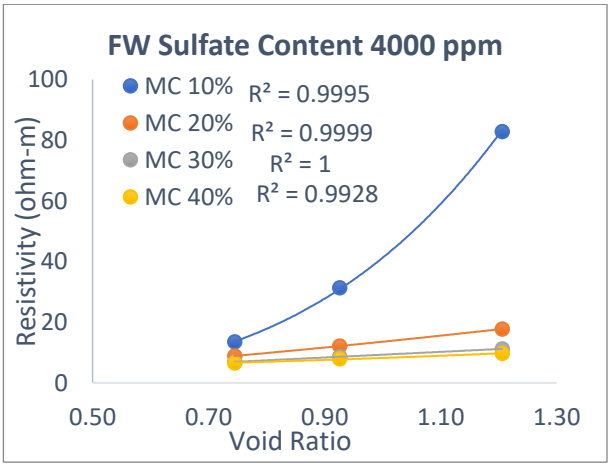
FW Sulfate Content 4000 ppm
MC 10% R² = 0.9995
MC 20% R² = 0.9999
MC 30% R² = 1
MC 40% R² = 0.9928
Resistivity (ohm-m)
Void Ratio
0
20
40
60
80
100
0.50
0.70
0.90
1.10
1.30

(c)

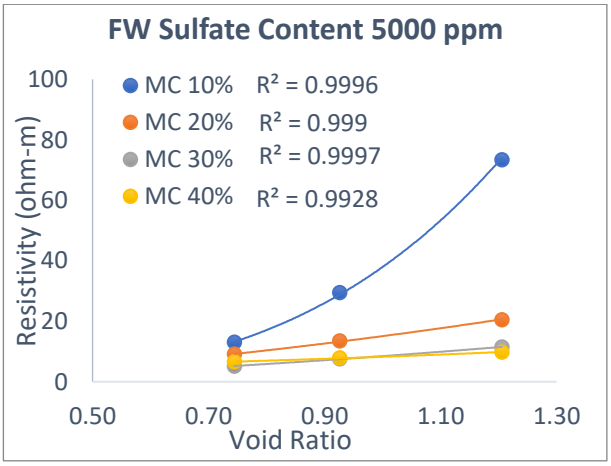
FW Sulfate Content 5000 ppm
MC 10% R² = 0.9996
MC 20% R² = 0.999
MC 30% R² = 0.9997
MC 40% R² = 0.9928
Resistivity (ohm-m)
Void Ratio
0
20
40
60
80
100
0.50
0.70
0.90
1.10
1.30

(d)

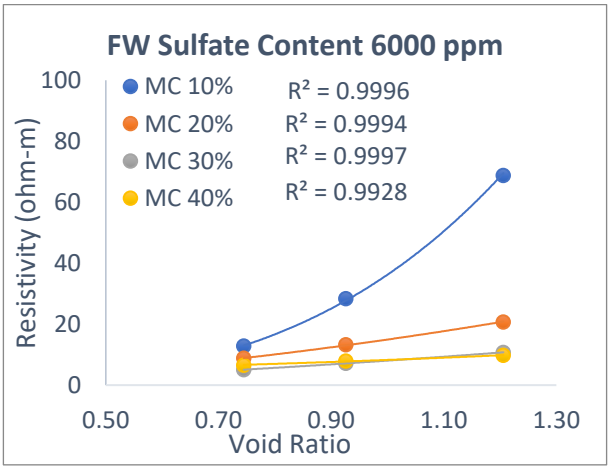
FW Sulfate Content 6000 ppm
MC 10% R² = 0.9996
MC 20% R² = 0.9994
MC 30% R² = 0.9997
MC 40% R² = 0.9928
Resistivity (ohm-m)
Void Ratio
0
20
40
60
80
100
0.50
0.70
0.90
1.10
1.30

(e)

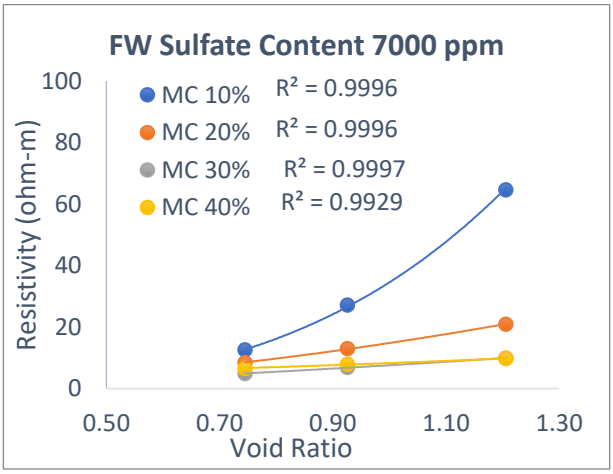
FW Sulfate Content 7000 ppm
MC 10% R² = 0.9996
MC 20% R² = 0.9996
MC 30% R² = 0.9997
MC 40% R² = 0.9929
Resistivity (ohm-m)
Void Ratio
0
20
40
60
80
100
0.50
0.70
0.90
1.10
1.30

(f)

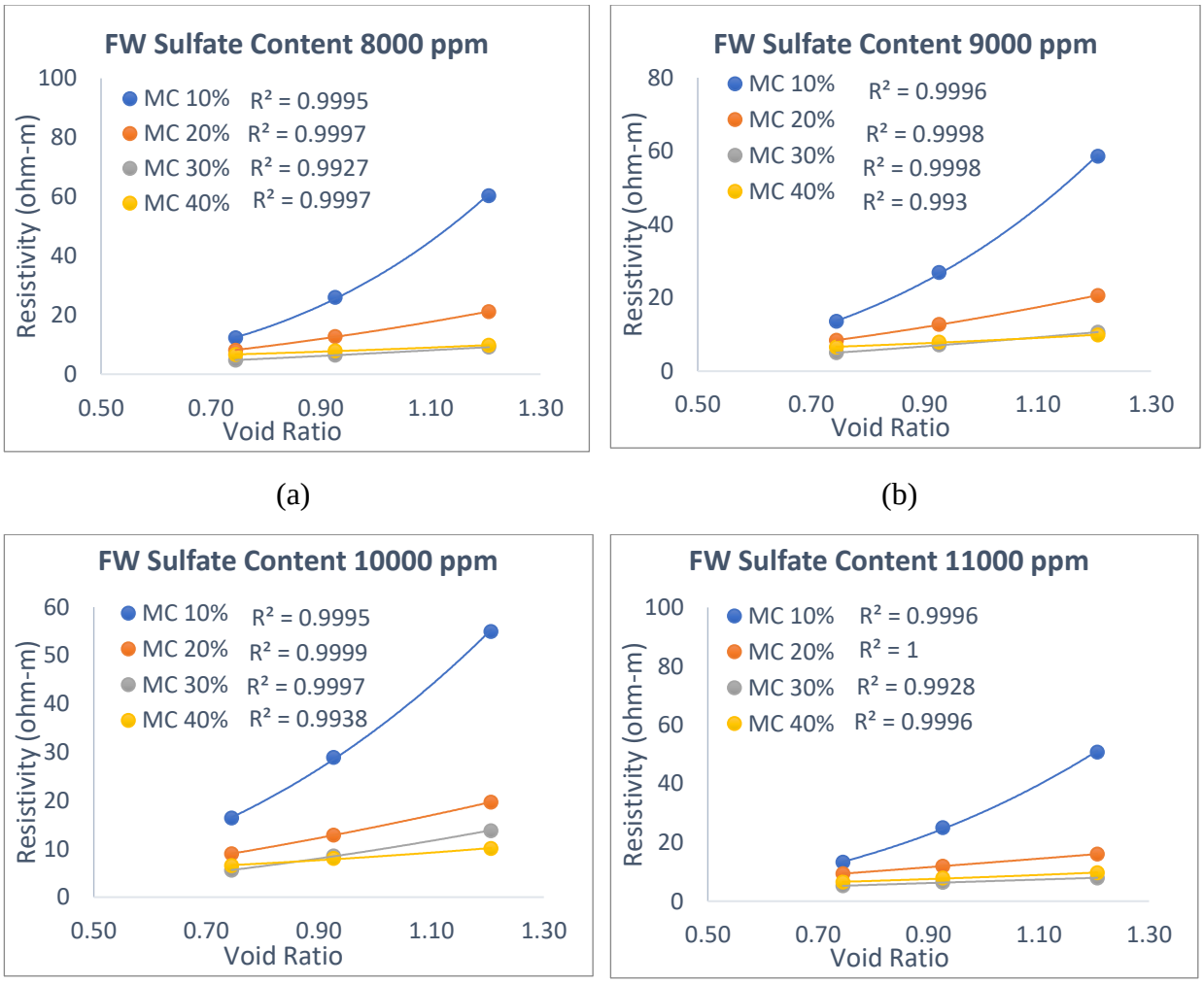

Figure 4-7: Relationship between electrical resistivity and void ratio.

The rate of change of resistivity with void ratio is not same for all the soil samples. It is observed from the graphs in Figure 4-7 that the rate of change of resistivity is higher in the lower sulfate content samples. As the sulfate content gets higher this rate of change in resistivity gets to a lower value.

4.3.2.3 Degree of saturation and resistivity

Figure 4-8 shows the relationship between resistivity and saturation level. Both the pattern of resistivity change and the trend of resistivity change with moisture content are same. Due to this, the resistivity in these moisture ranges has changed overall and decreased by 40 Ohm-m. The study of Mojid and Cho can be used to analyze the observed resistivity fluctuations as a function of moisture content (2006). According to the authors, moisture addition causes the double diffusion layer (DDL) on the clay surface to thicken, forming a bonding mechanism between the particles. Additionally, the precipitated ions on clay surfaces are more noticeable when exposed. Electrical conductivity is improved by exposing it to moisture. It is commonly acknowledged that there has been an increase in saturation, leading to a higher level of particle bridge formation. As a result, moisture bridges increase the current flow.

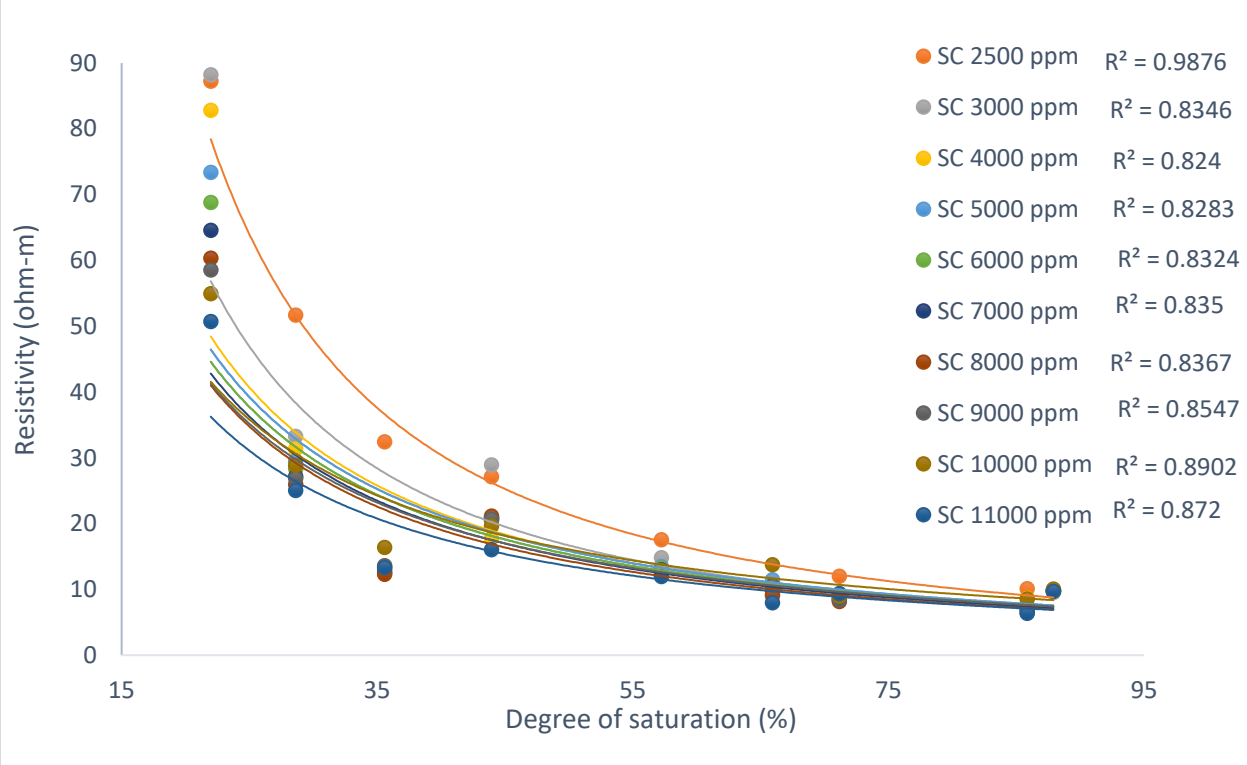

Figure 4-8: Resistivity and saturation level are correlated.

4.4 Resistivity Results for Sandy El Paso Soil

4.4.1 Influential Parameter Related to Soil Properties

Various influential parameters of soil properties are related to resistivity value i.e., fine content, clay content, activity, pore water conductivity, sulfate content, CEC & SSA. (Compacted El Paso samples were used to measure the effects of the soil characteristic on electrical resistivity values. Throughout the study degree of saturation was maintained to reduce the impact of saturation on the results of the resistivity. (Kibria & Hossain,2015). Various fixed degrees of saturation were taken to find out the influential parameter.

4.4.1.1 Sulfate Content and Resistivity

Sulfate ions in pore water play a major role in determining the resistivity value. The soil samples show higher conductivity when sulfate ions are present. In Figure 4-9, relationship between sulfate content and resistivity.

At lower moisture content of the resistivity goes down as the sulfate content goes up for all the varying unit weight. However, the rate of change in resistivity is very high for the 10% moisture content opposed to the lower rate of change in 20% moisture content. For the 30% and 40% moisture content the rate of change in resistivity is not very noticeable.

In Figure 4-10, it is observed that different unit weight will have impact on the resistivity value. For 10% moisture content, for all the sulfate content levels resistivity value for 11.8 KN/m^3 has significantly higher opposed to the 13.4 KN/m^3 or 14.9 KN/m^3. However, as the moisture content goes higher to 30% or 40% the effect of dry unit weight on resistivity value gets reduced.

There is an average 35 Ohm-m drop in resistivity value for the difference in moisture content of 10% to 30%. However, this difference is not same for all the sulfate content levels. As the sulfate content goes higher, this difference in resistivity for gain in moisture content goes lower. Though this trend is followed throughout all three-unit weight ranges, the amplitude of difference in resistivity for 10% and 30% is not same for all three-unit weight. For 13.4 KN/m^3 we can see average drop in resistivity of 17 Ohm-m for shifting in 10% to 30% moisture content and for 14.9

KN/m^3 we can see average drop in resistivity of 10 Ohm-m for shifting in 10% to 30% moisture content.

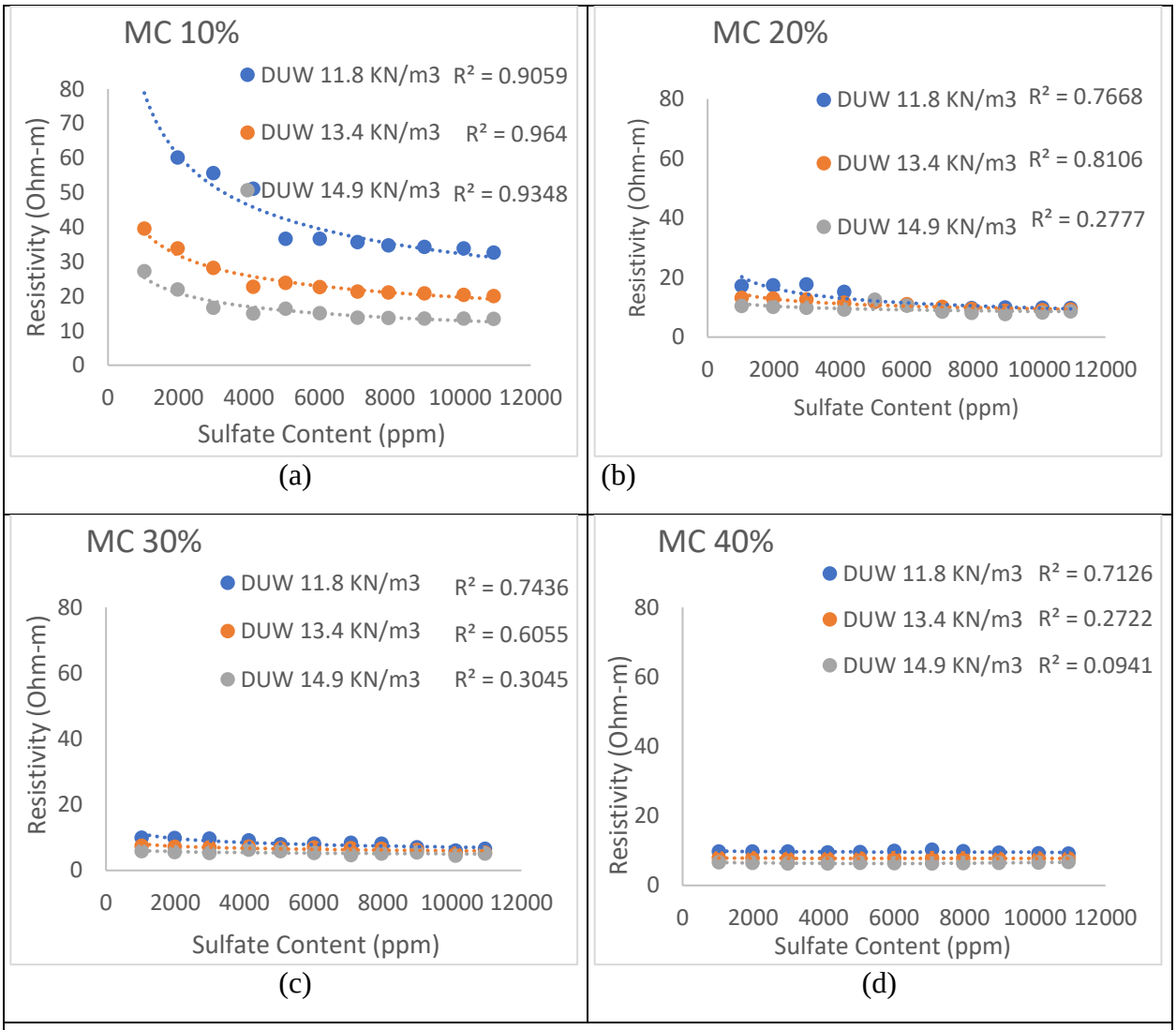

Figure 4-9: Relationship between sulfate content and resistivity in different moisture content level.

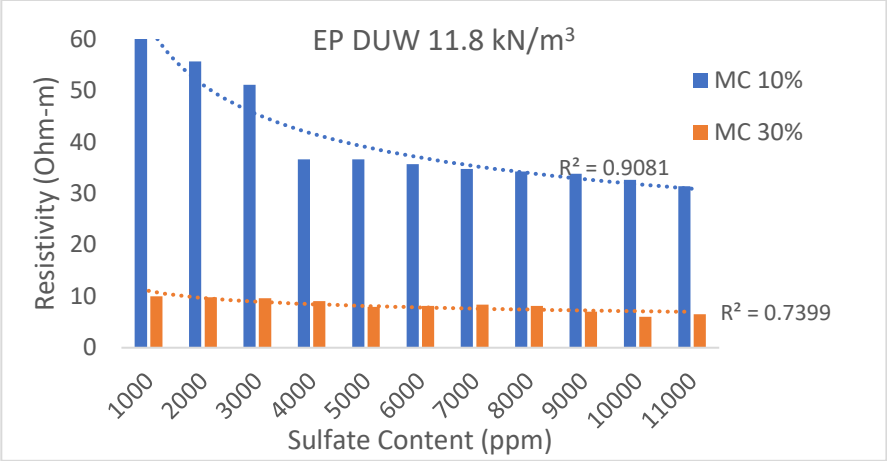

(a)

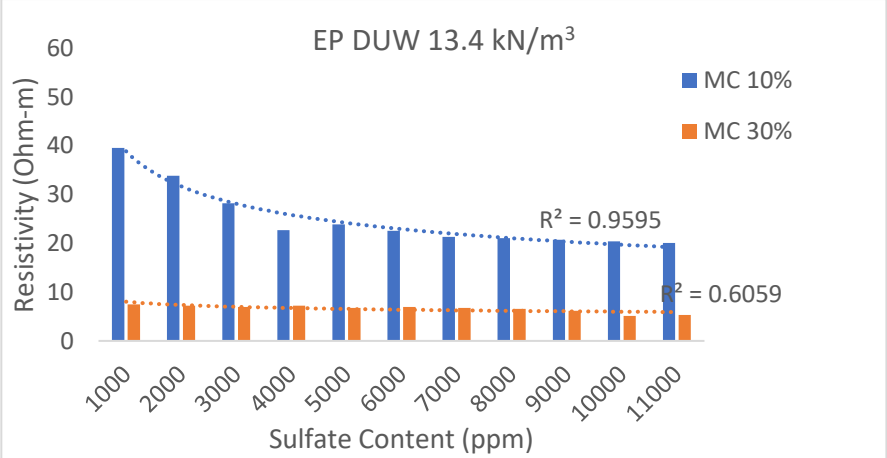

(b)

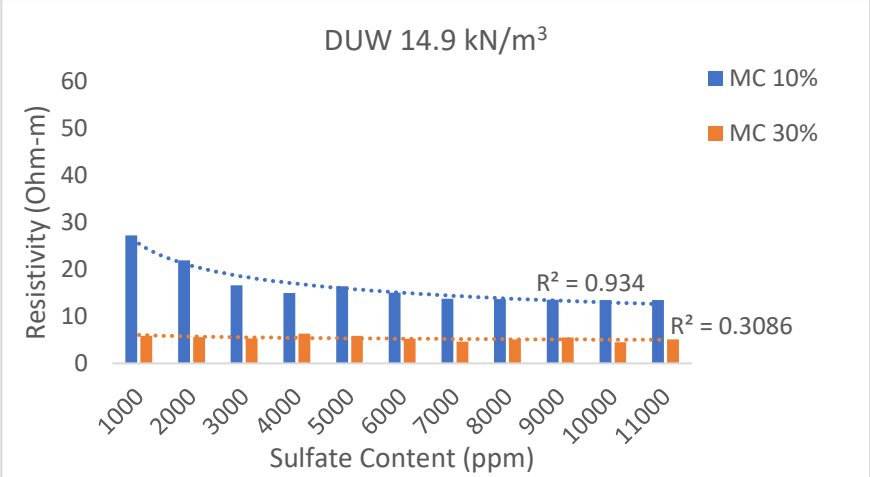

(c)

Figure 4-10: Resistivity vs Sulfate Content for different dry unit weight.

4.4.2 Influential Parameters related to Phase Relationship

El Paso soil sample had more sand content in it. To see the relationship among resistivity and the soil parameters tests were done on the El Paso sample.

4.4.2.1 Gravimetric Moisture Content and Resistivity

Figure 4-11 illustrates the variation of resistivity of sandy soil of El Paso district with different gravimetric moisture content at variable unit weight and sulfate content.

In this study average resistivity values for 11.8 KN/m^3 dry unit weight and 10%, 20%, 30%, 40% moisture content was found out to be 40.66 Ohm-m with standard deviation of 10.75 Ohm-m, 12.17 Ohm-m with standard deviation of 3.24 Ohm-m, 8.09 Ohm-m with standard deviation of 1.28 Ohm-m, 9.63 Ohm-m with standard deviation of 0.32 Ohm-m respectively.

For the case of 13.4 KN/m^3 and 10%, 20%, 30%, 40% moisture content resistivity value was found out to be 23.98 Ohm-m with standard deviation of 5.35 Ohm-m, 10.71 Ohm-m with standard deviation of 1.58 Ohm-m, 6.54 Ohm-m with standard deviation of 1.58 Ohm-m, 6.99 Ohm-m with standard deviation of 2.45 Ohm-m respectively.

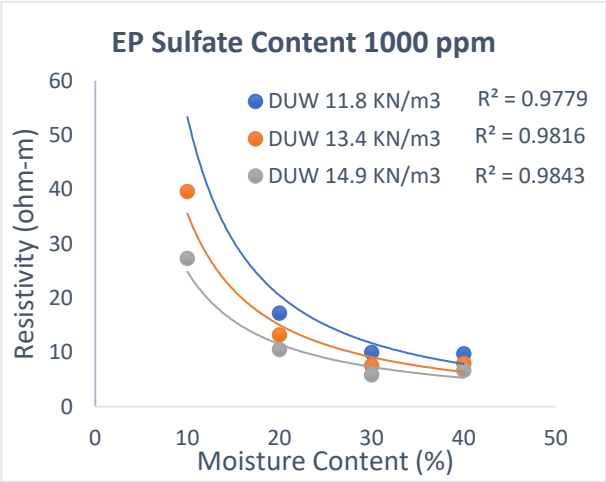

(a)

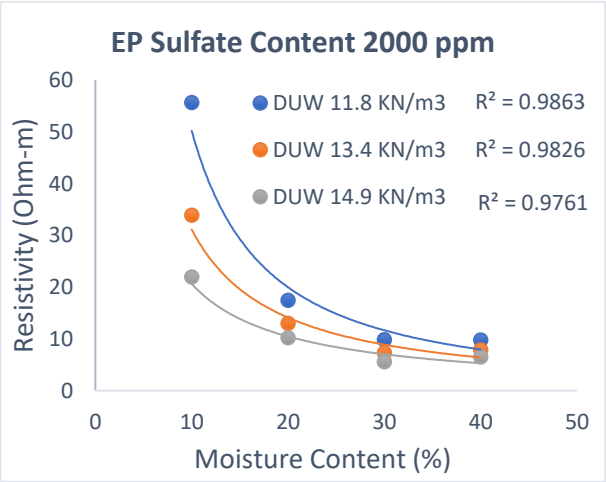

(b)

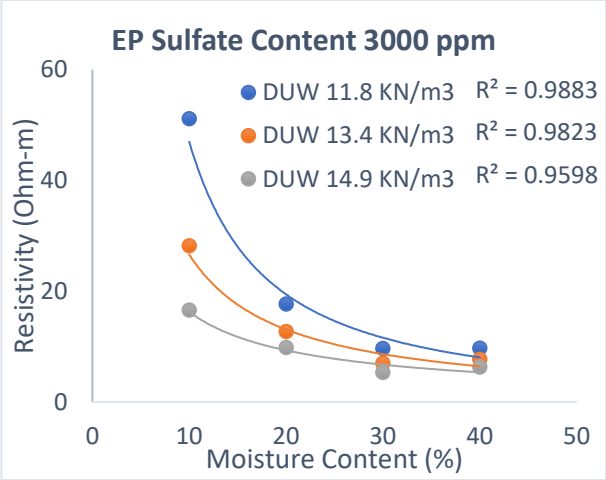
EP Sulfate Content 3000 ppm
DUW 11.8 KN/m3 R² = 0.9883
DUW 13.4 KN/m3 R² = 0.9823
DUW 14.9 KN/m3 R² = 0.9598
Resistivity (Ohm-m)
Moisture Content (%)
0
20
40
60
0
10
20
30
40
50

(c)

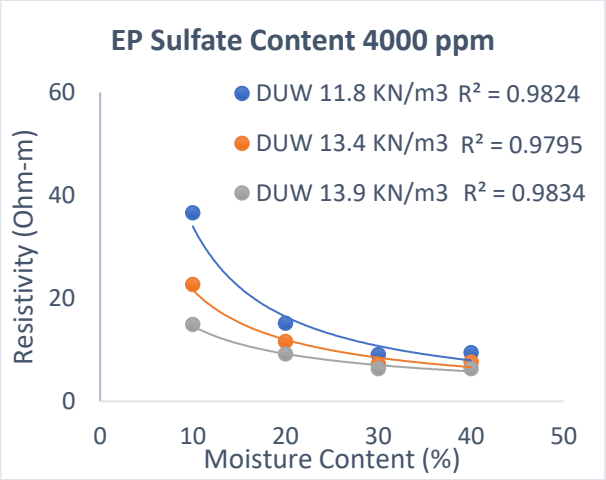
EP Sulfate Content 4000 ppm
DUW 11.8 KN/m3 R² = 0.9824
DUW 13.4 KN/m3 R² = 0.9795
DUW 13.9 KN/m3 R² = 0.9834
Resistivity (Ohm-m)
Moisture Content (%)
0
20
40
60
0
10
20
30
40
50

(d)

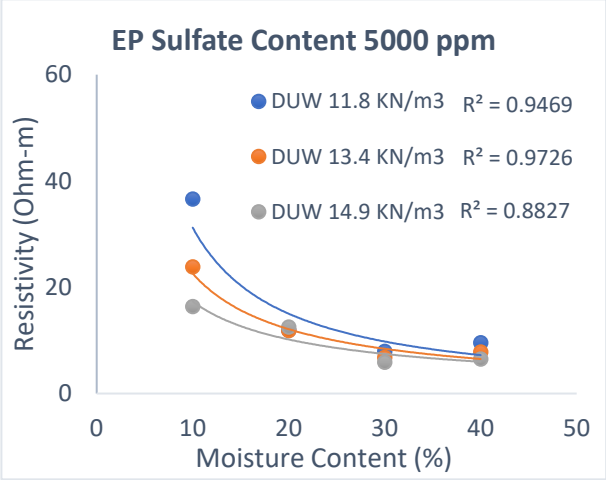
EP Sulfate Content 5000 ppm
DUW 11.8 KN/m3 R² = 0.9469
DUW 13.4 KN/m3 R² = 0.9726
DUW 14.9 KN/m3 R² = 0.8827
Resistivity (Ohm-m)
Moisture Content (%)
0
20
40
60
0
10
20
30
40
50

(e)

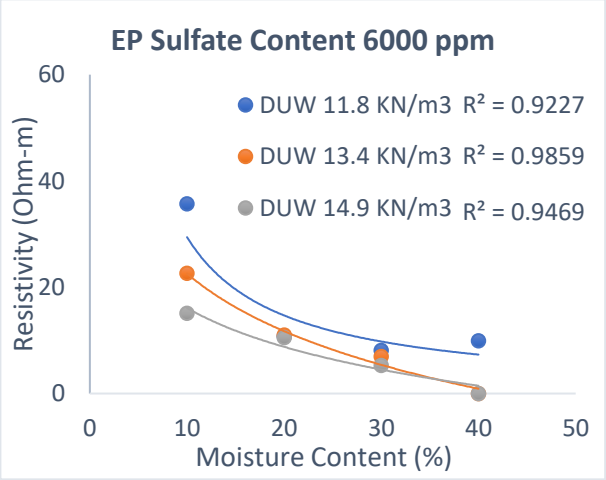
EP Sulfate Content 6000 ppm
DUW 11.8 KN/m3 R² = 0.9227
DUW 13.4 KN/m3 R² = 0.9859
DUW 14.9 KN/m3 R² = 0.9469
Resistivity (Ohm-m)
Moisture Content (%)
0
20
40
60
0
10
20
30
40
50

(f)

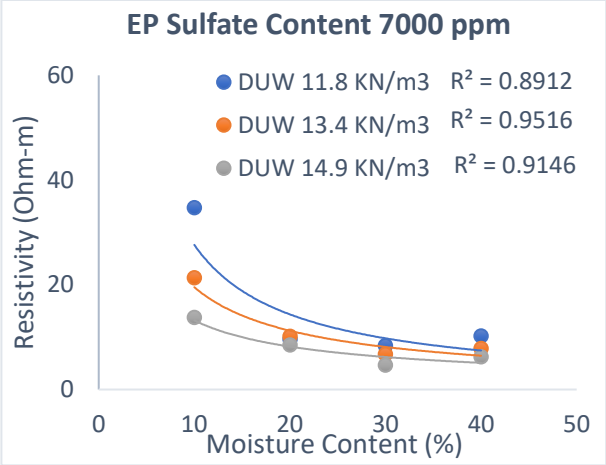

(g)

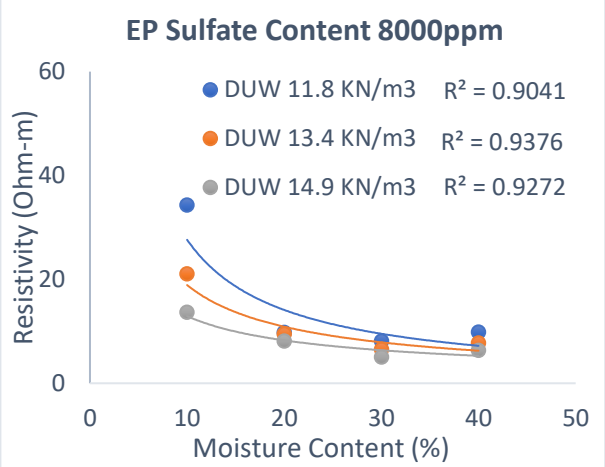

(h)

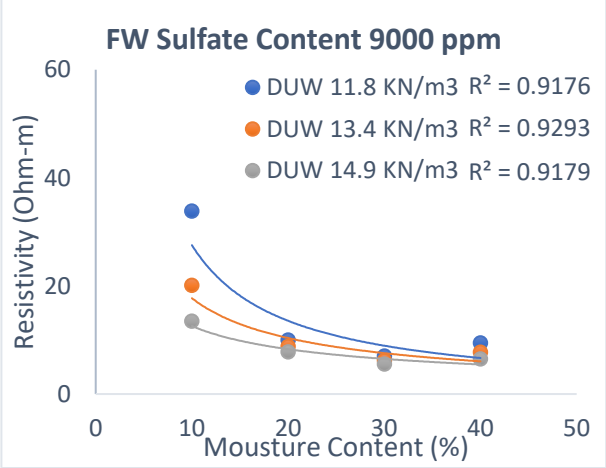

(i)

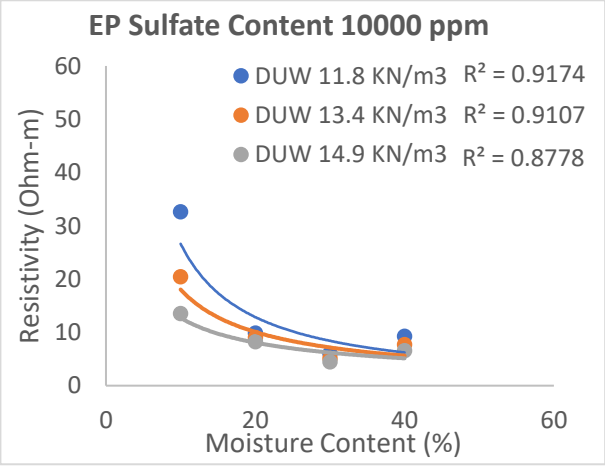

(j)

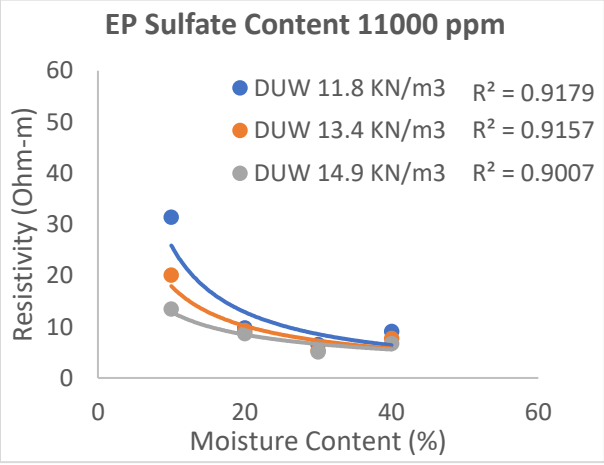

(k)

Figure 4-11: Electrical resistivity and moisture content of EP soil: a relationship.

The resistivity for soil with 14.9 KN/m^3 and 10%, 20%, 30%, 40% moisture content was found out to be 15.81 Ohm-m with standard deviation of 3.35 Ohm-m, 9.39 Ohm-m with standard deviation of 1.46 Ohm-m, 5.34 Ohm-m with standard deviation of 0.554 Ohm-m, 5.82 Ohm-m with standard deviation of 2.04 Ohm-m respectively.

4.4.2.2 Dry Unit Weight and Resistivity

In Figure 4-12 for different moisture content resistivity is expressed as a function of dry unit weight. It is seen that the resistivity decreases as the unit weight increase, however, the rate of decrease is not the same for all the sulfate content levels. The average decrease in resistivity for increase of unit weight from 11.8 KN/m^3 to 14.9 KN/m^3 is 77.7% for 10% moisture content, 57.17% for 20% moisture content, 44.48% for 30% moisture content and 31.5% for 40% moisture content.

The rate of change in resistivity with increasing unit weight for 10% moisture content is the highest. However, the rate decreases as the moisture content goes up.

Furthermore, another parameter is important while describing the relationship between unit weight and resistivity value. From the Figure 4-12, it is seen that the rate of change in resistivity with unit weight decreases with the increase of sulfate content.

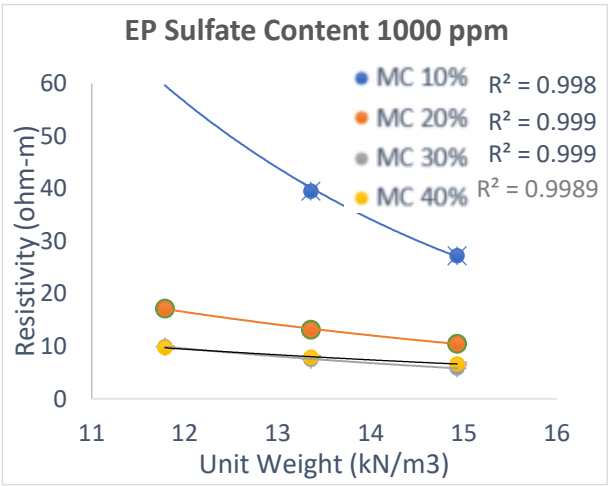

(a)

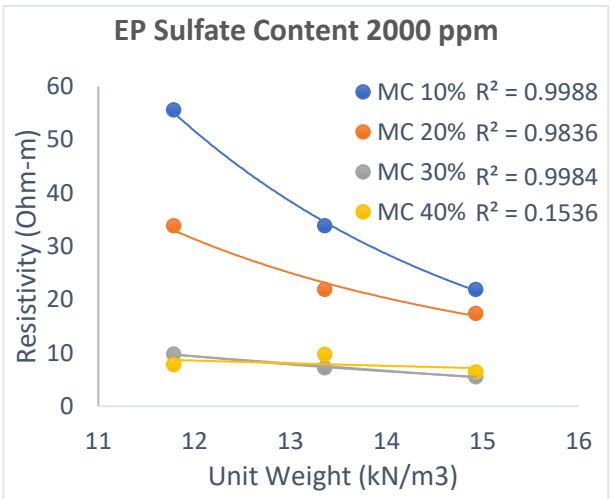

(b)

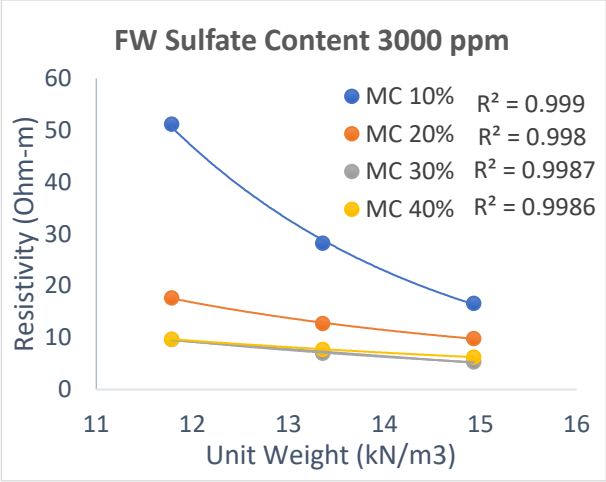
FW Sulfate Content 3000 ppm
MC 10% R² = 0.999
MC 20% R² = 0.998
MC 30% R² = 0.9987
MC 40% R² = 0.9986
Resistivity (Ohm-m)
Unit Weight (kN/m3)

(c)

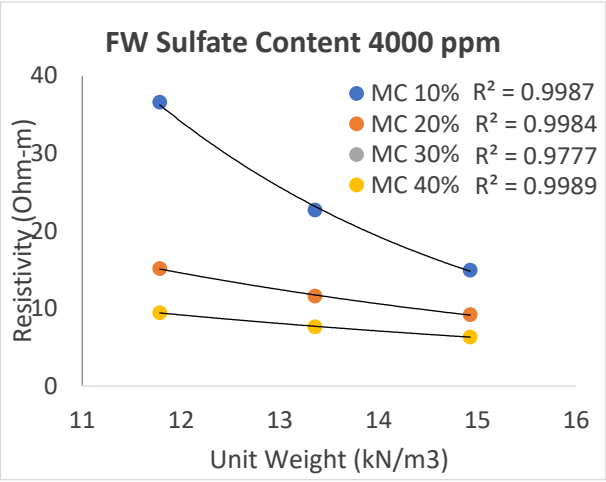
FW Sulfate Content 4000 ppm
MC 10% R² = 0.9987
MC 20% R² = 0.9984
MC 30% R² = 0.9777
MC 40% R² = 0.9989
Resistivity (Ohm-m)
Unit Weight (kN/m3)

(d)

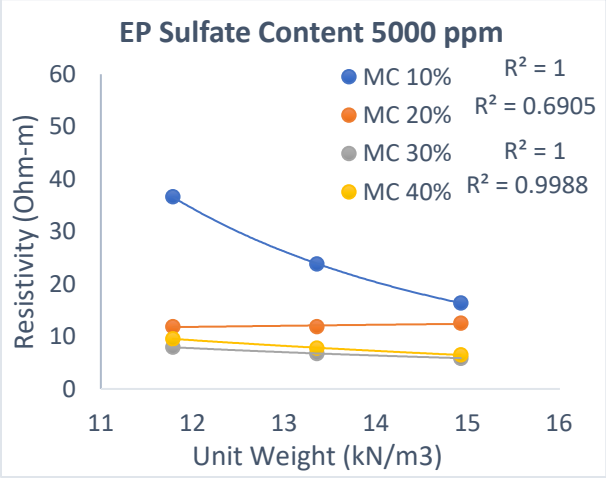
EP Sulfate Content 5000 ppm
MC 10% R² = 1
MC 20% R² = 0.6905
MC 30% R² = 1
MC 40% R² = 0.9988
Resistivity (Ohm-m)
Unit Weight (kN/m3)

(e)

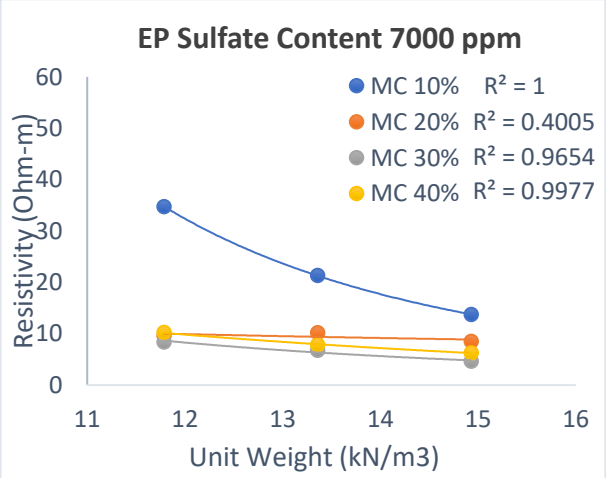
EP Sulfate Content 7000 ppm
MC 10% R² = 1
MC 20% R² = 0.4005
MC 30% R² = 0.9654
MC 40% R² = 0.9977
Resistivity (Ohm-m)
Unit Weight (kN/m3)

(f)

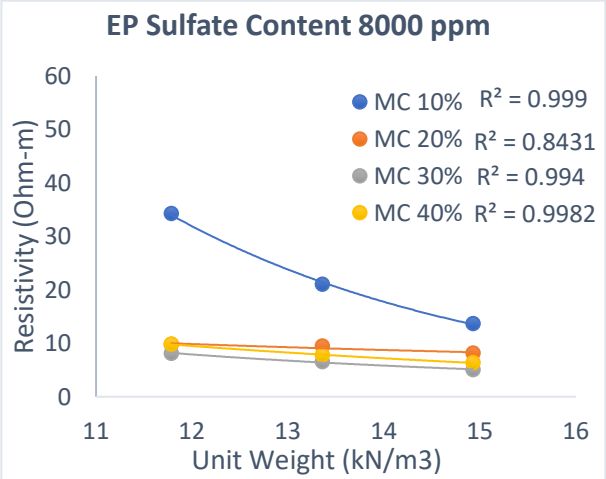
EP Sulfate Content 8000 ppm
MC 10% R² = 0.999
MC 20% R² = 0.8431
MC 30% R² = 0.994
MC 40% R² = 0.9982
Resistivity (Ohm-m)
Unit Weight (kN/m3)

(g)

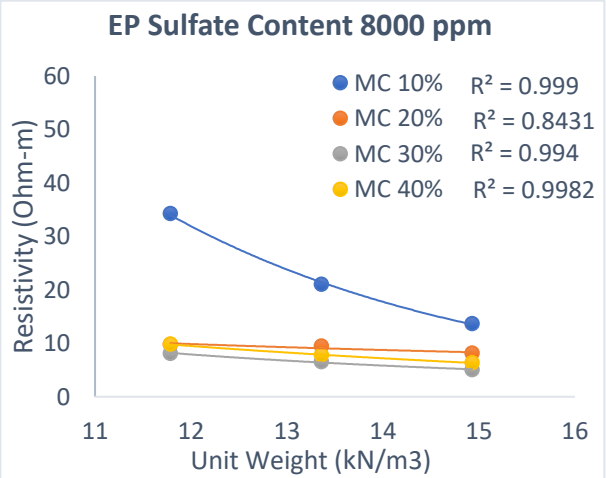
EP Sulfate Content 8000 ppm
MC 10% R² = 0.999
MC 20% R² = 0.8431
MC 30% R² = 0.994
MC 40% R² = 0.9982
Resistivity (Ohm-m)
Unit Weight (kN/m3)

(h)

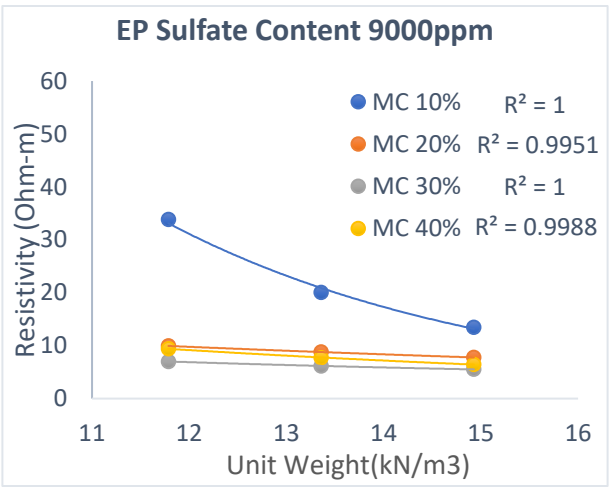

(i)

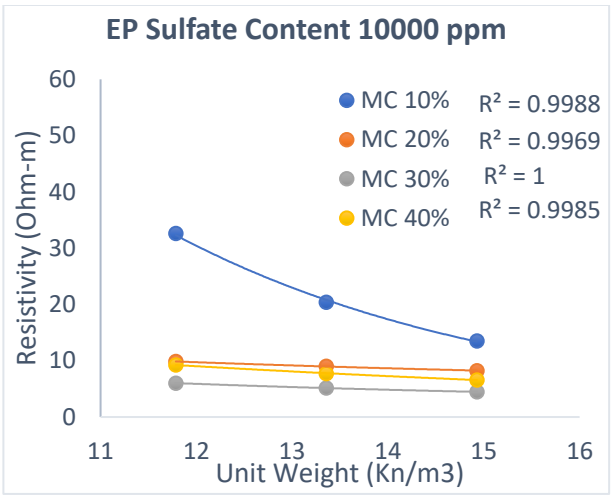

(j)

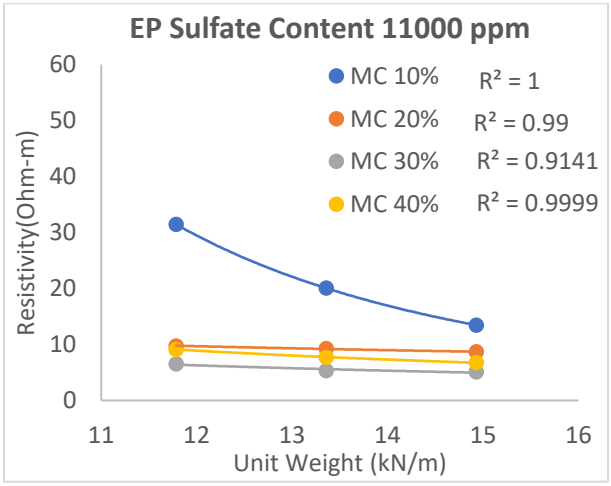

(k)

Figure 4-12: Relationship between resistivity and unit weight of compacted El Paso soil

4.4.2.3 Void Ratio and Resistivity

For the El Paso soil sample, the change in resistivity with change in void ratio at different moisture content was plotted in Figure 4-13. As void ratio was increasing the resistivity was increasing. However, depending on the soil sample type and moisture content in it, the rate of the resistivity change was varying. When the soil has more air void the electron carrying capacity decreases and thus resistivity values go up.

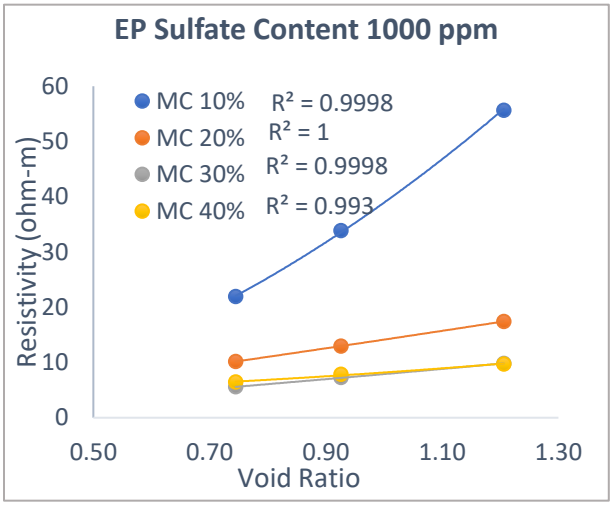
EP Sulfate Content 1000 ppm
MC 10% R² = 0.9998
MC 20% R² = 1
MC 30% R² = 0.9998
MC 40% R² = 0.993
Resistivity (ohm-m)
Void Ratio
0
10
20
30
40
50
60
0.50
0.70
0.90
1.10
1.30

(a)

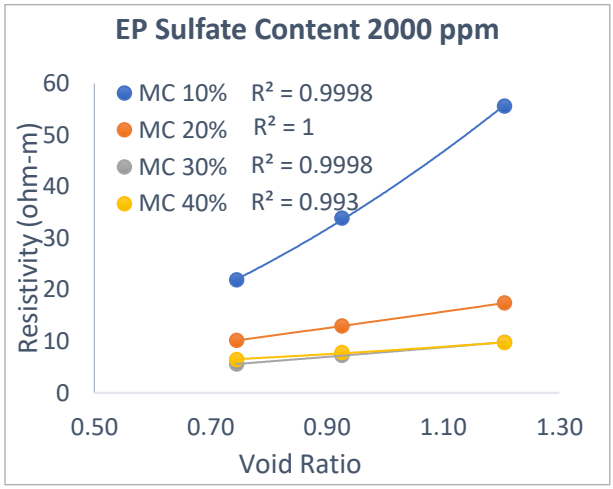
EP Sulfate Content 2000 ppm
MC 10% R² = 0.9998
MC 20% R² = 1
MC 30% R² = 0.9998
MC 40% R² = 0.993
Resistivity (ohm-m)
Void Ratio
0
10
20
30
40
50
60
0.50
0.70
0.90
1.10
1.30

(b)

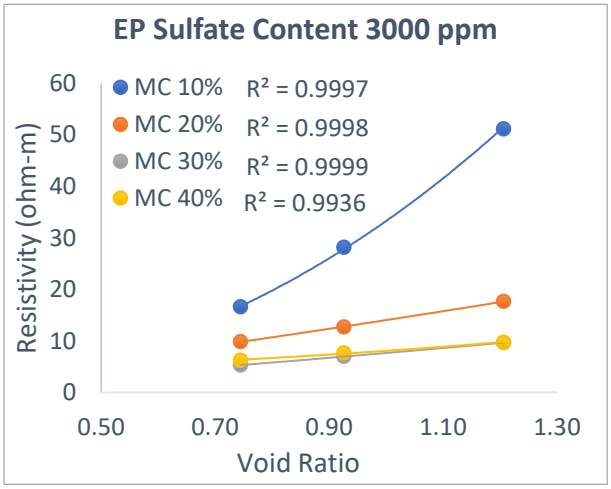
EP Sulfate Content 3000 ppm
MC 10% R² = 0.9997
MC 20% R² = 0.9998
MC 30% R² = 0.9999
MC 40% R² = 0.9936
Resistivity (ohm-m)
Void Ratio
0
10
20
30
40
50
60
0.50
0.70
0.90
1.10
1.30

(c)

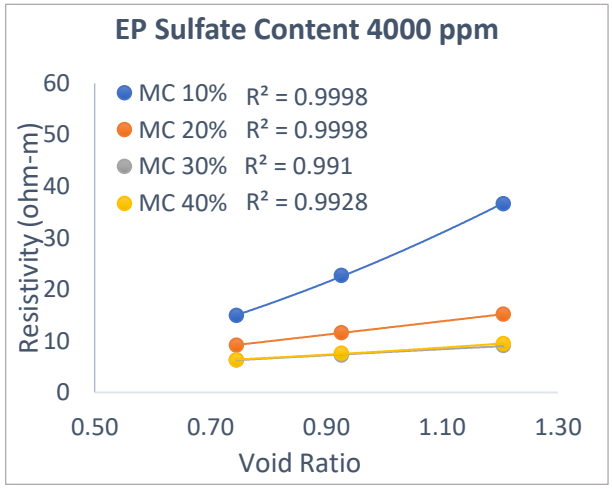
EP Sulfate Content 4000 ppm
MC 10% R² = 0.9998
MC 20% R² = 0.9998
MC 30% R² = 0.991
MC 40% R² = 0.9928
Resistivity (ohm-m)
Void Ratio
0
10
20
30
40
50
60
0.50
0.70
0.90
1.10
1.30

(d)

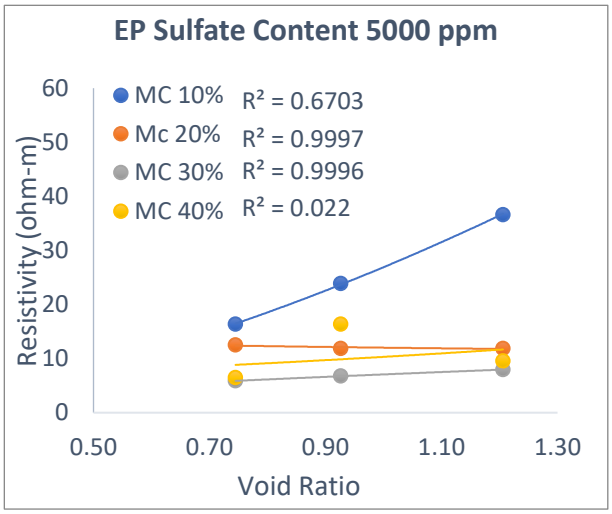
EP Sulfate Content 5000 ppm
MC 10% R² = 0.6703
Mc 20% R² = 0.9997
MC 30% R² = 0.9996
MC 40% R² = 0.022
Resistivity (ohm-m)
Void Ratio
0
10
20
30
40
50
60
0.50
0.70
0.90
1.10
1.30

(e)

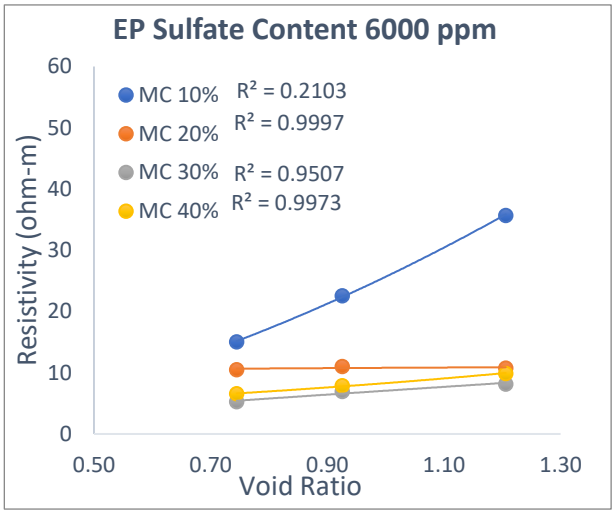
EP Sulfate Content 6000 ppm
MC 10% R² = 0.2103
MC 20% R² = 0.9997
MC 30% R² = 0.9507
MC 40% R² = 0.9973
Resistivity (ohm-m)
Void Ratio
0
10
20
30
40
50
60
0.50
0.70
0.90
1.10
1.30

(f)

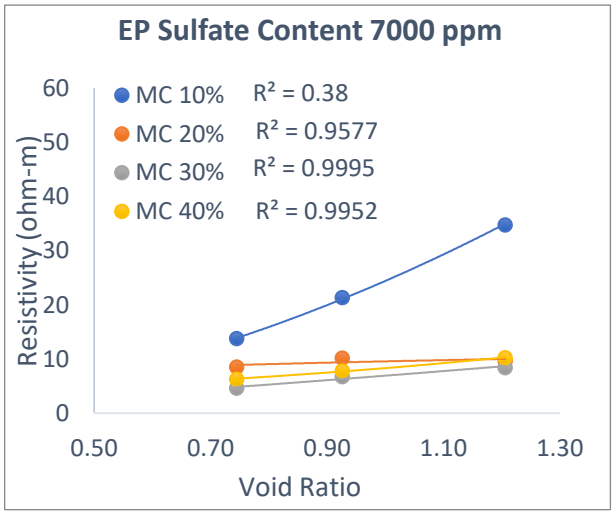
EP Sulfate Content 7000 ppm
MC 10% R² = 0.38
MC 20% R² = 0.9577
MC 30% R² = 0.9995
MC 40% R² = 0.9952
Resistivity (ohm-m)
Void Ratio
0
10
20
30
40
50
60
0.50
0.70
0.90
1.10
1.30

(g)

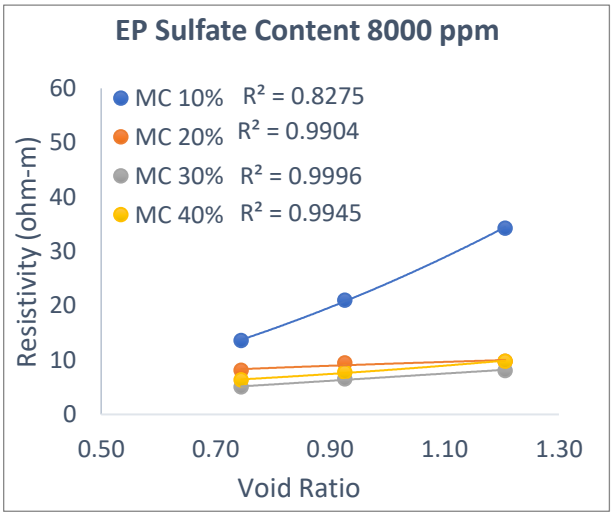
EP Sulfate Content 8000 ppm
MC 10% R² = 0.8275
MC 20% R² = 0.9904
MC 30% R² = 0.9996
MC 40% R² = 0.9945
Resistivity (ohm-m)
Void Ratio
0
10
20
30
40
50
60
0.50
0.70
0.90
1.10
1.30

(h)

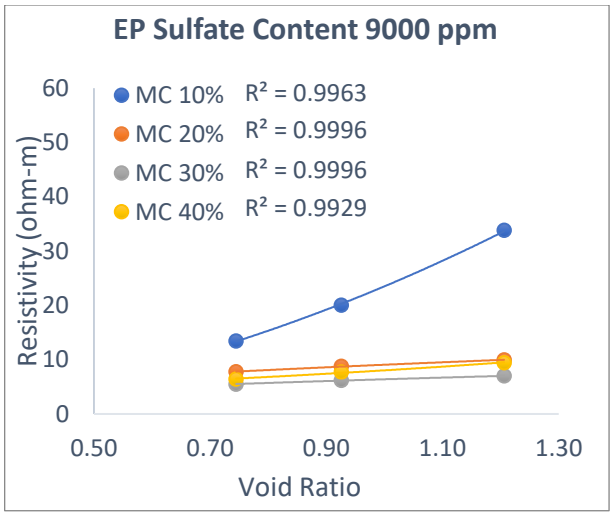

(i)

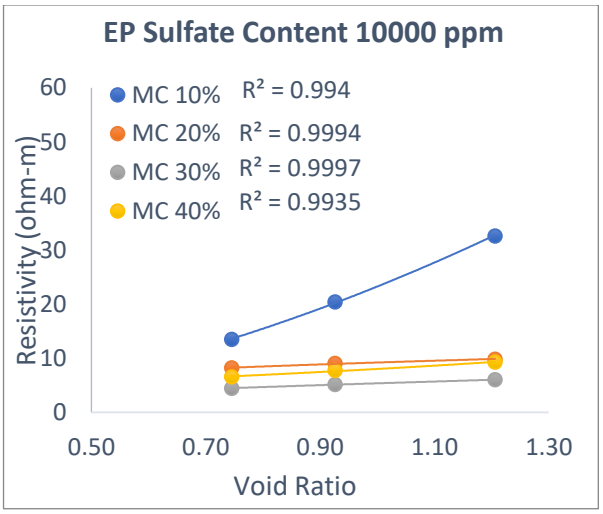

(j)

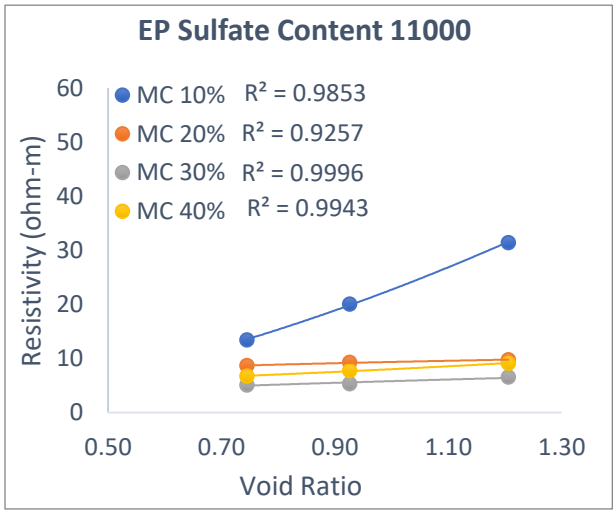

(k)

Figure 4-13: Relationship between electrical resistivity and void ratio.

4.4.2.4 Degree of Saturation and Resistivity

Figure 4-14 shows the relationship between resistivity and degree of saturation. The figure clearly shows as the degree of saturation gets closer towards 100% the resistivity values go down. This caused the resistivity to drop around 40-50 Ohm-m as the saturation levels get high from around 20% to 95%. The study of Mojid and Cho can be used to analyze the observed resistivity fluctuations as a function of moisture content (2006). According to the authors, moisture addition causes the double diffusion layer (DDL) on the clay surface to thicken, forming a bonding mechanism between the particles. Additionally, the precipitated ions on clay surfaces are more noticeable when exposed. Electrical conductivity is improved by exposing it to moisture. It is commonly acknowledged that there has been an increase in saturation, leading to a higher level of particle bridge formation. As a result, moisture bridges increase the current flow.

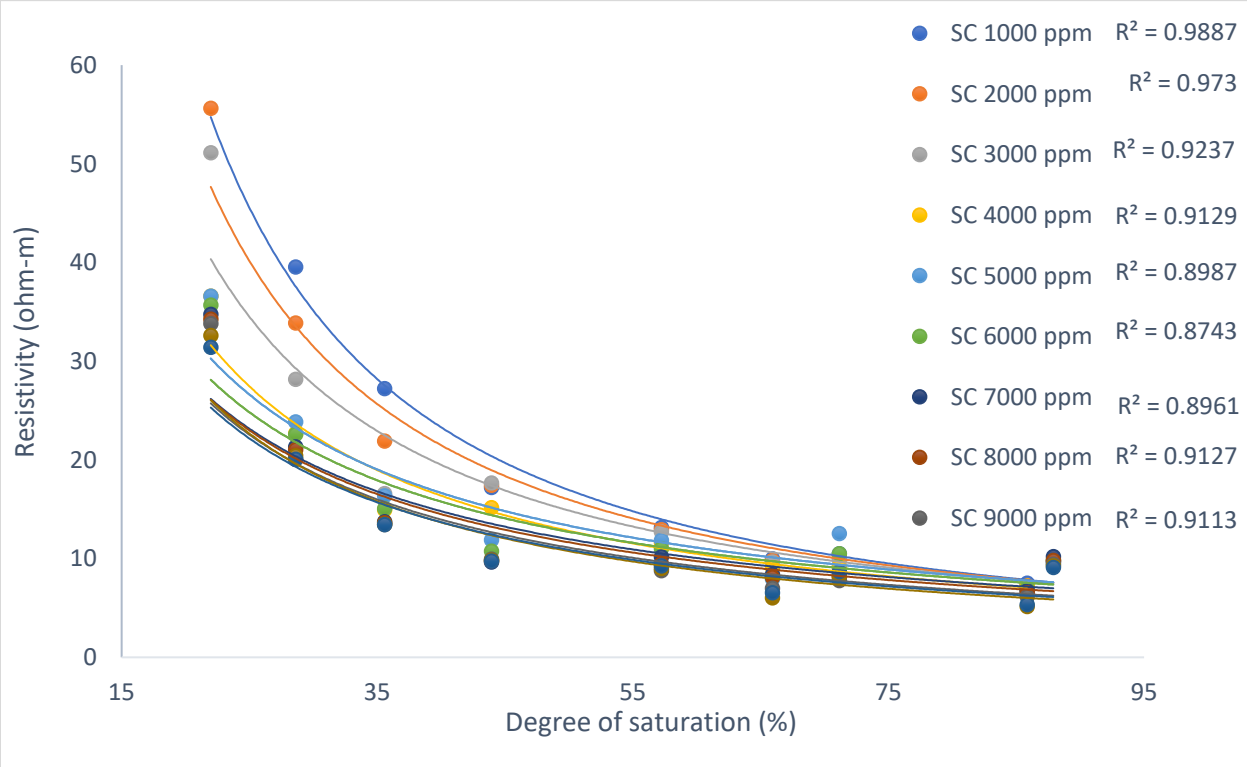

Figure 4-14: Relationship between electrical resistivity and degree of saturation.

CHAPTER 5: STATISTICAL ANALYSIS

5.1 Introduction

To characterize the electrical resistivity of soil, there aren't many electrical mixing models. Moisture from the soil must be removed in order to estimate conductivity from pore water conductivity. It is, however, challenging to execute.

The goal of this study is to create a statistical model that uses the other geotechnical features of soil to correlate electrical resistivity with sulfate content. The technique can be used to link the sulfate content of soil samples taken from compacted soils and their resistivity.

In this work, model assumptions were investigated, and multiple linear regression (MLR) studies were carried out using the statistical analysis application R-Studio. a list of the actions as seen in Figure 5-1, the MLR model was developed to contain.

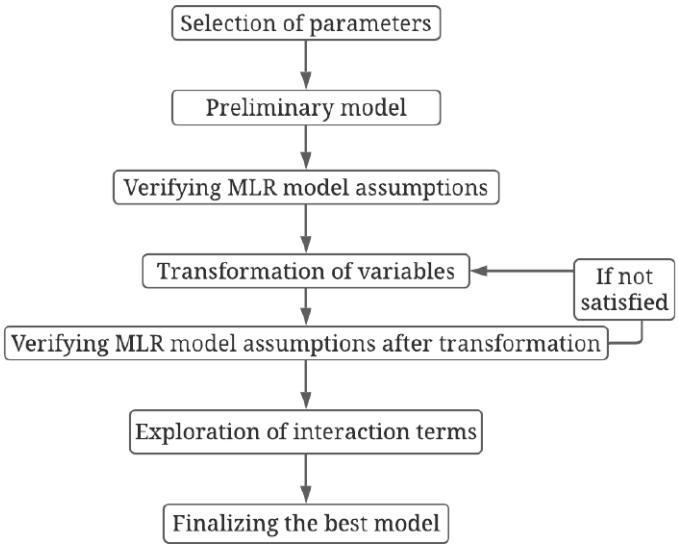

Figure 5-1: Model development steps

5.2 Parameter Selection for Model

Moisture content, unit weight, fine content all relates to geotechnical parameters. However, sulfate content in soil can’t be correlated with the geotechnical parameter as efficiently as other’s can be. In this study, the aim was to investigate the relationship between soil electrical resistivity and the sulfate content and geotechnical properties of soil using the intended models.

Predictors for the model were chosen so that there was little correlation between them. The created model might not be very accurate if the predictors exhibit a high level of collinearity. This could result in a lower regression coefficient, a higher variance, and difficulties articulating how a predictor's unit change affects the response (Pituch and Stevens, 2015). In practical situations, predictors can't always be controlled, and there is linkage between them. Multi-collinearity is the term used to describe the issue of interaction between predictor variables. If there is a high correlation between the predictors, the model's predictors will have a significant impact on the outcome. In this case, it might not be appropriate to adjust the predicted results for a unit change in a predictor variable. Three drawbacks of multi-collinearity in an MLR model include: a) lowering the coefficient of regression; b) making it difficult to assess the significance of the variables; and c) raising the variance (Stevens, 2012).

The objective of this study is to develop a Multiple Linear Regression (MLR) model to correlate Resistivity of soil with sulfate content, moisture content, fine content and dry unit weight so that sulfate content can be obtained from resistivity value rather that testing for sulfate content which is time consuming process. In this study, Resistivity(R) was modeled as response, while Moisture Content (MC), Dry Unit Weight (γ_d), Fine content(FC) and Sulfate Content(SC) were predictors.

The decision was made to incorporate all of the factors in the preliminary statistical model because all of the independent predictors have some influence on the response. These were the parameters' notations:

R= Resistivity (Ohm-m)

MC= Moisture Content (%)

FC= Fine content (%)

SC= Sulfate Content (ppm)

(γ_d) = Dry Unit Weight (kN/m^3)

According to research on the impact of important physical characteristics on the electrical resistivity of soil, dry weight and moisture content had a big impact on electrical resistance responses. Additionally, it was established how void ratio and volumetric moisture content affected electrical resistance. According to the phase relation of soil, the quantity of soil per unit weight of soil is inversely proportional with the number of voids it contains. (Figure 5-2).

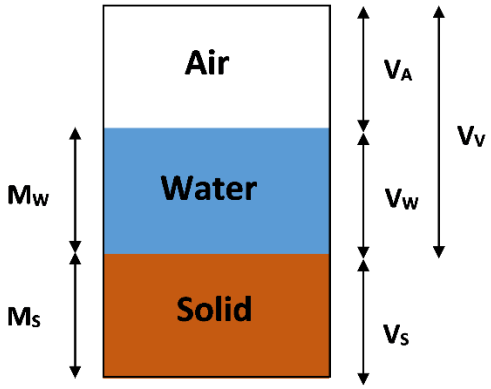

Figure 5-2: Relationship between soil phase (geoengineer.org)

Using the following equation, the degree of saturation can be estimated based in it's dry unit weight, gravimetric moisture content and void ratio:

$$\gamma_d = \frac{\gamma_w G_s}{1 + e}$$

Here, γ_d = dry unit weight, w = gravimetric moisture content, e = void ratio.

5.3 Multiple Linear Regression Analysis

A thorough explanation of the multiple linear regression analysis is provided in this section. A MLR equation was created to predict resistivity as a function of moisture content, fine content, sulfate content, and dry unit weight based on the results of the lab tests.

5.3.1 Correlation Analysis

No correlation should exist between the predictor variables (Kutner et al., 2005). However, in some circumstances, the predictor variables are frequently related to one another in practice. Multicollinearity is the presence of relationships between the independent variables. In these situations, it may be impossible to interpret the regression parameters in a useful way. The MLR model will have problems if the predictor variables have a high degree of correlation.

5.3.1.1 Response vs Predictor Plots

Figure 5-3 displays the relationship between the response variable and each of the predictor factors.. The relationship between the response and predictors are not following any trend.

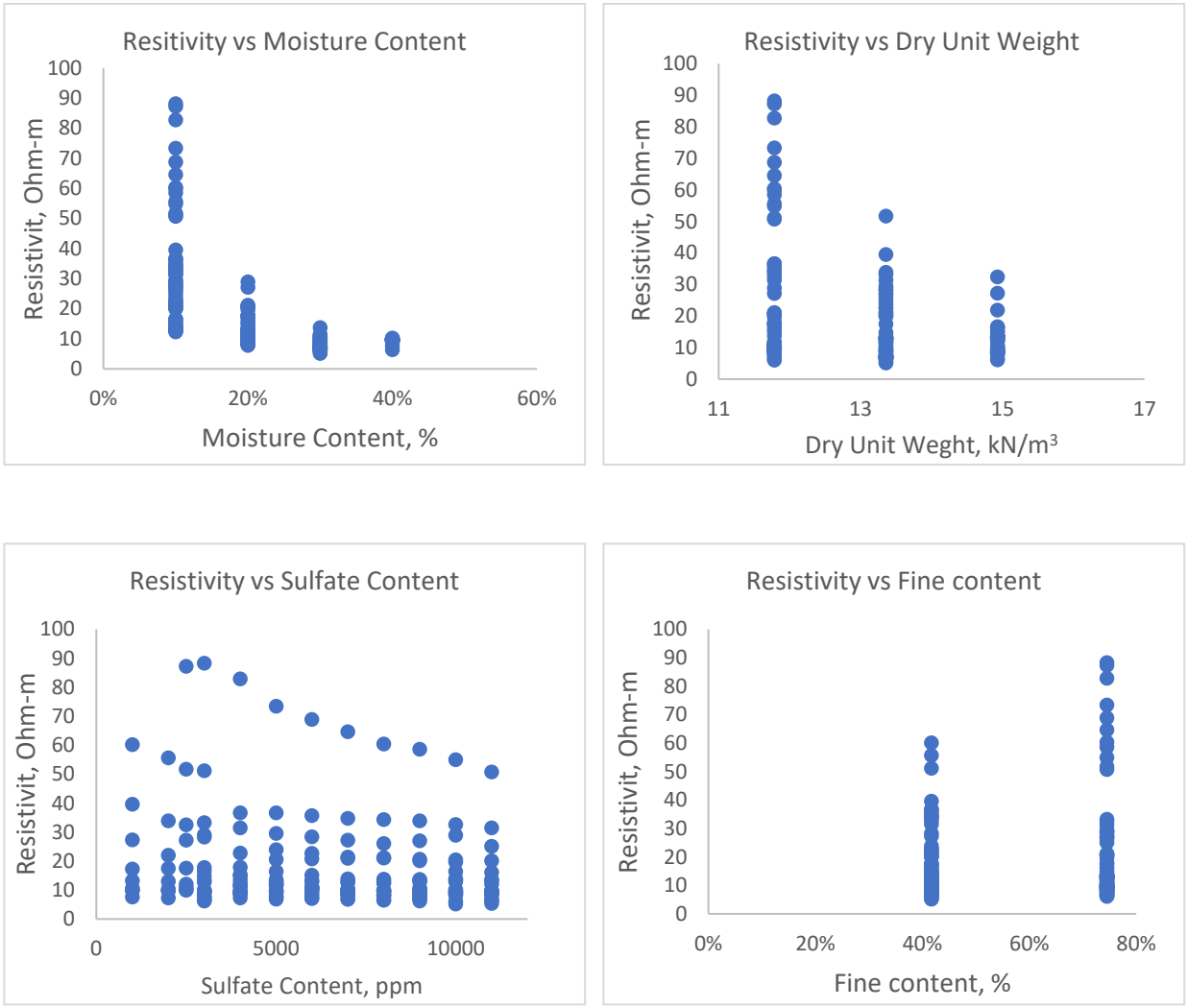

Figure 5-3: Response vs Predictor Plots.

5.3.1.2 Predictor vs Predictor Plots

The predictor vs. predictor plots can be used to assess the multicollinearity between predictor variables. There is no discernible association between any of the predictor variables, as shown by the predicting plot in Figure 5-4. Table 5-1 displays the Pearson Coefficients between the predictors. The Resistivity and Dry Unit Weight had the strongest correlation, which was -0.35. But according to Kutner et al. (2005), a correlation less than 0.7 can be regarded as poor. Therefore, no discernible collinearity between the predictor variables was found.

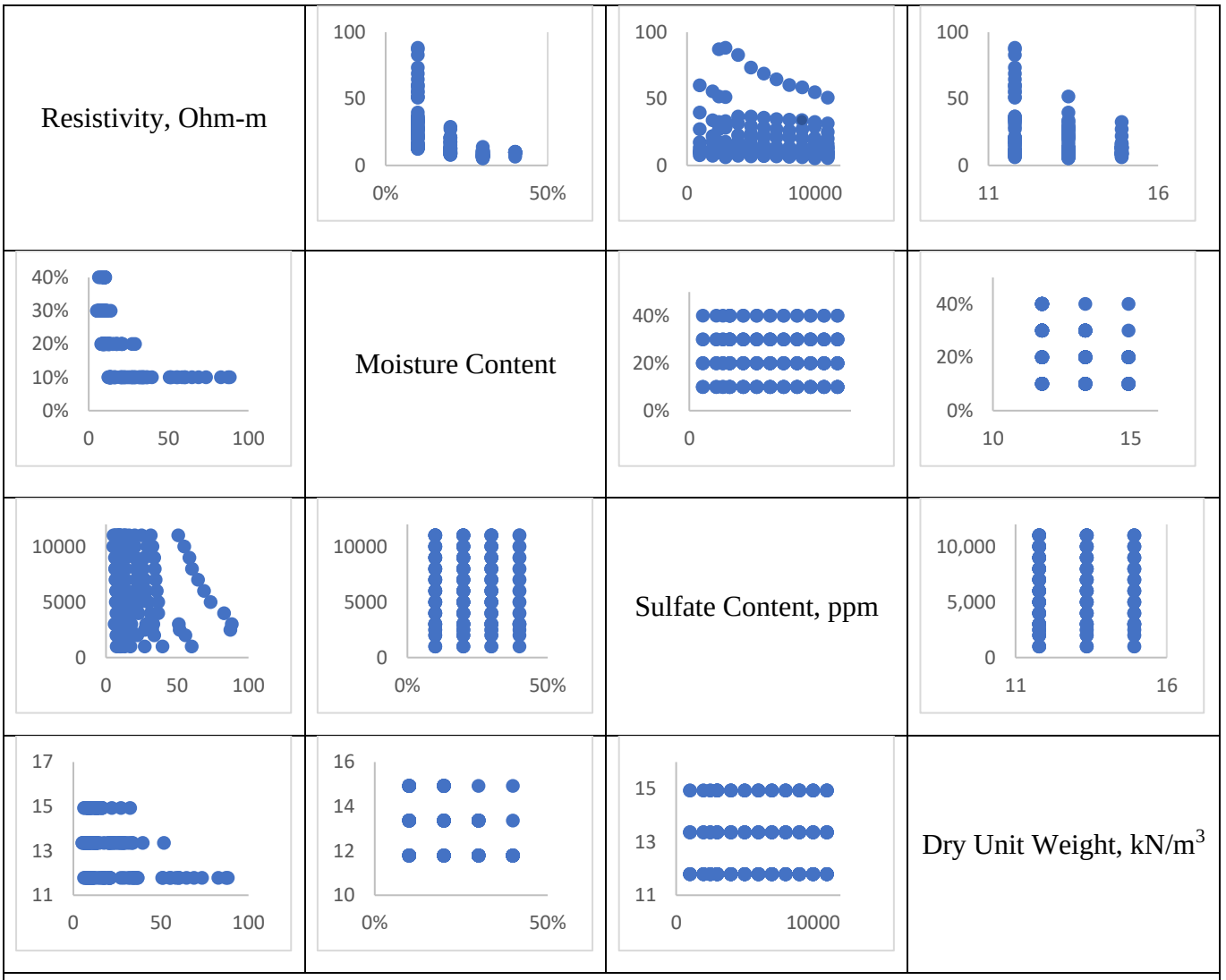

Figure 5-4: The correlation among the predictor variables (R, MC, SC, DUW)

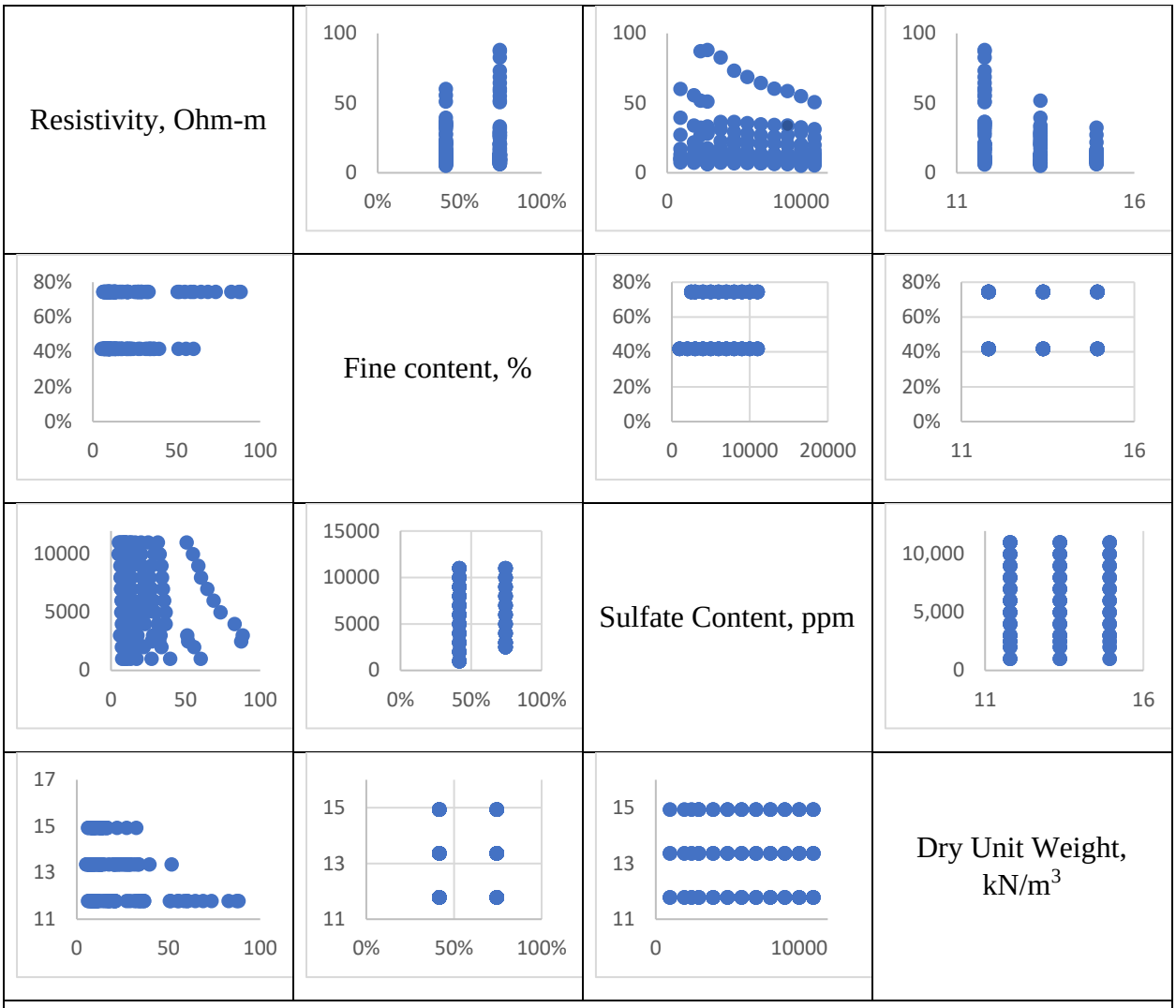

Figure 5-5: The correlation among the predictor variables (R, FC, SC, DUW)

Table 5-1: Correlation among the Predictor Variables

Variables	MC	SC	Dry Unit Weight	FC
MC	1	-0.025	-0.35	0.025
SC	-0.025	1	-0.018	0.072
Dry Unit Weight	-0.35	-0.018	1	-0.019
FC	0.025	0.072	-0.019	1

The linear correlation between the response and the predictor was also measured using the Pearson Correlation Coefficient. Table 6-2 shows the correlation between resistivity and predictor variable based on the statistical analysis. Negative values mean Resistivity will decrease with those predictors increasing. On the other hand, positive values mean resistivity will increase with FC increase.

Table 5-2: Correlation between the Resistivity and Predictor Variable

R	MC	DUW	SC	FC
1	-0.57	-0.27	-0.14	0.16

5.3.2 Development of Preliminary Model

A rudimentary model for multiple linear regression was created, correlating Resistivity (R) with Moisture Content (MC), Dry Unit Weight (DUW), Sulfate Content (SC) and Fine content (FC).

The preliminary MLR Model was found as follows:

$$R = \beta_0 + \beta_1 SC + \beta_2 MC + \beta_3 DUW + \beta_4 FC + \varepsilon_i \qquad (5.1)$$

Regression parameters include R= Resistivity (Ohm-m), MC= Moisture Content (%), FC= Fine Content (%), SC= Sulfate Content (ppm), and (d)= Dry Unit Weight (kN/m3). By minimizing the sum of squared errors for the model data, regression analysis is used to calculate the correlation coefficients 0, 1, 2, 3, and 4. I represents a random error.

When all other predictor variables are held constant, the correlation coefficients are physically significant because they can explain variations in the mean response per unit change of a predictor variable. The parameters of the regression were estimated by minimizing the total squared errors of the sample. The predictor factors are quantitative in nature. Multiple linear regression was performed on the model data.

In Tables 5-3 and 5-4, respectively, the parameter estimates and the analysis of variance (ANOVA) summary, are shown. The correlation coefficients' sign conventions are as one would anticipate and are in line with the findings of laboratory test data. Sulfate Content, Moisture Content, and Unit Weight all had negative coefficients, which meant that as they rose, the value of Resistivity fell. The corrected R2 was excellent and is acceptable, according to the ANOVA summary. The residuals' p-value was also very low. Thus, the initial fitted MLR equation can be displayed as follows:

Table 5-3: The parameter estimates

	Coefficient	Std. Error	t value	Pr(>|t|)
(Intercept)	78.9	$4.580e^{+00}$	17.225	$<2e^{-16}$
SC	$-4.3773e^{-04}$	$1.09e^{-04}$	-4.014	$8.91e^{-5}$
MC	-76.16	$3.826e^{00}$	-19.908	$<2e^{-16}$
DUW	-3.698	$3.3028e^{-01}$	-12.213	$<2e^{-16}$
FC	5.756	$1.988e^{+00}$	2.895	0.000434

Table 5-4: The analysis of variance (ANOVA) summary

Residual Standard Error	R^2	Adjusted R^2	F-Statistic	p-value
11.38	0.71	0.70	101.5	<2.2e-16

5.3.3 Verification of Preliminary Model

Some assumptions must be satisfied by the Multiple Linear Regression (MLR) model. Some statistical tests including graphical plots will be used to verify the following model assumptions:

- ✓ The correlation between the predictors and the response should be linear.
- ✓ The residuals ought to have a fixed variance.
- ✓ The residuals must follow a normal distribution.
- ✓ The residuals shouldn't automatically correspond.

5.4 MLR Model Form

Relationships between residuals, predictor variables, and residual, fitted values Plots are typically used to determine whether linear regression is applicable for a given data set. When the residuals are located within this range, the linear regression model can be applied.

A band that runs horizontally and is centered on an axis. There must be a random distribution of points in the residuals vs predictors and no discernible systematic trend. The linear regression model is inapplicable, and a quadratic term is required in the model if there is any curvature in the plots.

5.4.1 Constant Error Variance

Finding constant error variance or homoscedasticity is made simpler with the aid of plots that display residuals versus predictor variables and residuals versus fitted values. When the residuals are displayed against the predictor variables, they should be randomly distributed with no discernible trend. Similar to this, when residuals are displayed against fitted values, there shouldn't be any obvious trend. This confirms that an MLR model's constant error variance has been met. Any curved trend or funnel shape suggests the presence of non-constant variation. In this situation, the regression may not be accurate. By changing the variables, this condition can be lessened.

Figure 5-6 displays a scattered plot of residuals versus fitted values. However, the plot does not show any significant curvilinear tendency (shown by red). The residuals appear to be dispersed at random. By using RStudio to run the studentized Breusch-Pagan test, additional analysis was carried out. The test's p-value was 0.0591, which is higher than = 0.01 The residuals are homoscedastic at = 0.01 and the null hypothesis could not be rejected as a result. The completed model met the requirement of constant error variance.

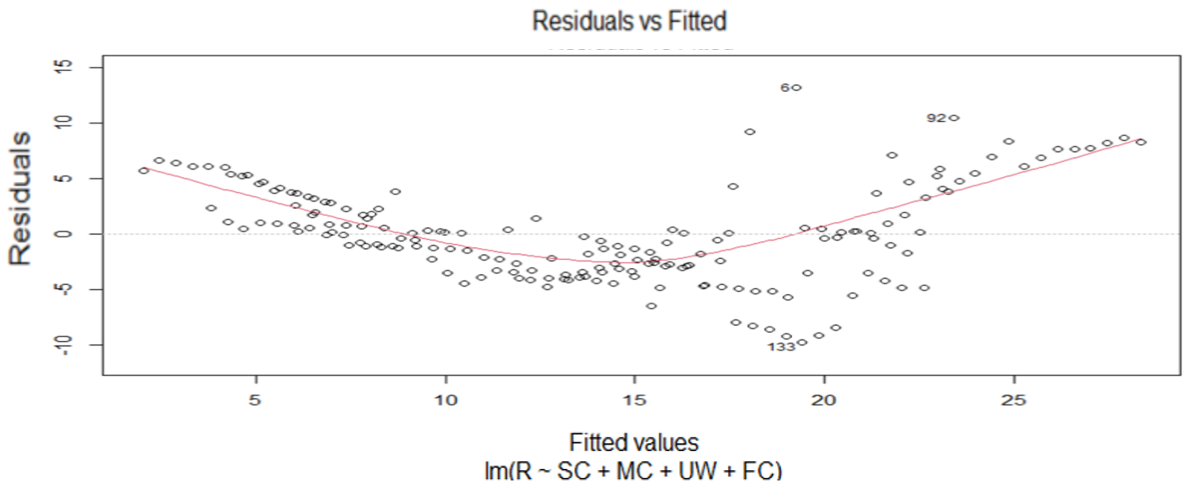

Figure 5-6: Residuals vs Fitted Values Plot for the Preliminary Model

5.4.2 Normality

The normal probability plot for the completed MLR model is shown in Figure 5-7. The plot reveals short tails on both sides. Shapiro-Wilk normality testing was done in RStudio to further confirm the normality assumption. The test produced an estimated p-value of 0.02, higher than 0.01. As a result, the null hypothesis could not be proven false, proving that the 146 residuals have a normal distribution with a =0.01. Figure 5-7's histogram depicts the normal distribution.

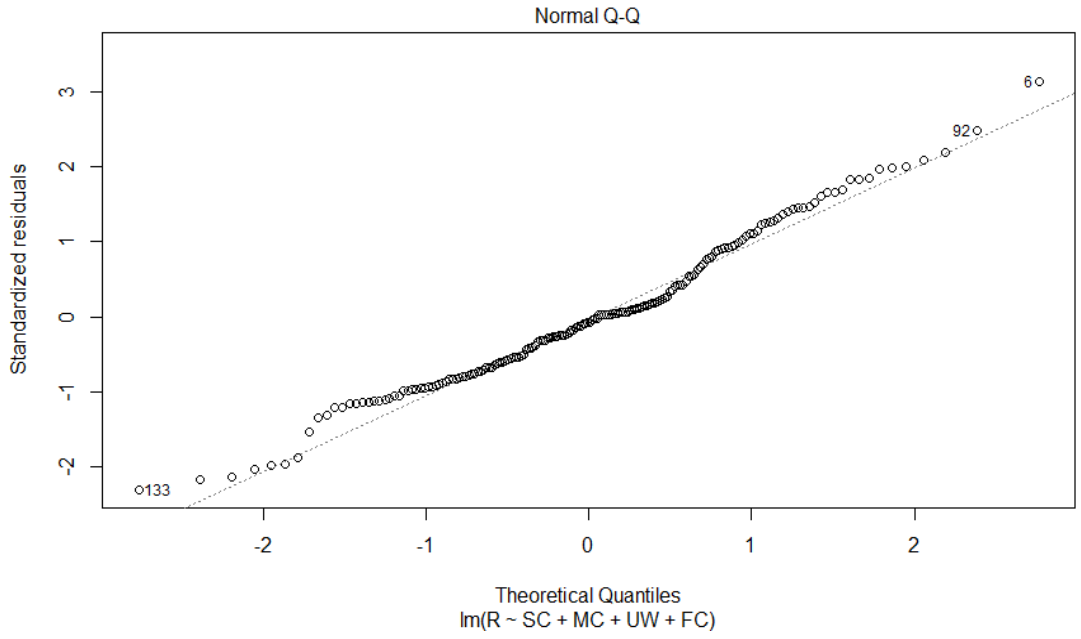

Figure 5-7: Normal Probability Plot for the Final Model

5.4.3 Outlier Test

A data set's outliers are some extremely rare observations. By dragging the fitted line disproportionately towards the extreme observation, they can trick the regression (Kutner et al., 2005). Several common tests in RStudio were used to determine whether there were any outliers. Outliers were found using the Bonferroni outlier test. Figures 5-8, 5-9, and 5-10 show the usage of DFFITS, DFBETAS, and Cook's Distance to assess the impact of the outliers in the initial model. DFFITS (Difference in Fits) calculates how much one observation affects the value anticipated. It is recommended that an observation be reported for further review if its absolute DFFITS value is more than 1 (for small to medium data sets). For medium to big data sets, an absolute DFBETAS value larger than 1 also recommends flagging the related observation. Also noted should be the observation where Cooks Distance (Di) > F (p, n p).

Several common tests in RStudio were used to determine whether there were any outliers. Outliers were found using the Bonferroni outlier test. The impact of the outliers on the final model was assessed using DFFITS, DFBETAS, and Cook's Distance. For this collection, the F-statistic for comparing the Cook's Distance was 1.151 for = 0.05. Additionally, it is advised that Di higher than 0.5 be looked at because it can have an impact (Faysal, 2017).

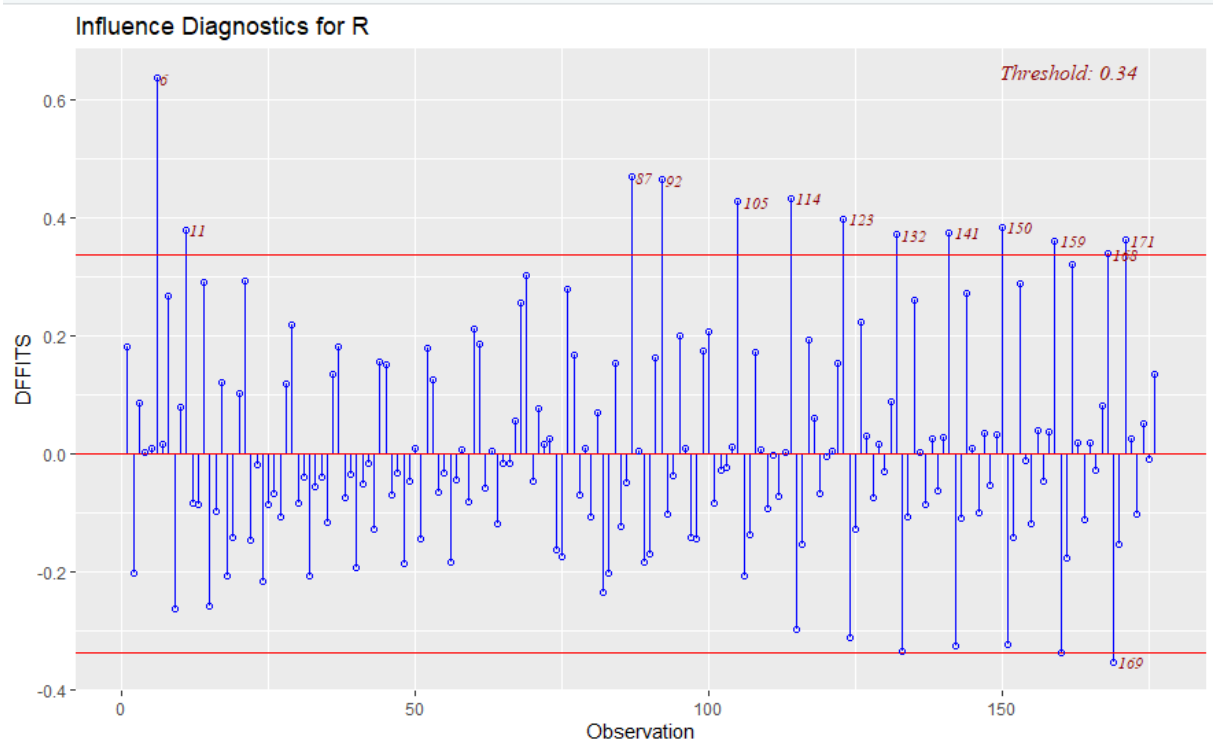

Figure 5-8: Outlier test by using DFFITS

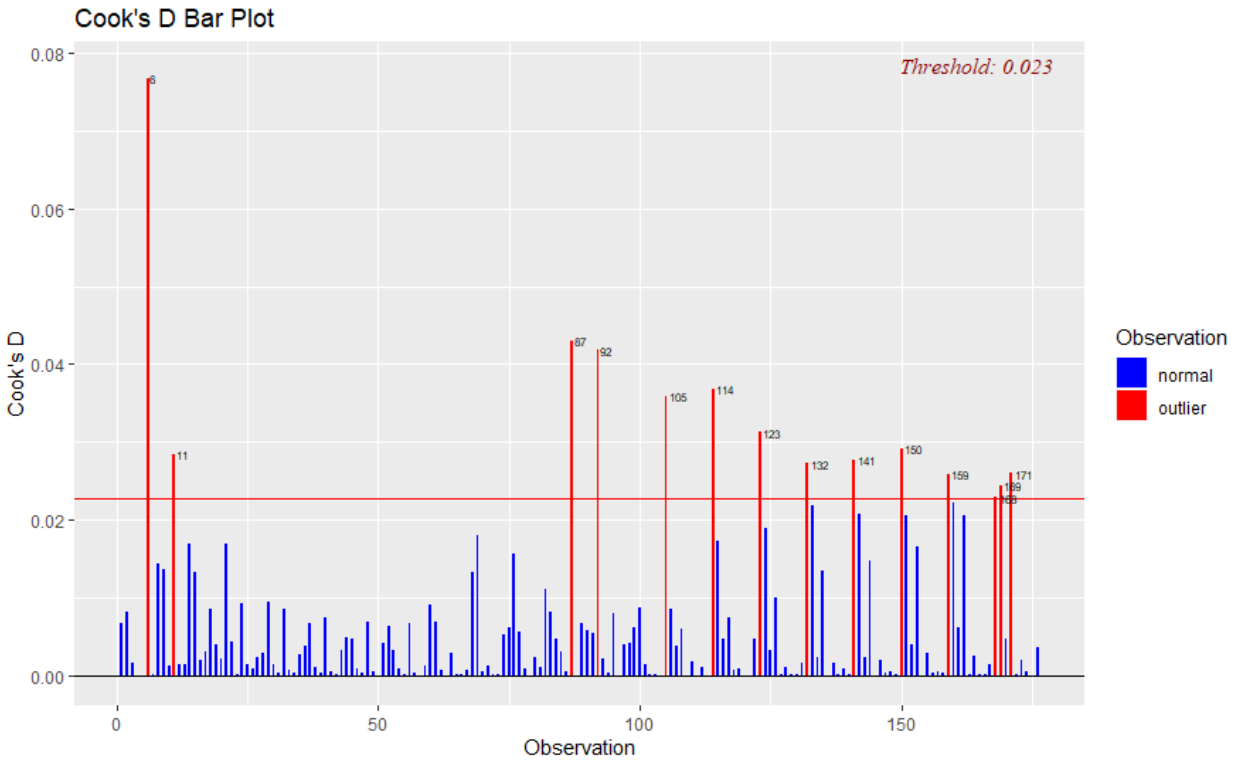

Figure 5-9: Outlier test by using Cook's Distance

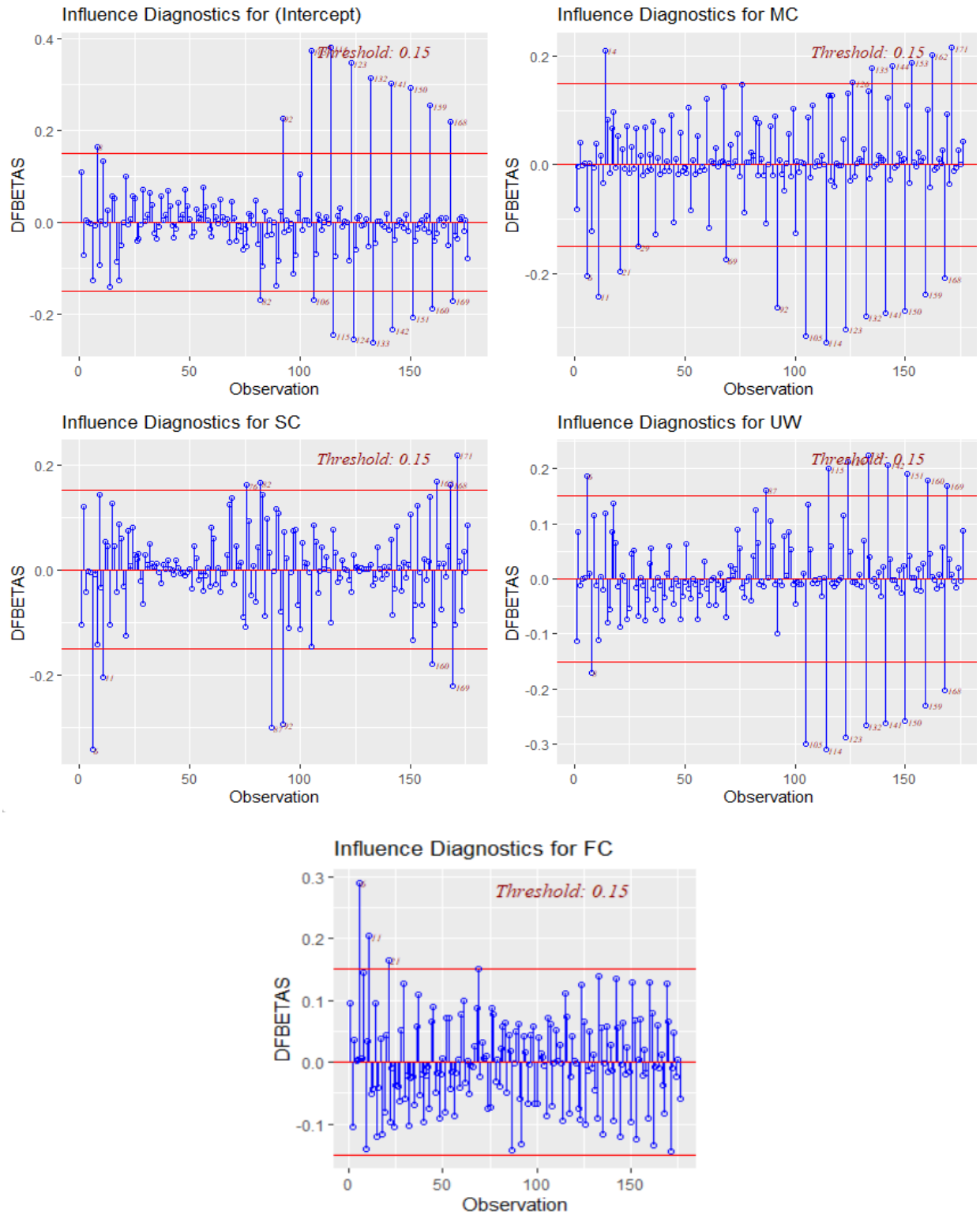

Figure 5-10: Outlier test by using DFBETAS

5.4.4 Multicollinearity

An essential presumption of an MLR model is that the predictors shouldn't have a lot of inter-predictor correlation. Multicollinearity in a model can be found using the Variation Inflation Factor (VIF), which measures how much the variation is inflated. Multicollinearity among the predictors occurs if VIF > 1. Only predictors with a VIF > 5 may provide a difficulty, though. A VIF greater than 10 denotes strong multicollinearity and a subpar estimation of the response. Therefore, it is better for the VIF to be below 5. All of the VIFs fall within the recommended range based on the VIF in Table 5-5. Therefore, there is no significant multicollinearity among the predictor variables.

Table 5-5: Variation Inflation Factors for the Preliminary Model

Variables	SC	MC	DUW	FC
VIF	1.01	1.36	1.36	1.02

5.4.5 Transformation of Variables and Check for MLR Assumptions

The response variable was not transformed because the preliminary model met the constant error variance and normality criteria.

5.4.6 Final Model Selection

To complete the best prediction model, three procedures were used in RStudio: the best subset technique, stepwise regression, and backward elimination.

5.4.7 Best Subset Selection

The parameters R2, adj. R2, Mallows Cp, and Bayesian Information Criteria are being taken into account for the optimum subset selection procedure (BIC). The technique chooses the model with the highest R2 and adj. R2, the lowest Mallows Cp, and the lowest BIC as the optimal model. Table 5-6 shows the results' executive summary. The best model, according to this methodology, consisted of a mixture of four predictor variables.

Table 5-6: The results' executive summary

Predictor Variables				R^2	Adjusted R^2	C_p	BIC
SC	MC	DUW	FC				
-	✓	-	-	0.4253	0.422	28.33	-78.5
-	✓	✓	-	0.663	0.66	7.56	-94.2
✓	✓	✓	-	0.6892	0.6838	6.76	-91.1
✓	✓	✓	✓	0.7037	0.70	4.98	-90.3

Therefore, the final model is as follows:

$$R = 78.9 - SC \times 0.0004377 - MC \times 76.16 - DUW \times 3.698 + FC \times 5.756$$

Where, R= Resistivity (Ohm-m),

SC= Sulfate Content (ppm),

FC= Fine content (%),

DUW,γ_d= Dry Unit Weight (kN/m^3)

MC= Moisture Content (%)

5.4.8 Stepwise Regression

Both the backward selection and the forward selection algorithms are used in the stepwise regression approach. The most important predictor variable is used first in the model. The

regression is run, and the parameters that will be taken into account are calculated. Then, other variables are gradually introduced in accordance with their importance. Until the model with the best criteria parameters is obtained, the process is repeated. The statistical significance tests are carried out using the F-statistic test (Kutner et al., 2005). The four predictor variables created the best model using this approach.

5.4.9 Validation of Final Prediction Model

The outcomes of the experimental tests were used to gauge the created multiple linear regression model's propensity for prediction. Figure 5-11 shows that the created model can anticipate 70.3% of the variance in resistivity caused by changes in the amounts of sulfate, moisture, dry unit weight, and fines.

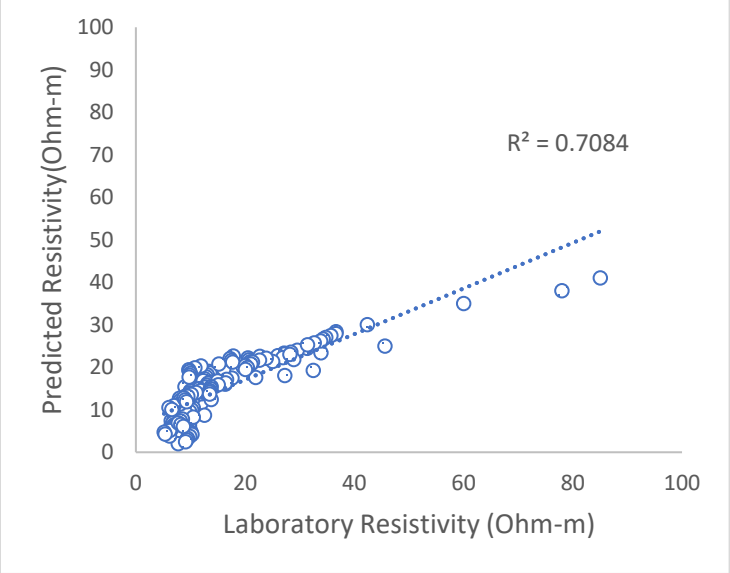

Figure 5-11: Validation of Final Prediction Model

A validation with fields data was also done. A small borehole having depth of 2.5 feet was done using hand augur. soil sample was taken from 2 feet. Three resistivity lines were done in Cedar Hill Site. One borehole was done every resistivity line using hand augur. Samples were collected using plastic bags for moisture content test, sieve analysis test unit weight test which were done in the laboratory. The field resistivity lines are shown in figure 5-12 and the parameters used for

the variables are represented in table 5-7. The error was less than 15% for the field sulfate content and predicted value by the multiple linear regression model.

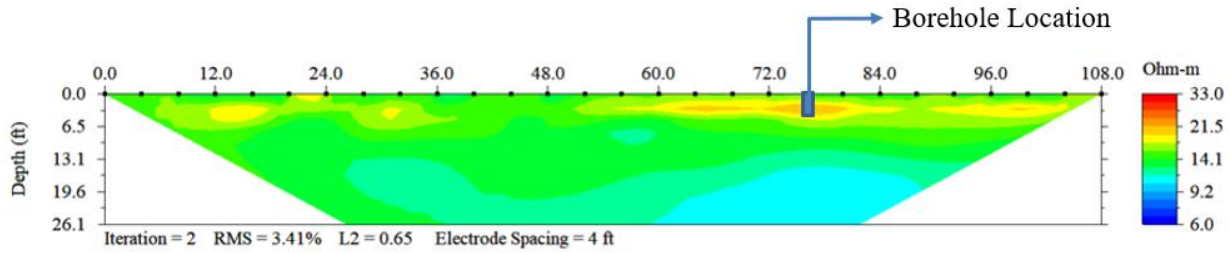

(a)

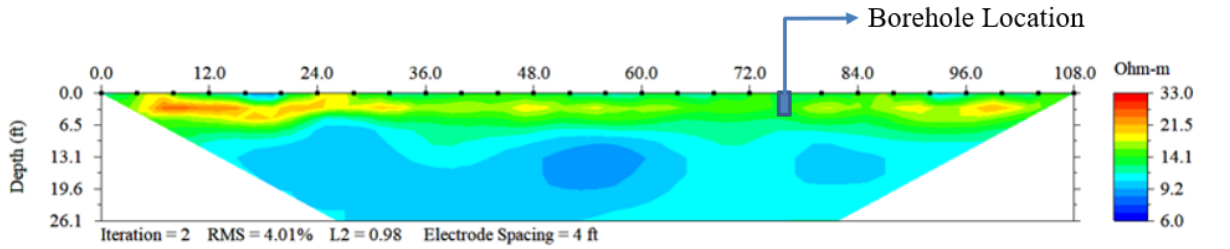

(b)

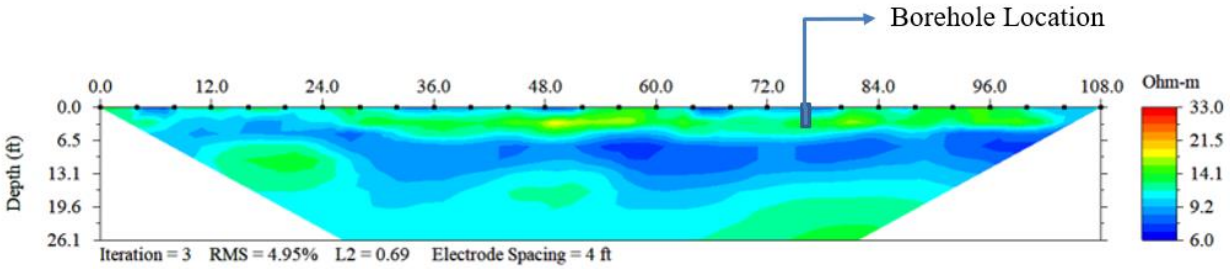

(c)

Figure 5-12: Resistivity line data for field validation.

Table 5-7: Data from field validation tests

Line	Borehole Depth	Moisture Content	Dry Unit Weight, kN/m^3	Fine Content	Resistivity Field	Sulfate Content (Lab Test)	Predicted Sulfate Content
(a)	2 feet	18%	13.3	74%	18 Ohm-m	4523 ppm	5200 ppm
(b)	2 feet	13%	14.1	0.65%	16 ohm-m	3540 ppm	3000 ppm
(c)	2 feet	19%	13.4	0.61%	16 Ohm-m	4390 ppm	5000 ppm

CHAPTER 6: CONCLUSIONS AND FUTURE RECOMMENDATIONS

6.1 Introduction

A continuous subsurface profile of a specific region can be successfully obtained using an electrical resistivity imaging survey (ERI). However, more research is needed before using this potential geophysical method in geotechnical engineering. The response of the soil to the changes is intricate and challenging to comprehend since the changes in soil parameters would alter the soil resistivity. In light of this, resistivity imaging can be used to obtain qualitative information for a field survey. In order to make electrical resistivity imaging research relevant in the engineering industry, a study on diverse soil samples was carried out.

The objective of this study was to assess the sulfate content of the soil using the electrical resistivity imaging data. In order to anticipate the sulfate concentration on the field, a statistical model has been created.

6.2 Summary and Conclusions

1. The soil samples for this experiment were collected from Fort Worth and El Paso.
2. Total 2 soil samples were selected from these two districts and after particle size distribution analysis and Atterberg limit test it was found that one soil sample was high plastic clay (Fort Worth) soil another was sandy (El Paso).
3. Existing sulfate content was measured following Tex-145 method where Fort Worth had 2500 ppm and El Paso had 1000 ppm of soluble sulfate in them. To identify the changes in electrical resistivity with sulfate content along with changing soil conditions, laboratory experiments were developed. This was done by adding sulfate to the Fort Worth and El Paso samples and doing resistivity testing for different compaction, moisture content combinations. In total 315 tests were done. 150 tests on Fort Worth Clayey Sample and 165 tests on El Paso Sandy Sample. All resistivity values were calibrated to a standard temperature of 15.5 °C.

4. To assess the effects of moisture content, sulfate content, dry unit weight, void ratio, and degree of saturation on electrical resistivity response of soil, electrical resistivity was plotted against soil characteristics. When resistivity was plotted against these parameters at various saturation levels, a typical declining trend was seen. However, there was a rising trend in the resistivity vs void ratio plot.
5. For development of multiple linear regression model, sulfate content, moisture content, fine content, dry unit weight was selected as important parameters influencing resistivity.
6. A multiple linear regression equation was created for compacted soil to explain how the sulfate content of the soil affected resistivity variations.
7. Validation of the model using laboratory data and field data.

6.3 Recommendation for Future Studies

1. The laboratory studies can be done with wide range of fine content soil samples.
2. Field resistivity values can be incorporated into the experimentation and statistical analysis for improvement of the accuracy of the statistical equation.
3. In addition to utilizing alternative currents with various frequencies in place of direct current, it is also possible to test the soil and measure the resistance response.
4. Only a dipole dipole array was used in this investigation. The electrical resistivity of soil can be determined using many types of arrays.
5. Different resistivity measuring tools can be used in the lab to account for the anisotropic component.

REFERENCES

1. John D. Nelson and Debora J. Miller (1992). “Expansive Soils Problems and Practice in Foundation and Pavement Engineering”, 259 pp. https://doi.org/10.1002/(SICI)1096-9853(19990825)23:10%3C1067::AID-NAG994%3E3.0.CO;2-E
2. Abu-Hassanein, Z. S., and Benson, C. H. (1996). "Electrical resistivity of compacted clays." *J. Geotech. Eng.*, 122 (5), 397-406.
3. Archie, G.E. (1942). “The Electrical Resistivity Log as an Aid in Determining Some Reservoir Characteristics.” *Trans. Am. Inst. Metall. Pet. Eng*., Vol. 146, pp. 54-62.
4. Anatja Samouëlian, Isabelle Cousin, Alain Tabbagh, Ary Bruand, Guy Richard (2005). “Electrical resistivity survey in soil science: a review.” *Soil and Tillage Research, Elsevier*, 83, pp.2, 173-193.
5. Chen, F.H. (1988). “Causes of Cracks on Recently Constructed Flexible Pavements: A Case Study on Kabati to Mareira Road in Kenya.” Foundations on Expansive Soils. 2nd Edition, Elsevier Science Publications.
6. B. M. Kouchaki (2017), “Laboratory Resistivity Measurements for Soil Characterization”, MSc Thesis, University of Arkansas.
7. Adhikary, S., Rana, S., Tasnim, J., & Islam, N. (2021). Dynamic Impact Factor Determination of an Existing Pre-stressed Concrete I-Girder Bridge Using Vehicle-Bridge Interaction Modelling. Journal of Civil Engineering and Construction, 10(3), 163-176.
8. Adhikary, S., Rana, S., Tasnim, J., & Islam, N. (2021). Dynamic Impact Factor Determination of an Existing Pre-stressed Concrete I-Girder Bridge Using Vehicle-Bridge Interaction Modelling. Journal of Civil Engineering and Construction, 10(3), 163-176.
9. F. I. Siddiqui and S.B.A.B.S. Osman (2012) “Electrical Resistivity Based Non-Destructive Testing Method for Determination of Soil’s Strength Properties” *Advanced Materials Research Vols*. 488-489, 1553-1557.
10. G. Kibria and M. S. Hossain (2012), "Investigation of Geotechnical Parameters Affecting Electrical Resistivity of Compacted Clays." *J. Geotech. Geoenviron. Eng.*, 138(12): 1520-1529
11. Tasnim, J. (2022). Reuse of Recycled Plastic for Subgrade Treatment. (M. Sc. Engg. Thesis, Department of Civil Engineering, The University of Texas at Arlington).

12. Hisyam Jusoh* and Syed Baharom Syed Osman (2017) "The Correlation between Resistivity and Soil Properties as an Alternative to Soil Investigation" *Indian Journal of Science and Technology*, Vol 10 (6)
13. Alsharari, B., Olenko, A., & Abuel-Naga, H. (2020). Modeling of electrical resistivity of soil based on geotechnical properties. Expert Systems with Applications, 141. https://doi.org/10.1016/j.eswa.2019.112966
14. John Pat Harris, Tom Scullion, Stephen Sebesta;Texas Transportation Institution, October 2002 "Laboratory and Field Procedures For Measuring The Sulfate Content Of Texas Soils".
15. Kibria, G., Hossain, M.S., Hossain, J., and Khan, M.S (2012), "Determination of Moisture content and Unit Weight of Clayey Soil using Resistivity Imaging (RI)" *GeoCongress 2012 © ASCE,* 3398-3407
16. L. Sebastian Bryson (2005), "Evaluation of Geotechnical Parameters using Electrical Resistivity Measurements" *Geo-Frontiers Congress*
17. Marina Kižlo, Arvids Kanbergs (2009), "The Causes of the Parameters Changes of Soil Resistivity", *The 50th International Scientific Conference „Power And Electrical Engineering.*
18. W. J. McCARTER (1984), "The electrical resistivity characteristics of compacted clays" *Geotechnique*
19. Pozdnyakov, A. I., Pozdnyakova, L. A., & Karpachevskii, L. O. (2006). Relationship between water tension and electrical resistivity in soils. *Eurasian Soil Science*, *39*(S1), S78–S83. https://doi.org/10.1134/s1064229306130138
20. Mojid, M. A., & Cho, H. (2006). Estimating the fully developed diffuse double layer
21. thickness from the bulk electrical conductivity in clay. *Applied Clay Science*, *33*(3–4), 278–286. https://doi.org/10.1016/j.clay.2006.06.002
22. Kutner, M., Nachtsheim, C., Neter, J., & Li, W. (2005). *Applied linear statistical models*.
23. Amato, M., Lapenna, V., Rossi, R., & Bitella, G. (2012). Multi-electrode Resistivity Imaging. In S. Mancuso (Ed.), Measuring Roots: An Updated Approach (pp. 189–211). Springer Berlin Heidelberg. https://doi.org/10.1007/978-3-642-22067-8_11
24. Archie, G. E. (1942). The Electrical Resistivity Log as an Aid in Determining Some Reservoir Characteristics. Transactions of the AIME, 146(01), 54–62.

https://doi.org/10.2118/942054-G

25. Barker, R. D. (1989). Depth of investigation of collinear symmetrical four-electrode arrays.
26. Geophysics, 54(8), 1031–1037. https://doi.org/10.1190/1.1442728
27. Bryson, L. S. (2005). Evaluation of Geotechnical Parameters using Electrical Resistivity
28. Measurements. Earthquake Engineering and Soil Dynamics, 740, 1–11.
29. Bryson, L. S., & Bathe, A. (2009). Determination of selected geotechnical properties of soil using electrical conductivity testing. Geotechnical Testing Journal, 32(3), 252–261.https://doi.org/10.1520/gtj101632
30. Campbell, R. B., Bower, C. A., & Richards, L. A. (1949). Change of Electrical Conductivity With Temperature and the Relation of Osmotic Pressure to Electrical Conductivity and Ion Concentration for Soil Extracts. Soil Science Society of America Journal, 13(C), 66–69. https://doi.org/10.2136/sssaj1949.036159950013000c0010x
31. Hossain, S., Dharmateja, M., & Hossain, J. (2010). Assessment of geo-hazard potential and site investigations using Resistivity Imaging. International Journal of Environmental Technology and Management, 13(2), 116 129. https://doi.org/10.1504/IJETM.2010.034297
32. Datsios, Z. G., Mikropoulos, P. N., & Karakousis, I. (2017). Laboratory characterization and modeling of DC electrical resistivity of sandy soil with variable water resistivity and content. IEEE Transactions on Dielectrics and Electrical Insulation, 24(5), 3063–3072. https://doi.org/10.1109/TDEI.2017.006583.
33. Hossain, S., Kibria, G., & Khan, S. (2019). Site investigation using resistivity imaging. CRC Press/Balkema.
34. Rhoades, J., Chanduvi, F., & Lesch, S. (1999). Soil salinity assessment: Methods and interpretation of electrical conductivity measurements.
35. Rhoades, J. D., & van Schilfgaarde, J. (1976). An Electrical Conductivity Probe for Determining Soil Salinity. Soil Science Society of America Journal, 40(5), 647–651. https://doi.org/10.2136/SSSAJ1976.03615995004000050016X
36. Samouëlian, Anatja;, Cousin, I., Richard, G., Tabbagh, A., & Bruand, A. (2003). Electricalresistivity imaging for detecting soil cracking at the centimetric scale. Soil Science Society of America Journal, 67(5), 1319–1326.
37. Zha, F., Liu, S., Du, Y., Cui, K., & Xu, L. (2010). Characterization of Compacted Loess

by Electrical Resistivity Method. Journal of Chemical Information and Modeling, 53(9), 1689–1699. https://doi.org/10.1017/CBO9781107415324.004

38. Zhou, Q., Shimada, J., Research, A. S.-W. R., & 2001, undefined. (2001). Threedimensional spatial and temporal monitoring of soil water content using electrical resistivity tomography. Wiley Online Library, 37(2), 273–285. https://doi.org/10.1029/2000WR900284
39. Braga, A. C. O., Malagutti F°_, W., Dourado, J. C., & Chang, H. K. (1999). Correlation of Electrical Resistivity and Induced Polarization Data with Geotechnical Survey Standard Penetration Test Measurements. Journal of Environmental and Engineering Geophysics, 4(2), 123–130. https://doi.org/10.4133/jeeg4.2.123
40. Singh, Shruti. (2022) Design of Crack Attenuating Mix using Waste Plastic.
41. Zahid, T. B., & Amanat, K. M. (2022). Minimum thickness of solid concrete floor slab with column line beams to avoid walking vibration discomfort. Structural Concrete.
42. Brunet, P., Clément, R., & Bouvier, C. (2010). Monitoring soil water content and deficit using Electrical Resistivity Tomography (ERT) - A case study in the Cevennes area, France. Journal of Hydrology, 380(1–2), 146 153. https://doi.org/10.1016/j.jhydrol.2009.10.032
43. Everett, M. (2013). Near-surface applied geophysics.
44. Akhtar, M.A., Mahjabin, S., Hossain, M.S., Mina, Z., Hossain, M.I., (2022). "Characterization of Eagle Ford Shale by Using Laboratory Electrical Resistivity Imaging." Proceedings from Geo-Congress 2022: Geophysical and Earthquake Engineering and Soil Dynamics (pp 159-168). Charlotte, NC: American Society of Civil Engineers
45. Robinson, D. A., Jones, S. B., Wraith, J. M., Or, D., & Friedman, S. P. (2003). A review of advances in dielectric and electrical conductivity measurement in soils using time domain reflectometry. Pubs.Geoscienceworld.Org.
46. Semenov, A. S. (1980). Electroexploration with method of natural electrical field (self200potential).
47. Sudha, K., Israil, M., Mittal, S., & Rai, J. (2009). Soil characterization using electrical resistivity tomography and geotechnical investigations. Journal of Applied Geophysics, 67(1), 74–79. https://doi.org/10.1016/j.jappgeo.2008.09.012

48. Tonks, D., Gallagher, E., & Geol, I. N. E. (2017). Grounds for concern: Geotechnical issues from some recent construction cases. Proceedings of the Institution of Civil Engineers: Forensic Engineering, 170(4), 157–164. https://doi.org/10.1680/jfoen.17.00008
49. Chikyala (2007). Experimental Studies to Address Strengths Of Limestone Cores, Sulfate Heave Problems In Limestone Cores And Tunnel Lining. The University of Texas at Arlington. http://hdl.handle.net/10106/116